REMOVAL OF MERCURY FROM WATER USING IRON(II) SULPHIDE NANOPARTICLES AND ULTRAFILTRATION MEMBRANE

A Thesis

by

MARIA CHRISTINA BISMONTE ORILLANO

Submitted to the Office of Graduate and Professional Studies of
Texas A&M University
in partial fulfillment of the requirements for the degree of

MASTER OF SCIENCE

Chair of Committee,	Ahmed Abdel-Wahab
Committee Members,	Eyad Masad
	Nimir Elbashir
Head of Department,	M. Nazmul Karim

May 2019

Major Subject: Chemical Engineering

ABSTRACT

In this study, reactive nanoparticulate FeS was used to remove Hg(II) from water with an ultrafiltration system. A dead-end ultrafiltration (DE/UF) system was developed to remove Hg(II)-contacted FeS from water in the presence of 0.01M anions (Cl^-, NO_3^-, SO_4^{2-}) and 1 mg/L HA in non-stirred mode using regenerated cellulose membrane. The DE/UF stirred mode was applied to evaluate the 'shear effect' on the rejection of Hg-contacted FeS. Batch tests reveal that complete Hg(II) removal was achieved in 10 minutes in the presence of anions and 60 minutes in the presence of HA. A cross-flow ultrafiltration (CF/UF) system was implemented to examine continuous removal of Hg-contacted FeS in the presence of 0.01 M anions using 1000 kDa polyethersulfone membrane. Experimental results showed that in the presence of anions, higher Hg(II) removal was observed compared to Hg(II) and FeS alone with slight decrease in pH and increased flux decline. The highest Hg(II) removal was achieved in the presence of HA with no pH effect despite significant impact on membrane permeability and slight Fe released during the desorption tests. The DE/UF stirred mode system exhibited reduced cake formation leading to less flux decline. In terms of membrane pore size, 100 and 300 kDa exhibited significant flux recovery despite greater flux decline compared to 30 kDa.

Overall, the developed ultrafiltration systems produced chemically stable Hg-contacted FeS particles that can be reused and disposed safely in the environment. In the DE/UF system non-stirred mode, Hg-contacted FeS achieved complete additional Hg(II) removal. However, the DE/UF stirred mode and the CF/UF system exhibited decreased additional removal capacity. These could be due to chemical variations in the FeS particles caused by the shear effect and tangential flow on the Hg(II)-contacted FeS. SEM/EDS analyses demonstrate that the Hg loading

on the membrane was higher in the presence of humic acid and anions. These findings present fundamental data that could be applied in the advancement of Hg(II)-contaminated water treatment using low cost FeS adsorbents and can serve as a guideline for continuous treatment of other toxic inorganic chemicals.

DEDICATION

This thesis is dedicated to God, my loving parents, Jose B. Orillano, Jr. and Vivian Z. Bismonte, my supportive brother, Juan Carlo. Also, this work is dedicated to my deceased grandparents, Jose Orillano, Sr. and Leoncia Buhayo, who helped raise me during my formative years in the Philippines.

ACKNOWLEDGEMENTS

I would like to thank my committee chair, Dr. Ahmed Abdel-Wahab, for his constant support and supervision throughout my research work. Moreover, I am grateful that he has given me the unique opportunity to be part of his environmental engineering research team and for the experience of conducting my experiments using world-class laboratory facilities. Also, I would like to extend my deepest gratitude to my mentor, Dr. Dong Suk Han (Shane), for his invaluable teachings and continuous guidance from the time I was doing literature review and conducting my first set of experiments to analyzing my results and drawing conclusions from my data. Furthermore, I would like to thank my committee members, Dr. Eyad Masad and Dr. Nimir Elbashir, for their guidance and support throughout the course of this research.

I would like to thank my parents for their love and sacrifices to help me get to where I am today. Also, I would like to thank my friends and family for being my source of inspiration and unwavering support. Above all, the glory, honor and thanks are to God.

CONTRIBUTORS AND FUNDING SOURCES

Contributors

This work was supported by a thesis committee consisting of Professor Ahmed Abdel-Wahab of the Department of Chemical Engineering, Professor Nimir Elbashir of the Department of Petroleum Engineering, and Professor Eyad Masad of the Department of Mechanical Engineering and under the guidance of Dr. Dong Suk Han of the Department of Chemical Engineering.

Funding Sources

This work was made possible by the Qatar National Research Fund under its National Priorities Research Program award number NPRP 4-279-2-094. Its contents are solely the responsibility of the authors and do not necessarily represent the official views of the Qatar National Research Fund.

NOMENCLATURE

A	Membrane area (m^2)
J	Flux ($L/m^2.hr$)
J_0	Initial flux ($L/m^2.hr$)
k	Empirical rate constant
n	Coefficient corresponding to the fouling mechanism
P_{zc}	Point of zero charge
t	Sampling time (min) (10, 30, 60, 120, and 180 min.)
V	Permeate volume (L)

TABLE OF CONTENTS

Page

LIST OF FIGURES

Page

LIST OF TABLES

Page

1. INTRODUCTION

This chapter explains the motivation behind this study along with the concept involved in selecting the use of reactive nanoparticulate mackinawite (FeS) and ultrafiltration systems. Then, this section concludes with the scope of this research and the structure of this thesis.

1.1. Motivation for this study

This study was fueled by two main global issues. The primary problem is associated with the alarming freshwater scarcity that threatens the sustainable development of humanity (*1-2*). The secondary issue is related to mercury (Hg) as one of the most common global pollutants, particularly in the aquatic environment, endangering several hundred million lives (*3-6*).

Water is a basic commodity for human survival. Critical water scarcity is experienced by roughly 67% of the world population (*1*). In 2015, the World Economic Forum reported that water crisis is the largest global risk (*1*). Influencing factors include the escalating number of global inhabitants, changing water consumption patterns, expansion of irrigated farming, essential energy production (produced during fuel extraction, water treatment prior to discharge/reinjection /recycling, processing, transportation of fuels, biomass development for biofuels etc.), and indispensable electricity and heat generation (*7*). Consequently, one solution is the utilization of wastewater (industrial and domestic) for beneficial uses. Furthermore, environmental regulations have become stricter in the past decade to diminish water pollution and contaminant discharges from agricultural and industrial facilities as well as urbanization complexes. Industrial wastewater contributes to majority of global water pollution with toxic metals such as mercury from artisanal and small-scale gold mining, coal burning, primary production of non-ferrous metals (Al, Cu, Pb, Zn), cement production, and oil and natural gas burning (*2, 6, 8*).

As a naturally occurring element, mercury is emitted from geologic reservoirs to the atmosphere (via coal combustion, artisanal and small-scale gold mining (ASGM), waste incineration, non-ferrous metals smelting, sludge combustion etc.) and the aquatic environment (from contaminated sites, chemical facilities, mining) as shown in Figure 1.1 (*4*, *6*). Outridge et al. (*6*) recently calculated the global estimates of the natural and anthropogenic Hg masses (in kilotons) in the atmosphere (0.35%), organic soil (12%), oceans (25%), and mineral soil (63%) since the pre-anthropogenic period (prior to 1450 AD) (Figure 1.2). Hg masses in the ocean are 82% natural and 18% anthropogenic as shown in Figure 1.2 (*6*).

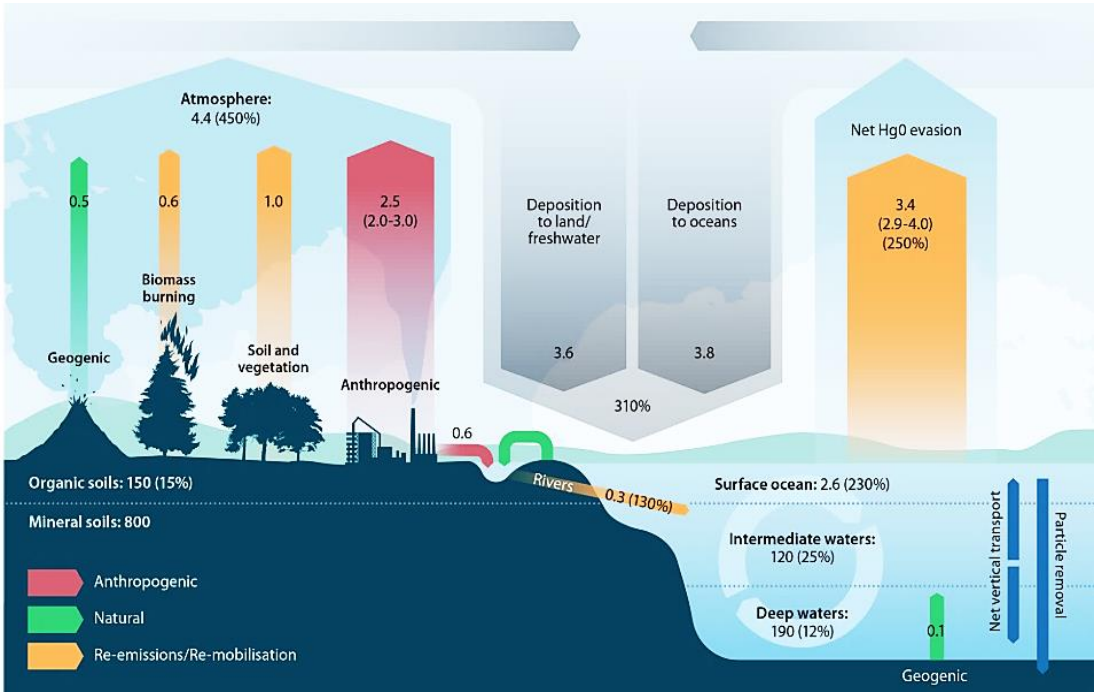

Figure 1.1: Global Hg cycle impacted by human activities since the pre-anthropogenic period (prior to 1450 AD) (Mass units in kilotons, fluxes in kilotons per year, percentages in bracket indicate approximate increase in mass/flux) (*6*). Reprinted with permission from the publisher, American Chemical Society.

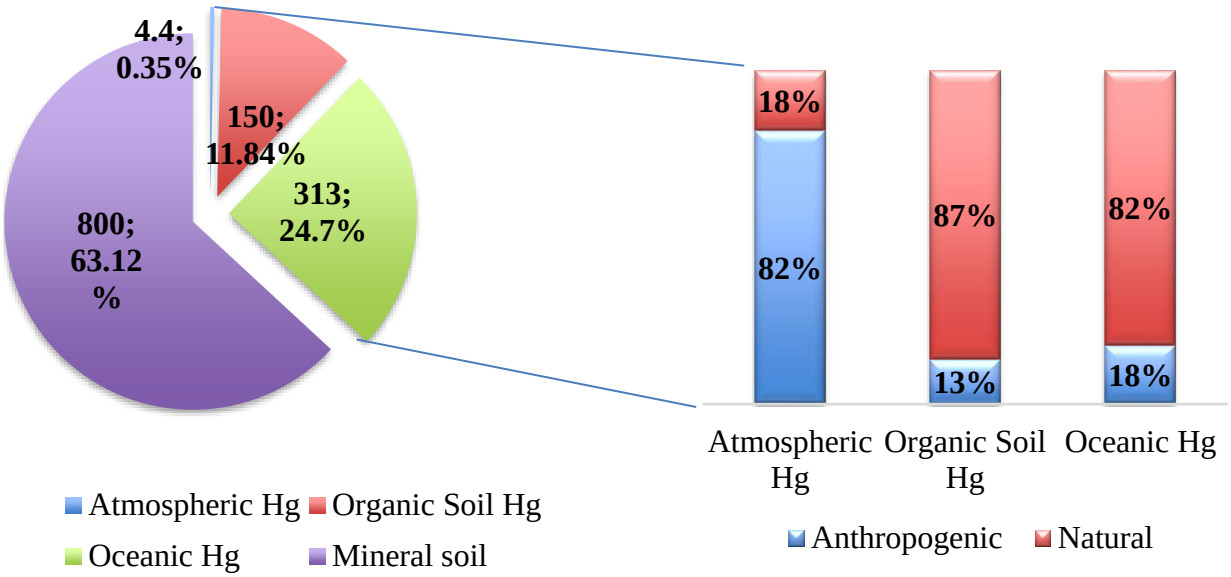

Figure 1.2: Recent estimates of natural and anthropogenic Hg masses in kilotons in the Global Atmosphere, Soil, and Oceans (*6*).

Mercury exists in multiple forms such as organic mercury (methylmercury or MeHg), inorganic mercurous salts (Hg(I)) and mercuric salts (Hg(II)) and elemental mercury (Hg (0)). Inorganic mercury present in seawater and sediments in coastal environments can be converted to MeHg, a neurotoxin, via natural bacterial reactions (*9-10*). Human exposure to organic compounds like MeHg is primarily through seafood consumption due to its bioaccumulation in the aquatic food chain. Factors that influence soluble Hg(II) conversion to MeHg include pH of the water, microbial activity, concentration of sulfates and chlorides, dissolved organic matter and Hg concentration (*9*).

It is crucial to treat soluble Hg(II) from water in order to prevent Hg bioaccumulation and prevent MeHg poisoning. In 1956, a notorious MeHg poisoning incident occurred in Minamata Bay, Japan with at least 100 deaths and thousands paralyzed after residents consumed contaminated fish. Analyses of sediment samples in the area showed concentrations around 600 ppm Hg and the lowest concentration found in fish collected from the area was 20 ppm present in

the fish collected (*11*). A similar incident occurred in Miigata City, Japan. Both tragedies resulted from the release of MeHg to the aquatic environment from chemical production factories, such as acetaldehyde and vinyl chloride, using mercury sulfate as a catalyst (*11-12*). The use of MeHg fungicide to chemically treat seed grains affected populations in Iraq, Guatemala and Pakistan that included bread in their diet (*13*). Symptoms of MeHg poisoning include behavioral disorders, insomnia, neuromuscular changes, kidney and thyroid damage (*11-13*).

During the past three decades, scientists and world leaders have held a number of International Conferences on Mercury as a Global Pollutant (ICMGP), US EPA (Environmental Protection Agency) and UNEP (United Nations Environment Program) policy events to highlight advancements in mercury science and provide guidance on addressing mercury pollution and implementing policy initiatives(*4*). In August 2017, a global treaty called the Minamata Convention on Mercury was implemented to protect human health and the environment from anthropogenic emissions and releases of mercury which is also linked to the United Nations' Sustainable Development Goals from 2015 to 2030 (*4*). Considering the dangerous risk of mercury pollution, the WHO (World Health Organization) declared that the maximum contaminant level of inorganic mercury in drinking water is 1 µg/L and the US EPA advised the acceptable discharge limit of total mercury is 5 µg/L in wastewater and 2 µg/L in drinking water (*3, 14-15*).

1.2. Technologies for mercury removal from water

In order to prevent Hg(II) conversion to MeHg in aquatic environments, several technologies have been developed to remove Hg(II) from water. These technologies are categorized into three main types: (i) physical (coagulation/flocculation, adsorption, filtration); (ii) chemical (chemical precipitation, ion exchange, electrocoagulation), and (iii) biological (bioremediation) as shown in Figure 1.3 (*2, 15-17*). Among these techniques, most water treatment

applications have been based on adsorption due to its simple, practical, economic, versatile, and highly effective process (*3*, *15*, *18*).

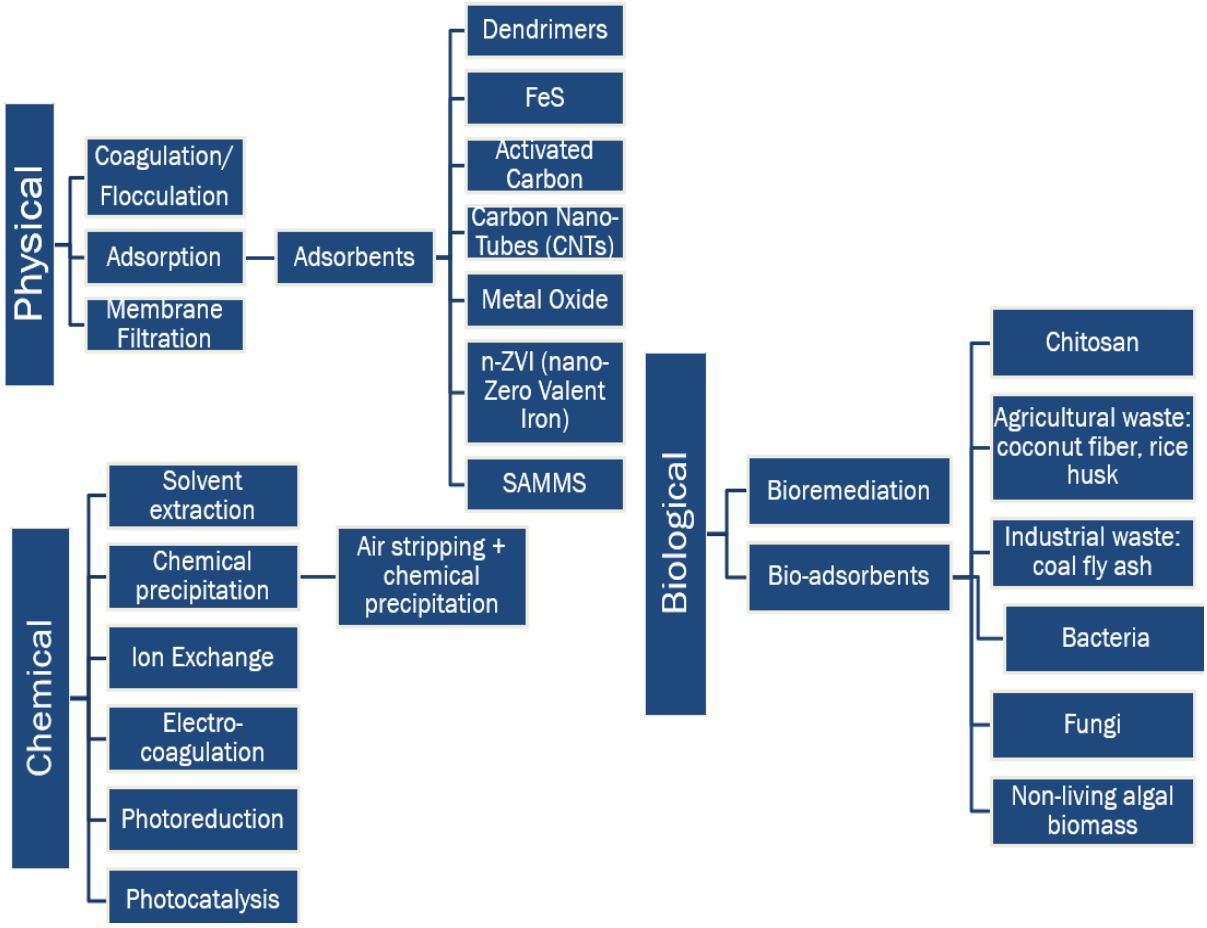

Figure 1.3: Type of Hg(II) removal technologies (*2*, *14-15*).

1.3. Mackinawite (FeS) as an effective Hg(II) adsorbent

Hg(II) is a soft Lewis acid that forms strong chemical bonds with soft Lewis bases such as the thiol functional group in sulfur-containing adsorbents. Consequently, insoluble Hg(II) sulfide solids are formed. Studies have shown that the accumulation and formation of MeHg are inhibited by the presence of sulfide minerals present in such anaerobic sediments with iron sulphides as one of the major sinks of mercury (*19-20*). Furthermore, naturally existing sulfide minerals such as

iron sulfide have been well established as a good Hg(II) scavenger in both aquatic waters and sediments (*19, 21-22*).

Iron sulfide minerals such as mackinawite (amorphous FeS), greigite (Fe_3S_4), and pyrite (FeS_2) are found in anoxic sediments (*23-24*). In aquatic environments, the first iron sulfide phase formed is mackinawite which then transforms to pyrite, and greigite is formed upon exposure of mackinawite to air (*25-27*). Though greigite and pyrite are relatively more stable forms of iron sulfides, mackinawite can persevere extensively at low temperatures and reduced environments (*3, 28-29*). Compared to greigite and pyrite, mackinawite is found to be highly reactive with several toxic metals such as arsenic and selenium (*27*). FeS has been reported as an efficient scavenger for various toxic metals in aqueous solutions. Mechanisms may involve surface precipitation, coprecipitation, adsorption or surface complex formation of Se(IV) and Se(VI)(*30*), Cr((VI)(*31*), As(III) (*32*), Tc(IV) (*33*), Cu(II) and Cd(II) (*34*), Mn(II) (*35*) and Hg(II) (*21, 36*).

The type of adsorbent for mercury removal from wastewater should satisfy the following two criteria: (i) Hg(II) adsorption must be thermodynamically and kinetically feasible; and (ii) the adsorbent must be environmentally benign and prevents growth of bacteria when released into the environment (*37-38*). The addition of FeS to water contaminated with Hg(II) results in immobilization of Hg(II) through the formation of mercury sulfide compounds such as HgS which has very low solubility constant of (2×10^{-53}) and can be filtered easily. Researchers have reported that the sorption mechanism of Hg(II) on FeS solid is strongly dependent on pH and concentrations of anions, natural organic matter, as well as other reaction conditions (*27, 36, 39*).

The possible reactions for the uptake of Hg(II) by FeS were presented by Jeong et al. (*21*), Skyllberg & Drott (*39*), and Gong et al. (*40*) :

Substitution or surface/Ion exchange:

$$FeS(s) + xHg(II) \leftrightarrow [Fe_{1-x}, Hg_x]S(s) + xFe(II) \quad (1.1)$$

Chemical precipitation following dissolution of FeS:

$$\mathrm{FeS(s)} + \mathrm{Hg(II)} \leftrightarrow HgS(s) + Fe(II) \quad (1.2)$$

Chemical precipitation following partial dissolution of FeS:

$$FeS(s) + H^+ \leftrightarrow Fe(II) + HS^- \quad (1.3)$$

$$Hg(II) + HS^- \leftrightarrow HgS(s) + H^+ \quad (1.4)$$

$$FeS(s) + Hg(II) \leftrightarrow Fe(II) + HgS(s) \quad (1.5)$$

Surface complexation:

$$\equiv FeS + Hg(II) \leftrightarrow \equiv FeS - Hg(II) \quad (1.6)$$

Using nanoparticles as sorbents for removing contaminants from water has gained considerable interest recently (*3, 40-46*).The two primary advantages of using nanoparticles are that they have large surface area for adsorption and that they can be chemically modified to enhance their affinity to target contaminants (*42*). The catalytic, optical and electronic properties of certain types of nanoparticles allow them to be used as redox active media and water treatment catalysts (*22, 47*). The challenge of using nano-scaled sorbents for contaminant removals in water treatment systems is removing these nano-scale sorbents from water as part of the treatment process (*42*). Nanoparticulate FeS has been extensively applied in Hg(II) removal from anoxic environments such as groundwater and estuaries (*22, 48*) but less in industrial wastewater from coal or gas-fired power plants which general has a low initial Hg(II) concentration (around 1000 µg/L). Hence, in order to apply nanoparticulated FeS for Hg(II) removal from industrial wastewater, the treatment process should reach the final Hg(II) concentration discharge limit of 1µg/L and include appropriate separation and disposal of final residual solids.

1.4. Ultrafiltration

Ultrafiltration is a widely used low pressure membrane separation process (pore diameters: 10-1000 Å), which effectively removes a variety of water pollutants such as suspended solids, organic matter, viruses, and bacteria (*49-52*). Therefore, this membrane filtration technique was chosen to separate the final residual solids after Hg(II) was adsorbed by FeS. Three types of filtration are frequently considered: (i) dead-end filtration (DE), (ii) crossflow filtration (CF), and (iii) stirred dead-end filtration. The feed solution is directed perpendicular to the membrane in dead-end filtration while the feed is forced through the membrane tangentially in cross flow filtration. The crossflow velocity in CF filtration is maintained through recirculation of the feed solution, however an increase in recirculation leads to increase in pumping costs (*53*). The main advantage of DE filtration its simple set up and operation which makes it the most economical UF filtration type (*54-55*). However, CF filtration is more widely used in practical applications due to its ability to adjust the crossflow velocity and thus reduce fouling to a certain extent. Stirred dead-end filtration combines the advantages of both DE and CF filtration systems (*56*).

Two filtration modes, constant pressure and constant flux, can be applied in a DE/UF system. In constant pressure, the driving force for filtration is kept constant so the permeate flux is proportional to the pressure and inversely proportional to the membrane resistance. Figure 1.4 shows a schematic of the various types of resistance that lead to flux decline during an ultrafiltration process. In a constant flux mode, the transmembrane pressure is increased over time to compensate for the increase in resistances due to flux decline. Flux decline modeling data produced by Kim and DiGiano (*57*) predicted insignificant difference in specific flux decline for constant pressure and constant flux modes for particles with diameter greater than 0.1 μm. However, for smaller particles, greater decline in specific flux with constant flux compared to

constant pressure mode was predicted. Furthermore, results from a pilot scale ultrafiltration experiment of secondary effluent showed that enhanced UF performance was observed for constant pressure, indicating that constant flux may produce comparatively faster fouling rates. Hence, constant pressure, dead-end ultrafiltration may have a more economic advantage compared to other modes (*53*, *57*).

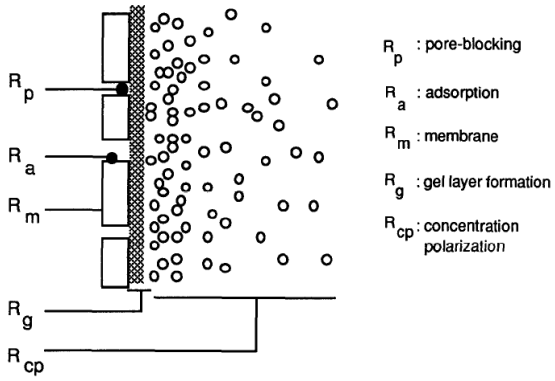

Figure 1.4: Types of resistance that cause flux decline in an ultrafiltration process, reprinted from Van den Berg & Smolders (*58*). Reprinted with permission from the publisher, Elsevier.

1.5. Scope of this research

Considering that the treatment of industrial wastewater is an inevitable solution to solving the global water crisis and that dissolved mercury must be treated to prevent methylmercury formation in anoxic bottom waters; this study is focused on understanding the mechanisms behind the reactive adsorption of Hg(II) onto nanoparticulate mackinawite (FeS) in the aquatic environment. To simulate a real water environment containing various anions and dissolved organic matter, this study aims to determine the effects of anions (Cl^-, SO_4^{2-}, and NO_3^-) and dissolved organic matter in the form of humic acid (HA) on the adsorption of Hg(II) onto FeS. For effective industrial wastewater treatment, this study combines Hg(II) removal from water by

nanoparticulate FeS and ultrafiltration to reject chemically stable residual solids that can be disposed safely. Hence, continuous contact filtration systems will be established to treat low initial concentrations of Hg(II) (i.e. 1000 µg/L in industrial wastewater) and reach the discharge limit of 1 µg/L Hg(II) using nanoparticulate mackinawite as an adsorbent.

The scope of this research involves: 1) Evaluating how fast Hg(II) is removed from water using nanoparticulate FeS in the absence and presence of anions and humic acid in order to identify the required contact time and efficient treatment conditions; 2) Studying the effects of anions (Cl^-, SO_4^{2-}, and NO_3^-) and humic acid on final solid rejection in the non-stirred and stirred dead-end ultrafiltration (DE/UF) system that was developed by our research group (*48*); 3) Studying the effects of anions (Cl^-,SO_4^{2-}, and NO_3^-) on final solid rejection in the cross-flow ultrafiltration (CF/UF) system established by our team (*59*); 4) Determining the stability of the Hg-contacted FeS deposited on UF membrane upon exposure to 0.1 M Sodium Thiosulfate solution; 5) Determining additional sorption capacity of the Hg-contacted FeS; and 6) Comparing the performance of the different ultrafiltration systems (non-stirred DE, stirred DE, and CF) combined with FeS adsorption for efficient Hg(II) removal from water.

1.6. Thesis Structure

The following sections include a summary of the literature review conducted then the methodology implemented to achieve the objectives of this research. Furthermore, the experimental results obtained and corresponding analyses are presented. Finally, the conclusions and recommendations for future work are discussed.

2. LITERATURE REVIEW

This chapter presents detailed information on the global sources, aquatic chemistry, and toxicity of mercury. Then, the different technologies applied for mercury removal from water are described in this section. Additionally, a comparison of the various types of adsorbents are presented.

2.1. Global mercury source

The most common forms of mercury (Hg) in the environment are elemental-metallic mercury, cinnabar ore (mercuric sulfide), organic methyl mercury, and mercuric chloride. Additionally, mercury is also present as an impurity in numerous minerals, fossil fuels, and coal. Based on recent studies, the Hg content (from anthropogenic emissions) in worldwide reserves include 4.4-5.3 Gigatons (10^9 tons) in the atmosphere, 250-1000 Gigagrams (Gg) in soils/sediments, and 270-450 Gg in oceans. From 1990 to 2010, an annual reduction of 1.5 to 2.2% in concentration atmospheric Hg(0) and Hg(II) wet deposition were observed in Europe and US due to significant efforts done to reduce anthropogenic Hg emissions (*8*). However, atmospheric Hg concentrations have increased in East Asia with increased oxidized Hg(II) in the tropical and subtropical regions (*8*). Consequently, 50% of total global wet Hg(II) deposition is predicted to occur in tropical oceans. In terms of global aquatic Hg emissions, China and India contribute to 50% of Hg releases into the marine environment which eventually discharges into the North Indian and West Pacific Oceans (*8*). Table 2.1 displays the main Hg sources in the aquatic environment. A summary of the primary (natural and anthropogenic) and secondary emission sources and impact is presented in Table 2.2.

Table 2.1: Dominant Hg sources in the aquatic environment (*8*).

Aquatic environment	*Dominant Hg source*
Inland freshwater	Artisanal and Small-scale gold mining (880 Mg/year) Terrestrial mobilization (170-300 Mg/year) Industrial and domestic wastewater releases (220 Mg/year)
Pelagic Ocean	Atmospheric deposition
Arctic Ocean	Erosion from rivers and the coast
Pacific Ocean	Enhanced Hg deposition from the Asian continent

Table 2.2: Summary of Hg emission types, sources, and environmental impact (*8*).

Emission	*Source*	*Impact*
Primary	Natural: Volcanic actions Biomass incineration Geogenic erosion	Intensify Hg(0) content in surface reservoir
	Anthropogenic: Artisanal and Small-Scale Gold Mining Coal-combusted power station and electricity generation Chlor-alkali industry Industrial facilities (paper and pulp, textile, chemical processing plants) Ingredient in wiring devices, switches, amalgam for teeth filling Catalysis of vinyl chloride monomer from acetylene Oil and gas industries Hazardous waste sites Pesticides	Intensify global Hg(0) content in the ecosystem
Secondary	Re-emission process of deposited Hg which is then reduced to Hg(0)	Re-allocation of reduced Hg (Hg(0)) within the ecosystem

2.2. Toxicity of mercury

Toxic mercury emission into the environment, most especially the marine areas, impose major threats to humans and aquatic life. Mercury has an atomic mass of 200.59 g/mol with a density of 13.6 g/cm^3 at 20^{0}C (*60-61*). In the aquatic environment, where inorganic mercury is converted to the chemo-toxic organic Hg compound, methylmercury (MeHg) enters the food chain through absorption in marine microorganisms and fish. Key parameters that affect the methylation process include presence of microbes, sulfides, dissolved oxygen, environmental temperature, pH, and salinity (*62*). Dangerous mercury exposure to humans, either through contaminated fish consumption (common and major pathway) or anthropological sources brutally affects the cardiovascular, genetic, immune, respiratory, reproductive, muscular, neurological, and nephrological systems (*61-63*). The strong binding capacity of MeHg to sulfhydryl and thiol groups disrupt enzymatic and hormonally activities in the body. Beckers and Rinklebe (2017) reported that around 80-90% of MeHg is rapidly transported throughout the body in the blood stream via the digestive tract. The kidney is the primary organ at risk and roughly 10% of MeHg resides in the brain (*61*). Table 2.3 displays the list of health consequences of Hg to humans. Accordingly, Hg concentration limits and safe consumption limits of contaminated fish have been imposed by the World Health Organization (acceptable daily intake: 0.71 µg Hg/kg body weight, blood level: 40-200 µg Hg), European Food Safety society (provisioned tolerable weekly intake: 1.6 µg Hg/kg body weight, max. residual levels: 0.5 mg/kg of other fish, 1 mg/kg for large predatory fish), United Nations Food and Agricultural Organization (maximum allowable limit:0.5 mg/kg for other fish and 1 mg/kg for large predatory fish) and other numerous governing establishments (*62*).

Table 2.3: Health consequences of Hg exposure to humans(*62-63*).

System	***Symptoms***
Cardiovascular	Coronary dysfunction, Atherosclerosis, Cardiomyopathy, heart palpitation
Genetic	Hindrance of protein production, teratogenesis, block of hormonal/enzymatic activities
Immune	Lymphoproliferation, Immuno-suppressant/stimulant
Respiratory	Pneumonitis, bronchitis
Reproductive	Infertility, reduction in sperm count, menstrual disorder
Muscular	Muscle atrophy, loss of coordination
Neurological	Epilepsy, Schizophrenia, bipolar disorder, Dementia, Parkinson's disease
Nephrological	Kidney dysfunction

2.3. Aquatic Chemistry of Mercury

Dissolved mercury occurs in various forms such as aqueous elemental Hg(0), inorganic Hg(II), and organic species (methylmercury(MeHg), dimethylmercury(Me_2Hg), and ethylmercury (EtHg))(*64*). Elemental aqueous Hg(0) and inorganic Hg(II) occur simultaneously through redox reactions in oxic and anoxic waters as shown in Figure 2.1 (*64*). Hg(0) is rather unreactive and is released into the atmosphere via volatilization(*65*).

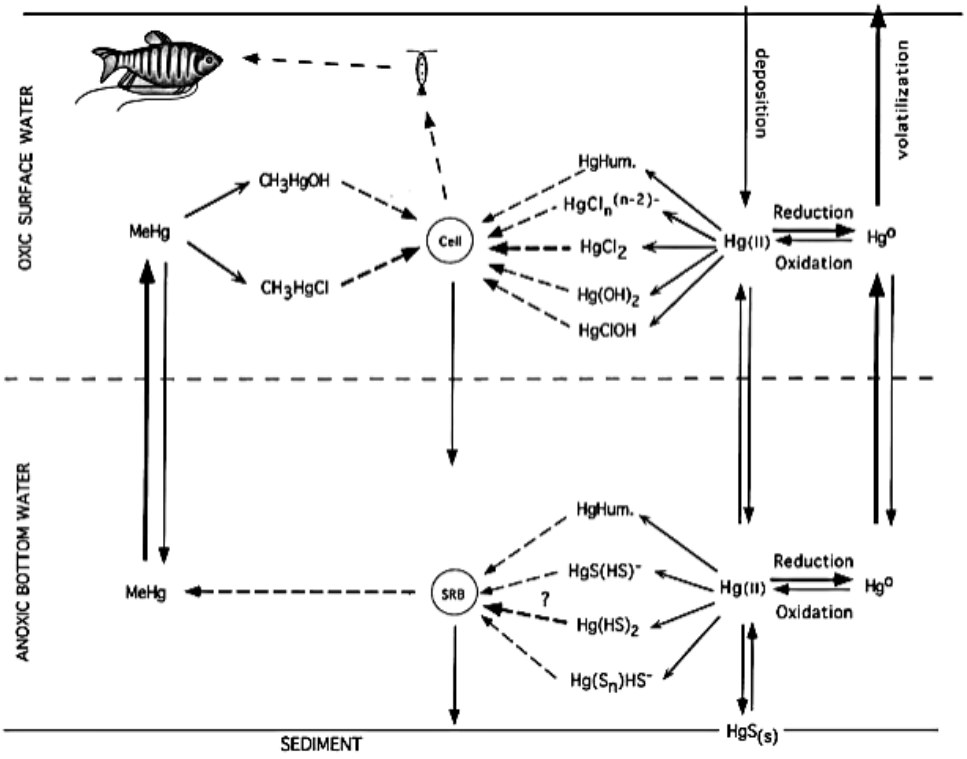

Figure 2.1: The aquatic cycle of mercury produced by Morel et al. (*64*). Reprinted with permission from the publisher, Annual Reviews, Inc.

In surface water, inorganic mercury (Hg(II)) forms complexes with chloride and hydroxide ions. According to Morel et al. (*64*), the dominant species in seawater (pH 8.3, $[Cl^-]$= 0.4 M) was $HgCl_4^{2-}$ion. In freshwater (pH 5.5-8.0, $[Cl^-]$= 0.01 - $10^{-4.5}$M), the dominant species were HgClOH, $HgCl_2$, $Hg(OH)_2$, and $HgCl_3^-$ ions(*66*). The presence of other inorganic ligands such as NO_3^-, SO_4^{2-}, PO_4^{3-}, and F^-did not considerably influence the speciation of Hg(II) in aqueous solutions (*67-69*).

Similarly, in Figure 2.1, oxic surface water contains Hg(II) and Hg(0), Hg-Cl and Hg-OH complexes (HgClOH, $HgCl_2$, $Hg(OH)_2$, and $HgCl_n^{(n-2)-}$), and MeHg with chloro- and hydroxo-complexes (CH_3HgCl and CH_3HgOH). In anoxic bottom water, Hg(II) forms soluble complexes with sulfide from sediments ($HgS(HS)^-$, $Hg(HS)_2$, $Hg(S_n)HS^-$) which undergo biological

methylation via sulfate reducing bacteria to form MeHg. Additionally, the metastable solid mercury sulfide, HgS(s) (black metacinnabar), forms at room temperature and pressure. In solution, black metacinnabar transforms to red cinnabar over time. Both HgS(s) forms have extremely low solubility product constant ($K_{sp} = 10^{-54}$). $HgCl_2$ is highly soluble in water whereas HgCl and HgS are insoluble (*64*). In addition to Hg redox transformations, biomethylation, and complexation of Hg(II) with chloride and hydroxide ions under anoxic conditions, Hg(II) also forms strong complexes with dissolved organic matter (DOM) such as humic acids (HA) (*70*). This Hg(II)-HA complexation may be important in controlling the speciation, and methylation of aqueous Hg in the aquatic environment. Hg(II) species forms strong bonds with the functional groups (thiol (-SH) or reduced sulfur (-S))present in DOM at high concentration ratios ([DOM]/[Hg]) which results in reduced biomethylation(*71*). Abiotic reduction of Hg by humic acid was also reported by Allard and Arsenie (1991) . Conversely, it has been reported that Hg(II)-cysteine complexes, where smaller molecular weight –SH groups are present, result in high methylation rates (*70, 72*). Studies by Gu et al. (*70*) showed that DOM, in the form of humic acid (HA), has the ability to reduce Hg(II) to Hg(0) and form Hg(0)-DOM complexes via ligand-induced oxidative complexation. They proposed the reactions shown in Equations 2.1-2.4: (i) physicochemical sorption, (ii) ligand-induced oxidative complexation, (iii) oxidation of Hg(0) to Hg(II), and (iv) complexation of Hg(II) with the thiol groups (*70*).

$$2R - SH + Hg(0) \rightarrow R - SH \cdots Hg(0) \cdots HS - R \quad (2.1)$$

$$R - SH \cdots Hg(0) \cdots HS - R \rightarrow R - S - Hg(II) - S - R + 2H^+ + 2e^- \quad (2.2)$$

$$R - S - S - R' + Hg(0) \rightarrow Hg(II) + R - S^- + R' - S^- \quad (2.3)$$

$$Hg(II) + R - S^- + R' - S^- \rightarrow R - S - Hg(II) - S - R' \quad (2.4)$$

2.4. Comparison of dissolved mercury removal technologies

A comparison of the Hg(II) removal technologies is displayed in Table 2.4. Several treatment techniques are efficient for large-scale Hg(II) removal such as coagulation/flocculation/flotation, chemical precipitation, ion exchange, and photoinduced reduction (*2, 14-15*). However, to achieve the maximum allowable Hg(II) concentration in drinking water (1 µg/L) from solutions with low initial Hg(II) concentration, treatment processes such as adsorption, membrane filtration, solvent extraction, electrocoagulation, bioremediation, photocatalysis, and air stripping with chemical precipitation are effective (*2, 14-15*).

2.4.1. Adsorption

Several mechanisms can be applied to separate dissolved metal ions in aqueous solutions such as adsorption, surface precipitation, co-precipitation, and absorption. Adsorption is mostly applied to treat wastewater with low initial concentrations of mercury. This technique involves a two-dimensional accumulation of the adsorbate molecules at the adsorbent-water interface in the presence of intermolecular interactions between the adsorbate and adsorbent (*73-75*). Such intermolecular interactions involve (i) surface complexation reactions which includes inner-sphere surface complexation between the metal ion and the surface functional group, (ii) electrostatic interactions caused by outer-sphere complexation between the metal ion and the surface of the solid phase, (iii) hydrophobic expulsion of metal complexes with highly non-polar organic solute, and (iv) adsorption of metal-polyelectrolyte complexes (surfactants) formed by reduced surface tension (*73-74, 76*).

Table 2.4: Comparison of various Hg(II) removal technologies

Technique	*Description*	*Advantages*	*Disadvantages*	*Main parameters for optimum efficiency*	*References*
Coagulation/ Flocculation/ Flotation	Formation of low soluble heavy-metal compounds (carbonates, hydroxides, sulfides) in order to increase the density of colloid particles and allow them to settle down for removal. Flocculants are added such as $Al_2(SO_4)_3$, $Fe_2(SO_4)_3$ and $FeCl_3$, polyaluminiun chloride, polyferric chloride to agglomerate the destabilized particles and form larger particles. This process is followed by straining/flotation/filtration. E.g. Organic ligand functionalized silica (2-mercaptobenzothiazole/aminopropylbenzoylazo-2-mercaptobenzothiazole/Quinolinol	Cost effective High selectivity for Hg(II) ions	High sludge formation, large usage of coagulants/flocculants, low reusability of harmful chemicals, require additional removal techniques such as precipitation, spontaneous reduction for complete removal	Type/dosage of coagulant, pH, T, alkalinity, mixing conditions	(*2, 77*)
Adsorption	Adsorbents are used to extract the heavy metal ions in the aqueous solutions through physico-chemical interactions with the active sites.	Effective removal of Hg(II) at Low initial concentration, Low OPEX, Low fouling, Reuse of regenerated adsorbent, various types of adsorbents have been developed (with their effectiveness dependent on high surface area, functional groups)	Desorption Adsorbent disposal environmental impact	Adsorbents Carbon Nano-Tubes (CNTs) - thiol derived	(*2, 15, 17*)

Table 2.4 Continued

Technique	*Description*	*Advantages*	*Disadvantages*	*Main parameters for optimum efficiency*	*References*
Membrane Filtration	Pressure-driven technique that separates solid particles based on the size, solution concentration, pH and applied pressure through a permeable membrane.	Suitable for low toxic metal ion concentration, High selectivity and efficiency, Large treatment capacity, Limited space required, Low pressure	Pre-treatment of wastewater is required for membrane preservation, High OPEX, Membrane fouling particularly due to dissolved organic matter (DOM), Low selectivity, Instability under high pressure operations	Particle size, solution concentration, applied pressure, pH, membrane permeability	(*15*, *17*)
Solvent extraction	Hg(II) is extracted from the solution using cationic extractants (e.g. capryilic acid dissolved in chloroform, LIX 34 (4-n-dodecyl-9-benzenesulphonamide), thiophosphinic acid) at low pH (1).	High Hg(II) removal	Requires secondary treatment (complex stripping process), used extraction solvents create secondary pollutant into the environment, Time-consuming Difficult liquid-liquid separation	pH, initial Hg(II) concentration,	(*15*)
Chemical precipitation	Chemicals are added to the solution to alter the pH in order to prevent dissolution of the toxic metal-precipitates. Then, the sedimented metal precipitates are isolated and removed from the solution. Hydroxide precipitation involves precipitants such as Ca(OH)2, NaOH. Sulfide precipitation includes sulphide precipitates which have lower solubility compared to hydroxide precipitates. Precipitants used can be FeS and CaS (solids).	Simple design and operation, Highly effective for high toxic metal ion concentration, Low CAPEX, Simple operation, Ease of handling, Quick metal recovery, Good settling capacities	High OPEX, not suitable for low toxic metal ion concentration, sludge handling, presence of complexing agents in water can hinder precipitation, requires additional treatment such as sedimentation or filtration to remove the insoluble precipitates, large amounts of chemicals required	pH, Type of precipitants, Dosage of precipitant	(*2*, *17*)

Table 2.4 Continued

Technique	*Description*	*Advantages*	*Disadvantages*	*Main parameters for optimum efficiency*	*References*
Ion exchange	Substitution of Hg(II) with benign metal ions using an ion exchange resin (i.e. material used to recover/extract the metal ions). For high initial concentration, zeolite cationic exchanger is preferable. Zeolite contains Al and Si atoms bound by hydrogen bridges to form a crystalline structure.	High selectivity and removal efficiency, Regeneration of resin is feasible, Cationic exchange resins are suitable for treating high toxic metal concentration in the solution while anionic exchange resins are efficient for treating low toxic metal concentrations.	Fouling of the ion exchange resin in case of high Hg(II) concentration in the solution (especially in the presence of NOM), Secondary pollutants are formed from the regeneration of resins using chemical reagents, High OPEX	pH, presence of natural organic matter (NOM), Synthetic or natural resin, Cationic or anionic exchange resin,	(*2*)
Electro-coagulation	Contaminants present in the solution can be adsorbed by active intermediates produced by the hydrolysis of metallic ions generated by electrolysis. For instance, electricity applied to the anode is used to generate coagulants such as Al and Fe while H_2 is generated from the cathode.	Feasible operation, no chemical additives, Synergize with electricity generated from wind/tidal/solar/biogas Can be combined with ozone/adsorption/ultrasound processes	Sustainable end-use sludge management Lab-scale phase using synthetic water Highly dependent on electricity (i.e. High OPEX), indirect pollution via fossil fuel resources, Low performance and stability of anode and cathode (fast consumption/passivation)	Current density, Type of power supply, Electrocoagulation time, pH, temperature, agitation, initial concentration	(*78-79*)
Bioremediation	Soluble Hg(II) ions are converted to insoluble elemental mercury catalyzed by microbial enzymes. Aerobic/anaerobic processes are applied to convert dissolved Hg(II) into less soluble mineral forms like sulfides.	Environmentally friendly Cost effective No sludge generation Safe and simple process	Highly dependent on enzymatic activity; Requires strict monitoring of microbial growth (nutrients, optimum toxic metal concentration, pH, temperature); Further research required for development	Optimal levels of pH, available nutrients for essential growth of microbes, temperature, toxic metal concentration to prevent toxic conditions	(*80*)

Table 2.4 Continued

Technique	*Description*	*Advantages*	*Disadvantages*	*Main parameters for optimum efficiency*	*References*
Photocatalysis	Photocatalytic degradation of several forms of aqueous mercury e.g. Hg(II) to Hg(0) stimulated by UV excitation. Photocatalyst such as nano-particulate TiO_2 is used	Efficient at pH 10 (basic conditions) Simultaneously removes toxic metal and organic pollutants, Less harmful by-products generated	Requires a long time to reach high removal efficiency In acidic condition, organic additives are required such as formic acid, methanol, and oxalic acid	pH due to speciation variation of Hg and surface charge of TiO_2 nanoparticles	(*38, 81-82*)
Photoinduced reduction	UV radiation is used to reduce Hg(II) to Hg_2Cl_2 precipitant instead of Hg(0) in the presence of Cl^- (5 g/L) and Fulvic Acid (2 g/L). With an initial concentration of 1000 mg/L Hg(II), 70% was removed at pH 3 with 90 min UV irradiation (300 W medium pressure mercury lamp) using real wastewater	Simultaneously removes toxic metal and organic pollutants, Less harmful by-products generated	Requires additional treatment by adsorption or chemical precipitation Requires long time to reach high removal efficiency Limited to lab scale Potential high OPEX due to UV radiation dependency	UV radiation, dosage of adsorbent	(*83*)
Combination: air stripping + chemical precipitation	The concept involves reducing Hg(II) to Hg(0) by adding low levels of stannous (Sn(II)) chloride in water, then removing volatile Hg(0) from water by air stripping (>100 ng/L to 10 ng/L)	Cost effective ($0.10 to $0.20 per m^3), Greater than 90% Hg(II) removal efficiency Sn does not affect mercury methylation No secondary pollutants generated No off-gas treatment required	Sn (non-toxic) bioaccumulation but not at increased levels Requires further research and development	Dosage of $SnCl_2$	(*84-85*)

Two types of heavy metal adsorption mechanisms were reported by previous researchers: specific adsorption (more selective, less reversible, chemisorbed inner-sphere complexation) and non-specific adsorption or ion exchange (less selective, weak, outer-sphere complexation) (*73-74, 76*). In specific adsorption, surface complexation occurs in the form of a reaction between an ion present in the solution and the surface functional groups of an adsorbent (*73, 86*). However, in non-specific ion (cation) exchange, cations from the adsorbent surface are replaced with the cations from the solution. Hence, this cation exchange consists of metal ions and charged adsorbent surfaces held by weak covalent bonds (outer-sphere complexation) (*73, 87*).

Conversely, surface precipitation involves the formation of a three-dimensional network of a new solid phase through its repeated development in three dimensions (*75*). Hence, adsorption is a two-dimensional process and surface precipitation involves a three-dimensional sorption mechanism. Furthermore, a continuum often exists between surface complexation and surface precipitation (*75*). Co-precipitation occurs during the formation of the substrate (precipitate) which comprises of both the aqueous heavy metal from the solution and the species from the dissolution of the adsorbent. (*74, 88*). Additionally, absorption or solid state diffusion, is the diffusion of an aqueous metal ion into the solid phase and is three-dimensional in nature (*74, 89*). For instance, heavy metals get absorbed onto minerals such as clay and metal oxides by diffusing into the lattice structure and become fixed into the pore spaces.

2.4.1.1. Comparison of different types of Hg(II) adsorbents

Over the past decade, numerous research studies have been dedicated to developing superior classes of adsorbents to improve Hg(II) adsorption, enhance reusability, and reduce toxic by-products for safe disposal, and lower synthesis costs (*3, 15, 18*). A comparison of the different

types of Hg(II) adsorbents and list of sorption capacities in descending order are displayed in Table 2.5 and Table 2.6, respectively.

Table 2.5 Comparison of different types of Hg(II) adsorbents

Type of adsorbent	*Advantages*	*Disadvantages*	*Resources*
Activated carbon	High surface area, porosity, adaptability	High cost	(*2*)
Carbon Nanotubes	Consist of cylindrical single-walled/multi-walled graphite sheets with superior properties (mechanical, magnetic, chemical, and thermal stability, catalytic properties, high specificity) Large surface area (250 m^2/g) Regeneration of adsorbent is feasible	High production cost which limits large scale implementation Strong tendency to accumulate and limited functional groups Requires pre-treatment (acid/oxidative treatment/enhancement with functional groups/saturation with metals/metalloids	(*2*)
Metal-Oxide	Highly effective Regeneration of adsorbent is feasible e.g. Fe_3O_4, ZnO, MDN, TF-SCMNPs	High production cost which limits large scale implementation Strong tendency to agglomerate-require pretreatment Toxic to humans (exposure via skin, inhalation, ingestion)	(*90*)
nano-TiO2 as a photocatalyst	high surface area, selective sorption through chelation of the toxic metal ions to the surface sustainable approach to water treatment because it can use sunlight as source of energy	Strong tendency to aggregate Difficult to regenerate	(*38*, *81*)
n-ZVI	High surface area, high active site density Selective surface reactivity Improved mobility Spherical shaped particles with a davg=30.6 nm (avg. diameter) Regeneration is effective	High production cost which limits large scale implementation Strong tendency to agglomerate-require pretreatment (modified with aquatic plant Azolla filiculoides pumice support)	(91-93)

Table 2.5 Continued

Type of adsorbent	*Advantages*	*Disadvantages*	*Resources*
SAMMS	Large surface area, high density of sorption sites, high reactivity and selectivity (pore size: 2-10 nm, SA: 1000 m^2/g) Rate adsorption rate irrespective of Hg(II) initial concentration or pH of the solution	Complex synthesis of SAMMS leads to high CAPEX Limited to lab-scale application	(*94-96*)
FeS, FeS2	High removal efficiency within 10 minutes Low cost and applicable in large scale treatment facilities Regeneration and reuse are feasible	Requires anaerobic conditions Tendency to agglomerate (stabilized by biomaterial/Al_2O_3 etc.)	(*48, 97*)
Dendrimers Hyperbranched polymers	Adaptable physicochemical properties and distinctive topological structure Highly selective Strong mechanical and thermal stability	Complex synthesis, not feasible for large scale use Highly dependent on pH, contact time, initial concentration, temperature Regeneration to be further investigated	(*18, 91, 98*)
Chitosan Biopolymer	Eco-friendly (biodegradable, biocompatible, non-toxic) Low cost Regeneration and reusability are feasible Can be applied over a wide range of pH	Requires chemical/physical modification to improve mechanical and thermal stability Hg(II) removal efficiency affected by presence of anions	(*98-99*)
Fungal biomass	Good sorption capacity due to its abundant cell wall material. It can grow in natural environment conditions Regeneration of fungi bioadsorbent is done by immobilizing the biomass with polymer matrices (PVA and calginate gels).	Further research required for large scale application Low reusability	(*2, 80*)

Table 2.5 Continued

Type of adsorbent	*Advantages*	*Disadvantages*	*Resources*
Bacterial adsorbent	Abundant resource Smaller size Flexible in usage	Adsorption only occurs during the growth phase of the biosorbent.	(*80*)
Non-living algal biomass	Adsorption occurs at the surface of the cell wall Dependent on the pH, temperature, contact time Desorption of algal biomass for reuse can be done using HCl or HNO_3 Dual usage for biofuel resource and wastewater treatment	Further research required for large scale application	(*2, 80*)
Agricultural waste: Coconut fiber/pith Rice husk	Eco-friendly, high adsorption capacity Easy to use Inexpensive and abundant resource	Further research required for large scale application Low reusability	(*2, 93, 100*)
nano-Zero Valent Iron (nZVI)	Small particle size, large surface area, high reactivity High removal efficiency through adsorption, precipitation, co-precipitation, reduction of Hg(II) to Hg(0) due to Fe^{2}+ and H_2 from Fe(0) dissolution	High cost Complicated synthesis Corrosive passivation/reactivity loss Permeability loss Tendency to agglomerate Low mechanical stability Further pre-treatment is required to improve stability of nZVI	(*92-93*)
Industrial waste: Coal Fly Ash	Abundant resource, low cost, highly efficient Lower environmental impact Functional group: Silica, Alumina and Magnetite Dependent on density, particle size, surface area Eco-friendly safe disposal	Efficiency depends on chemical treatment Desorption/Regeneration of adsorbent is inefficient	(*2*)

Table 2.6: Sorption capacities of different Hg(II) adsorbents

Adsorbents	Adsorption capacity (mg/g)	Initial Hg(II) concentration	Efficiency of Hg(II) removal (%)	Functional groups	Dosage	pH	T(C)	Optimum time (min)	Regeneration	Interaction mechanism	Ref.
Cyanuric chloride modified SiO_2/Al_2O_3 as the carrier of L-cysteine methyl ester dendrimer	**3079**	100 mg/L	99.8	Cyanuric (triazine) groups	0.1 g	6	25	45 min	12	pseudo-second-order, chemisorption	(*101*)
CMC/Gelatin/Starch stabilized FeS	**1726 1939 1989**	1 mg/L	99	Sulfide group	0.2 g/L	7	30	240 min		co-precipitation and complexation	(*3*)
FeS	**769.2**	1 mg/L	>96	Sulfide group	0.12 g/L	7	30	<60 min		Pseudo-second order; chemisorption	(*97*)
Activated Carbon	**724**										(*91*)
Sulfur rich microporous polymer (SMP)	**595.2**	200 ppb		Sulfur atoms	20 mg/60 mL Hg(NO3)2 sol	1	25	3 min	4	Pseudo-second order; chemisorption	(*102*)

Table 2.6 Continued

Adsorbents	Adsorption capacity (mg/g)	Initial Hg(II) concentration	Efficiency of Hg(II) removal (%)	Functional groups	Dosage	pH	T(C)	Optimum time (min)	Regeneration	Interaction mechanism	Ref.
Graphene Oxide and Tin (IV) Disulfide (SNS2) composite	**342.02**	19.58 ppm	99.1	COOH group of GO, Sulfide group of SnS2	10 mg GO-SnS2/10 mL Hg	0.5-11	30			Physisorption and Chemisorption	(*103*)
Pumice supported-nanoscale zero valent iron	**332.4**	40-100 mg/L	99.1	hydroxyl groups		8.13	25 C	60 min	4	0.5 min - physisorption, then reduction to Hg(0)	(*92*)
Al2O3 supported - FeS	**313**	1 mg/L	99	Sulfide group		3-9	30	60 min	5	co-precipitation and complexation	(*24*)

Table 2.6 Continued

Adsorbents	Adsorption capacity (mg/g)	Initial Hg(II) concentration	Efficiency of Hg(II) removal (%)	Functional groups	Dosage	pH	T (C)	Optimum time (min)	Regeneration	Interaction mechanism	Ref.
PAMAM (polyamidoamine) Dendrimer: SiO2-G0-SA SiO2-G1.0-SA SiO2-G2.0-SA	**182 304 364**	0.002-0.004 mol/L		N atoms of amino group Oxygen group, Phenyl groups		6	35	180 min		pseudo-second order, film diffusion process as the rate determining step	(*18*)
SAMMS	**270**	1.84 mmol/L	99	thiol group	matrix solution of 100 mmol/L KI	9	25	120 min		chemisorption	(*94-95*)
nano-TiO_2	**166.6**	100	99.9	150 W medium pressure mercury lamp+0.01M CuSO4 sol		10					(*81, 91*)

Table 2.6 Continued

Adsorbents	Adsorption capacity (mg/g)	Initial Hg(II) concentration	Efficiency of Hg(II) removal (%)	Functional groups	Dosage	pH	T (C)	Optimum time (min)	Regeneration	Interaction mechanism	Ref.
Peach stone based activated carbon (PSAC)	**59.5**	40-450 mg/L or ppm	94.1-99.5	Oxygenated acidic group (hydroxyl, alkoxy-compounds)	4 g/L	4	25			Pseudo-first order kinetic model; physisorption	(*104*)
Coal based activated carbon (CAC)	**48.9**	40-450 mg/L or ppm	94.1-99.5	Oxygenated acidic group	4 g/L	4	25			Pseudo-first order kinetic model; physisorption	(*104*)
Coconut husk activated carbon (CHAC)	**44.9**	40-450 mg/L or ppm	94.1-99.5	Oxygenated acidic group Amido, amino, carboxyl, acetamido, phenolic, alcohols and esters.	4 g/L	4	25			Pseudo-first order kinetic model; physisorption	(*104*)

Table 2.6 Continued

Adsorbents	Adsorption capacity (mg/g)	Initial Hg(II) concentration	Efficiency of Hg(II) removal (%)	Functional groups	Dosage	pH	T(C)	Optimum time (min)	Regeneration	Interaction mechanism	Ref.
Chitosan Natural polysaccharide obtained from deacetylation of chitin (fungal cell wall)	**43.3**	20-500 mg/L		Amino and hydroxyl groups	2g chitosan/10 mL10 mL of 0.2 M ethylhexadecyldimethyl ammonium bromide solution in dichloromethane	3	25	45 min	10	pseudo-second-order, chemisorption	(*98*)
FeS_2	**9.9**	1 mg/L	>96	Sulfide group	1 g/L	7	30	<60 min		Pseudo-second order; chemisorption	(*97*)
Coal Fly Ash (CFA) - Zeolite LTA		10 mg/L	94		50 g/L	2.5				Pseudo-second order; chemisorption	(*105*)

Table 2.6 Continued

Adsorbents	Adsorption capacity (mg/g)	Initial Hg(II) concentration	Efficiency of Hg(II) removal (%)	Functional groups	Dosage	pH	Temperature (C)	Optimum time (min)	Regeneration	Interaction mechanism	Ref.
Bacteria - Vibrio parahaemolyticus (PG02); Vibrio parahaemolyticus (PG02)		10 mg/L 0.1 mg/L	80 70	ketones, aldehydes and carboxyl groups							(*80*)
Fungi - Candida parapsilosis		0.1	80	carboxyl, phosphoryl, hydroxyl, imidazole						intracellular precipitation, ion exchange, complexation	(*80*)

2.4.1.2. Nanomaterials used to remove Hg(II) from aqueous solutions

Advancements in Hg(II) removal have been focused on applying and developing nanoadsorbents due to their vast surface area, incomparable porosity, and adjustable surface attributes leading to superior Hg(II) adsorption capacities. The presence of various functional groups on the nanoadsorbents surface and short diffusion pathway dictate the efficiency of Hg(II) involving interactions such as complexation and ion-exchange (*15*). Nevertheless, the main drawbacks of utilizing nanoadsorbents include the usage of toxic reagents in the synthesis process, agglomeration when treating real wastewater (due to the presence of anions, organic matter etc.), and corrosion of magnetite-built nanocomposites in acidic environments. Hence, future studies could address the modification of nanomaterial structure to overcome the current limitations, efficient retrieval of nanomaterials in the marine environment to reduce potential ecological impact or improve regeneration/reuse of spent nanoadsorbents, and determine ecofriendly synthesis procedures (*15*).

Dendrimers

Recently, hyper-branched polymers known as dendrimers have become promising nanoadsorbents in the field of medical science, catalysis, and water treatment due to their adaptable physicochemical properties and distinctive topological structure (*96*).The structure of dendrimers synthesized by Kurniawan for Hg(II) removal involves interior branch cells, terminal NH_2 branch cells, and a core of ethylene diamine held together by covalent bonds. The presence of high density NH_2 terminal branches and functional groups in the interior allow metal ion adsorption onto the surface of dendrimers. Sun et al. (*106*) studied Hg(II) adsorption using silica-gel supported Polyamidoamine (PAMAM) dendrimers and reported adsorption capacities in the range of 0.5-1.5 mmol Hg^{2+}/g of the dendrimers (*106*).

Carbon nanotubes

Carbon nanotubes (CNTs) are allotropes of carbon made of graphite with a cylindrical structure. They possess strong adsorption capacity, electrical and mechanical properties, larger surface area with more than 250 m^2/g, chemical stability, catalytic properties which enhances immobilization of soluble contaminants, uniform pore distribution and ability to bond specific contaminants to their exterior walls(*107-109*). Synthesis techniques of CNTs include cold vapor deposition, catalytic development, laser ablation and arc discharge (*96*). Two main forms of CNTs exist, which are single walled CNTs (SWCNT) and multi-walled CNTs (MWCNT). The concentration of functional groups on CNT's exterior walls can be increased by acidic or oxidative pre-treatment with HNO_3 and NaClO, and by coating with MnO_2 and Ceria. A commercially feasible MWCNT synthesis method was reported by Shang et al. (*110*). High yield MWCNTs on a large scale was produced by pyrolysis of polypyrrole nanotubes at 900^0C in N_2 environment (*110*). Studies reported by Tawabini et al. (*107*), Shadbad et al. (*108*), and El-Sheikh et al. (*109*) have shown that the application of MWCNTs for removal of Hg(II) from water achieved 90-100% removal. One of the main limitations of implementing this technique is the high production cost of CNTs (*96, 111*).

Metal oxides-based nano-adsorbents

Metal oxides-based nano-adsorbents can be effective for removing inorganic contaminants from water (*96*).Pilot scale data was presented by Pacheco et al. (*37*) and reported 99% Hg(II) removal efficiency by alumina nanoparticles which were prepared using sol-gel technology. A similar Hg(II) removal efficiency was achieved using nanoparticulate humic acid-coated Fe_3O_4 prepared by co-precipitation (*112*). According to Liu et al. (*112*), coating Fe_3O_4 nanoparticles with humic acid improved material stability and Hg(II) removal efficiency; and reduced aggregation of

the nano-adsorbents in the solution without affecting their magnetic properties. Reuse of spent Fe_3O_4 magnetic nanoparticles was feasible since HA-coated Fe_3O_4 particles with adsorbed metals can be retrieved from water via magnetic separation techniques at low magnetic fields (*112*).

Sheela et al.(*46*) investigated adsorption properties of Hg(II) with ZnO nanoparticles. ZnO nanoparticles which were synthesized via precipitation achieved maximum adsorption capacity for Hg(II) of 714 mg/g at pH of 5.5 and temperature of 30^{o}C(*46*). Additionally, Lisha et al. (*113*) examined the adsorption capacity of Hg(II) on manganese dioxide nanowhiskers (MDN) synthesized by reduction of potassium permanganate using ethylaclohol. They reported almost 100% Hg(II) removal efficiency with an initial Hg(II) concentration of 10 mg/L and a dose of 10 mg MDN/250 mL solution at pH 6-9 and temperature of 30^{o}C (*113*). An alternative to conventional metal-oxide adsorbents was presented by Hakami et al. (*114*). They reported high Hg(II) removal efficiency using thiol-functionalized mesoporous silica-coated magnetite nanoparticles (TF-SCMNPs) (*114*). Although metal-oxide nanoadsorbents can effectively treat water contaminated with Hg(II), information on the adsorption mechanism is still limited. Also, applying this technique at industrial scale is limited by high cost production of the metal oxides nano-adsorbents (*37, 96*).

Nanoscale zero-valent iron

Nanoscale zero-valent iron (nZVI) has a reduction potential of -4.4 V with surface area roughly 30 times greater than granular Fe (*96*). nZVI has been widely applied for remediation of sites contaminated with chlorinated compounds. The nZVI have potent water treatment properties due to their increased surface area and high active site density, ability to reduce and stabilize various cations, selective surface reactivity, and improved mobility and portability in remote subsurface aqueous environments (*96*). Liu et al. (*92*) reported a 99% Hg(II) reduction to Hg(0)

using pumice-supported nZVI (P-nZVI) nano-adsorbents . With a specific area of 32.2 m^2/g, the removal capacity of was 332.4 mg Hg/g of P-nZVI.

Self-Assembled Monolayers on Mesoporous Silica (SAMMS)

Another nano-adsorbent that is applied to remove metal ions from water is Self-Assembled Monolayer on Mesoporous Silica (SAMMS). The common hydrocarbon formula of SAMMS is $X-(CH_2)_n-Y$, where X is the head group (e.g. $-SiCl_3$), and Y is the bonding group (e.g. $Si(OCH_3)_3$). SAMMS consists of an arrangement of engineered mesoporous ceramic substrates (pore size: 2-10 nm, SA: 1000 m^2/g) with self-assembled monolayers (SAM) of well-organized functional groups (*96*). Such nanoadsorbents have large surface area, high density of sorption sites, high reactivity and selectivity. Mattigod et al. (*95*) created a thiol-SAMMS to remove Hg(II) from water. Alkylthiols present in SAMMS act as a Lewis base which have high affinity to Lewis acids such as Hg(II).98.9% removal efficiency of an initial Hg(II) concentration of 10 mg/L was achieved using 200 mg of thiol-SAMMS (*95*).It was reported that pH did not have a significant effect on the Hg(II) adsorption using thiol-SAMMS. However, the complex synthesis of SAMMS limits its application on a commercial scale (*94-95*).

2.4.2. Membrane filtration

Adsorption with low-priced and accessible adsorbents is known to be an effective and economic option for treating wastewaters with low concentrations of Hg(II). Additionally, membrane filtration is highly efficient in treating heavy metal-contaminated water. However, the limitations of applying membrane filtration include permeate flux decline due to membrane fouling (*17*). Hence, this study involves the combination of the synergistic treatments of nanotechnology, adsorption, and membrane filtration to treat low concentrated Hg(II)-

contaminated water using nanoparticulate FeS adsorbents and a dead-end ultrafiltration membrane system.

Membrane filtration techniques like reverse osmosis (RO), nanofiltration (NF) and ultrafiltration (UF) are widely used for water purification due to their flexibility, ease of scale-up and easy maintenance and operation. Ultrafiltration membranes can be utilized for removing these nanoparticles from water. Laboratory-scale experiments have to be conducted to investigate such systems specifically for aqueous Hg(II) removal (*42*).

Available types of membrane filtration processes are microfiltration (MF), ultrafiltration (UF), nanofiltration NF) and reverse osmosis (RO). The pore size ranges of these membrane processes are: 0.75-7.5 kDa (0.1-1 nm), 15-47 kDa (2-5 nm), 1-500kDa (5-100 nm), and 1.5-7.5 MDa (80-500 nm), for RO, NF, UF, and MF respectively (*115*). Urgun-Demitras et al. (*116*) evaluated different membrane processes for Hg(II) removal from oil refinery wastewater (*116*). They reported that RO and NF processes were able to meet the target Hg(II) effluent concentration initially at around 20 bars. However, an increase in pressure (>34.5 bars) resulted in considerable increase in flux decline and fouling rate as well as deterioration of permeate quality. Membrane permeability was reported to be obstructed by rapid solids accumulation and concentration polarization occurring on the membrane surface. UF and MF membrane combined with precipitation processes effectively obtained less than 1.3 ng/L of Hg(II) concentration at lower operating pressures (around 2.8 bars). A full scale unit consists of ultrafiltration preceded by precipitation and sedimentation was applied to remove Hg(II) from wastewater (*117*). This process achieved an effluent stream with Hg(II) concentration below the 0.2 µg/L detection limit.

2.4.3. Nanoparticulate-enhanced ultrafiltration

The integration of nanoparticulate adsorbents and ultrafiltration systems has been reported as a viable approach for removal of metal ions from water (*44, 48, 59, 118*). Adsorption of contaminants coupled with ultrafiltration systems not only achieves high contaminant removal efficiency but also allows for regeneration of spent adsorbents. The feasibility of recovering Cu(II) ions from aqueous solutions using a combination of polyamidoamine (PAMAM) dendrimers and dead-end ultrafiltration was investigated by Diallo et al.(*119*). They used atomic force microscopy to assess the correlation between membrane fouling and dendrimer sorption (*119*). Another study conducted by Jawor and Hoek (2010) compared the performance of polymer and zeolite removal capacity of cadmium ions from water and separated the nanoparticulate metal complexes using dead-end stirred ultrafiltration membrane system. The successful removal of Hg(II) and As(III) with initial concentrations of 500 µg/L and 1000 µg/L, respectively was accomplished by implementing a polymer enhanced ultrafiltration method conducted by Jana et al. (*120*) . Furthermore, the complexation of polyacrylic acid sodium salt (PAASS) coupled with ultrafiltration for the removal of Hg(II) and Cd(II) ions from aqueous solution was reported by Zeng et al. (*121*). Similarly, Han et al. (*48*) developed a continuous contact dead-end ultrafiltration system to remove the stable final residue formed when Hg(II)-contaminated water was treated using nanoparticulate FeS. It was reported that this technique resulted in effective rejection of Hg(II)-contacted nanoparticulate FeS. The stability of final residue was confirmed when no Hg(II) release was detected after contact with 0.1M sodium thiosulfate solution which was used as a strong inorganic ligand for desorption of Hg(II). The ultrafiltration experiments were conducted using both non-stirred and stirred mode, with more efficient Hg(II) removal in non-stirred mode because quick FeS oxidation by shear flow occurred in stirred mode (*48*).

2.4.4. Chemical precipitation

Chemical precipitation has been the most widely used mercury water treatment process due its simplicity and inexpensive operational costs. The effectiveness of this process is greatly dependent on pH, presence of natural organic matter and other compounds, chemical dosage, and sludge handling (*17*, *122*). Hg(II) ions in water react with added chemical reagents to form insoluble precipitates. Hydroxide precipitation and sulfide precipitation are the most common chemical precipitation processes. The advantages of hydroxide precipitation are low cost, relatively uncomplicated process and easy pH control. However, significant amounts of comparatively low density sludge are produced during the process which involves disposal and dewatering issues (*17*). Additionally, amphoteric metal hydroxides and presence of other metals can cause solubility problems since the ideal pH for the precipitation of one metal can cause another to dissolve back into the solution. Also, the presence of complexing agents in water can hinder metal hydroxide precipitation. Sulfide precipitation is the most common method to treat wastewater contaminated with inorganic mercury (*17*). Non-amphoteric metal sulfide precipitates possess considerably lower solubilities than hydroxide precipitates. Thus, sulfide precipitates can accomplish high metal removal over a wide pH range compared to hydroxide precipitates and produce relatively thick sulfide sludges and thus more convenient dewatering and disposal processes. Neutral or basic conditions are recommended for mercury precipitation with sulfide to avoid formation of toxic H_2S fumes which are produced in acidic environments.

Although chemical precipitation has been the conventional treatment of heavy metals removals from aqueous solutions due to its simple design and efficient treatment of highly concentrated wastewater, it is relatively ineffective for wastewater with low concentrations of

heavy metals (*17*). Furthermore, increased operational costs are attributed to handling of sludge produced in large quantities in precipitation processes.

2.4.5. Ion exchange resins

Hg(II) removal from water and wastewater via ion exchange method involves the replacement of toxic metal ions with benign ones. This relatively simple technique allows efficient treatment especially when large volumes of diluted solutions are treated (*123-126*). Dabrowski et al. (*126*) provided a review of the different types of ion exchangers for Hg(II) removal which are evaluated at both laboratory scale and industrial scale. Strongly acidic cation exchangers, selective ion exchangers, and weakly and strongly basic anion exchangers can be used to treat Hg(II) contaminated water. For example, the ion exchanger ImacTMR, a styrenedivinylbenzene copolymer, produced by AkzoZoutChemie has been used for industrial scale removal of Hg(II) from solutions such as electrolytic brines of chlor-alkali plants (*123-126*). The macroporous structure of Imac TMR consists of thiol and sulphonic groups, which have a +135 mV redox potential and a capacity of 240 g Hg/dm^3 of ion exchanger. Additionally, the Imac TMR process achieved high Hg(II) effluent quality and regenerated liquid containing mercury was recycled into the treatment process. Srafion NMRR is another type of ion exchanger that contains S and N functional groups which has sorption capacity of 545 g Hg/ kg of ion exchanger and was applied to treat Hg(II) contaminated industrial wastewaters (*123-126*). Zhao et al. (*127*) evaluated using weakly basic exchange resins for treatment of Hg(II) contaminated drinking water based on Lewis acid-based interactions. The optimum pH condition for this process was reported to be neutral to basic, and the presence of humic acids deterred the process since humic acids can form complex compounds with mercury.

Ion-exchange processes achieve high treatment and removal capacity and obtain fast kinetics. Despite these advantages, the regeneration of spent ion-exchange resins leads to critical secondary pollution which increases costs. Hence, ion exchange processes remain uneconomical for treating wastewater with low concentrations of heavy metals. Furthermore, the presence of natural organic matter such as humic acids (HA), capable of forming Hg-HA complexes, would negatively affect the performance of ion-exchange resins (*17, 125, 128*).

2.4.6. Electrocoagulation

In electrocoagulation, contaminants present in the solution can be adsorbed by active intermediates produced by the hydrolysis of metallic ions generated by electrolysis. Nanseu-Njiki et al. (*79*) evaluated Hg(II) removal by electrocoagulation using aluminum (anode) and iron (cathode) electrodes. 99% Hg(II) removal efficiency was reported at a current density of 3.125 A/dm^2. Table 2.7 provides a list of successful electrocoagulation experiments (*129-132*) .

Table 2.7: List of electro-coagulation experimental results

Initial concentration (mg/L or ppm)	*Hg(II) Removal efficiency (%)*	*Electrodes*	*Current density (A/m^2)*	*pH*	*References*
4	99	Al-Fe	250-312.5	7	(*129*)
50	98.5	Fe-Fe	9V	4.5	(*130*)
41	99.95	Al-Fe	40	3-7	(*131*)
20	99	Al-Stainless Steel	30	3-7	(*132*)
0.10-0.50	98	Al-Fe	15	7	(*133*)

2.4.7. Bioremediation

Aerobic bioremediation is a biological process for treating mercury-contaminated water by converting soluble Hg(II) to insoluble elemental mercury catalyzed by microbial enzymes such as mercury reductase (*134*). Another process is then used to separate elemental mercury. Also, anaerobic and aerobic processes can be applied to convert dissolved mercury into less soluble mineral forms like sulfides (*135*). This process is usually followed by precipitation or passage through an activated carbon bed prior to disposal. This process requires optimal levels of pH, availability of nutrients like yeast and sucrose which are essential for growth of microorganism, temperature to sustain biological operations, contaminant concentration to avoid toxic conditions to prevent microbial growth (*135*).

An example of a pilot scale bioremediation was reported by Wagner at al. (*136*). The treatment system involved the enzymatic reduction of dissolved mercury to Hg^0 from chlor-alkali electrolysis wastewater using an enzyme-catalyzed bioreactor coupled with an activated carbon filter. The system consisted of a 700-L, fixed bed, aerobic bioreactor catalyzed by *Pseudomonas* strains with Pumice granules as the catalyst carrier (mainly Al_2O_3 and SiO_2). The influent wastewater, containing 3-10 mg/L of initial mercury concentration, was neutralized using H_3PO_4 or NaOH and supplied to the bioreactor at 0.7-1.2 m^3/hr. Final Hg concentration of 50 µg/L was obtained after treatment through the bioreactor and a final concentration of approximately 10 µg/L was achieved after the activated carbon filter stage. However, this method is highly dependent on the enzymatic activity of the microorganisms. The strains have to be fed regularly and protected from poisonous conditions such as high initial Hg levels, temperature and unsuitable pH values (*136*).

2.4.8. Air stripping

Looney et al. (*85*) reported the effectiveness of combining chemical reduction and air stripping to treat Hg(II)-contaminated water with low initial concentration. The concept involves reducing Hg(II) to Hg^0 by adding low levels of stannous (Sn(II)) chloride in water, then removing volatile Hg^0 from water by air stripping. With initial Hg(II) concentrations of around 138 ng/L, approximately 94% removal efficiency was achieved at Sn:Hg stoichiometric ratios ranging from 5 to 25 (*85*). Batch experimental results confirmed that rapid reduction of Hg(II) to Hg^0 was attributed to the addition of Sn(II). This method does not produce secondary wastes and has low capital, maintenance, and operation cost. With the predicted mass discharge and contaminant concentration in released air, off-gas treatment is not usually required. Data from pilot-scale experiments show that chemical reduction coupled with air stripping can achieve final mercury concentrations in the range of 1 – 10 ng/L after wastewater treatment. To fully develop this treatment system and evaluate its reliability, further studies should be conducted on the environmental impact of stannous (Sn(II)) chloride and additional information of the stoichiometry should be obtained (*85*).

3. METHODOLOGY*

This chapter specifies the materials used in performing the lab experiments, synthesis of nanoparticulate FeS, and the procedure implemented for the batch tests. Furthermore, this section introduces the systematic approach applied to evaluate the performance of the dead-end and cross-flow ultrafiltration experiments in the absence and presence of anions and humic acid. Additionally, the techniques and equipments used to analyze the aqueous and solid phase samples are explained this chapter.

3.1. Materials

All chemicals with analytical grade quality or higher were dissolved in deoxygenated, deionized water (DDW). Deionized water was obtained by passing distilled water from a Barnstead mega-pure distillation device through a Labconco purifier system. Subsequently, the deionized water was purged with 99.99% N_2 (g) for two hours to produce deoxygenated, deionized water. Nanoparticulate FeS was synthesized using sodium sulfate nanohydrate ($Na_2S.9H_2O$, Alfa Aesar,) and iron (II) chloride tetrahydrate ($FeCl_2.4H_2O$, Sigma-Aldrich). Mercury stock solutions were prepared using mercuric chloride ($HgCl_2$) obtained from Mallinckrodt Chemicals, Phillipsburg, NJ. Sodium thiosulfate anhydrous ($Na_2S_2O_3$) was purchased from AMRESCO. Anions used in this study were in the form of sodium sulfate anhydrous (Na_2SO_4) obtained from BDH, sodium chloride (NaCl) purchased from Fischer Scientific, and sodium nitrate ($NaNO_3$) manufactured from Sigma-Aldrich. Humic acid (HA) was purchased from Sigma-Aldrich.

*Reprinted from Water Research, Vol 53, Han, D.S.; Orillano, M; Khodary, A.; Duan, Y.; Batchelor, B.; Abdel-Wahab, A.; "Reactive iron sulfide (FeS)-supported ultrafiltration for removal of mercury (Hg(II)) from water", 310-321, Copyright 2014, with permission from Elsevier and "Effects of anions on removal of mercury(II) using FeS-supported crossflow ultrafiltration" by Han, D. S.; Orillano, M.; Duan, Y.; Batchelor, B.; Park, H.; Abdel-Wahab, A.; Nidal, H..; 2017. *Nova Science Publishers, Inc.*, 129-152, Copyright 2017 by Nova Science Publishers, Inc.

All the solutions prepared in this study was adjusted to pH 8 using 0.1M NaOH and 0.1 M HCl. The pH was monitored using a Thermo Scientific pH meter calibrated using Orion three buffer solutions (4.0, 7.0, 10.0). All the batch experiments were conducted in an anaerobic chamber filled with 99.9 % N_2. Reaction vessels were suspended using an end-over-end rotary mixer and the samples were filtered using 0.02 µm Anodisc membrane filters (Whatman).

A dead-end flow, ultrafiltration membrane system was set up with low pressure-driven stirred cell UF system provided by Millipore Co, where an 800 mL glass reservoir container is connected to a 300 mL glass cell with a 31.7 cm^2 membrane area. Pressure was maintained at 1 bar by a compressed N_2 cylinder connected to the system. Ultrafiltration membranes made of regenerated cellulose (RC) with a diameter of 63.5 nm of different molecular weight cutoff (MWCO) values were used to investigate the separation of the nanoparticulate metal complexes in the solution (i.e. 30, 100, 300 kDa).

As for the crossflow ultrafiltration membrane experiments, the Cogent µscale Tangential Flow Filtration System was used with a Pellicon XL 50 cassette equipped with a polyethersulfone UF membrane (MWCO=1000 kDa, d=50 cm^2) (Figure 3.1). The PES UF membrane was positioned in layers separated by spacers to transfer feed and permeate water as shown in Figure 3.2.

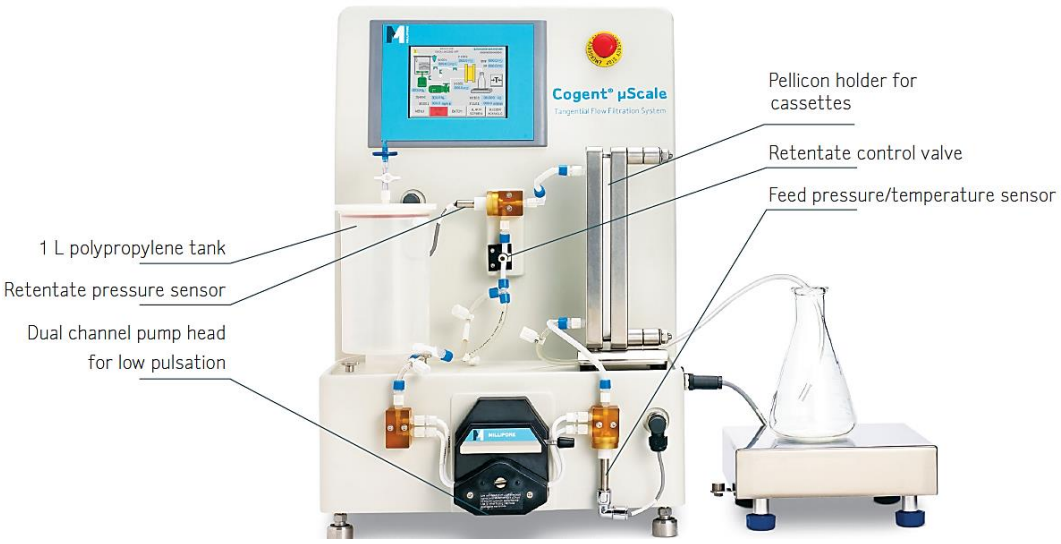

Figure 3.1: Cogent µscale Tangential Flow Filtration System set up used for the CF/UF membrane experiments.

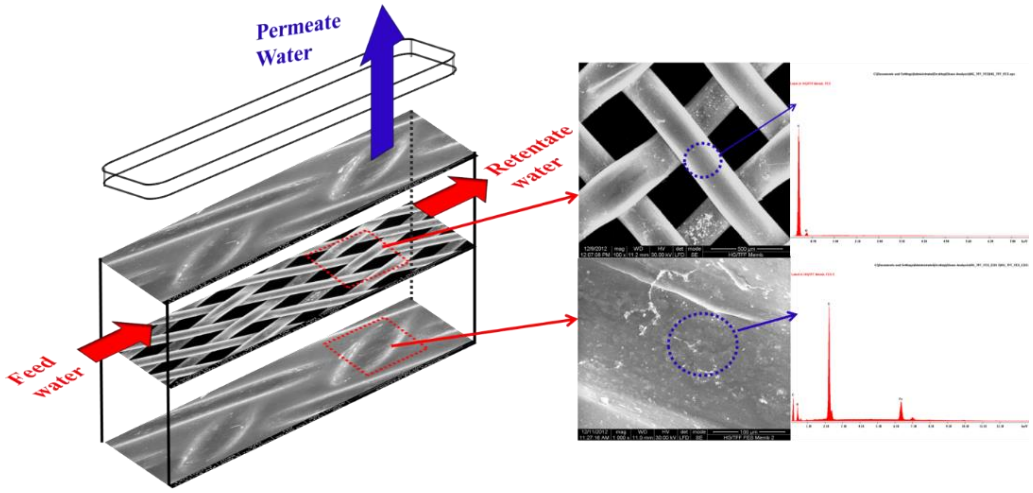

Figure 3.2: Graphic illustration of the feed, retentate, and permeate water flows through the polyethersulfone (PES) Pellicon XL cassette (MWCO=1000 kDa) in the CF/UF system. Reprinted with permission from the publisher, Nova Science Publishers, Inc. (*59*).

3.2. Synthesis of nanoparticulate FeS

Optimizing the aging time to synthesize nanoparticulate FeS would result in a more economical process especially during scale-up. Following procedures reported by Hayes et al. (*137*), the synthesis of nanoparticulate FeS is conducted in an anaerobic chamber, filled with 95% N_2, using $Na_2S{\cdot}9H_2O$ and $FeCl_2{\cdot}4H_2O$ followed by three days aging. The procedure to prepare 2 g/L FeS (amorphous mackinawite) at pH 8 involved the preparation of DDW in which 1 L of de-ionized water was purged with 99.99% N_2(g) for 2 hours and stored in the anaerobic chamber. 0.1M of $Na_2S.9H_2O$ and 0.1 M of $FeCl_2.4H_2O$ were placed in 500 mL bottles each using DDW and then mixed a final volume of 1 L polyethylene bottle followed by 3 days of aging (*27, 137*). In order to remove the excess sulfur element observed in the formed FeS suspension, the prepared 1L-FeS solution was transferred to 45mL centrifuge bottles, and was centrifuged for 10 minutes at the room temperature at 10,000 rpm (*48*). The water collected at the top of each centrifuge bottle was decanted and the solids were transferred into another bottle and washed with DDW. Then the centrifuge process was repeated more than three times to ensure the removal of any excess iron or sulfur compounds found in the solution. Next, in order to determine the amount of FeS produced, five pre-weighed vials were each filled with 1 mL of the washed FeS solution and then placed in the oven to dry. The weight difference for each vial was calculated and averaged, and the finally obtained value indicated the amount of nanoparticulate FeS present in 1 mL of the washed FeS solution ('x' g/L). From this stock solution of nanoparticulate FeS, 1 g/L of FeS is obtained by dilution with DDW and the solution was adjusted to pH 8 using NaOH (1, 0.1 and 0.01 M) or HCl (1, 0.1 and 0.01M) solutions. Except for centrifugation and freeze-drying, the procedures were conducted in an anaerobic chamber filled with 99.99% N_2 gas.

3.3. Batch experiments

Batch experiments were conducted to determine how fast Hg(II) was removed from water using nanoparticulate FeS. These tests were conducted in an anaerobic chamber filled with 99.9% N_2 to ensure anaerobic condition. All the reaction containers, experimental equipment, reagents and pH meter were equilibrated in the anaerobic chamber for one day prior to conducting the experiments. All solutions used for batch tests were prepared using DDW in which 1 L of deionized water was purged with N_2 for two hours. The pH of all the solutions was set to 8.0 ± 0.2 using 0.01M, 0.1M and 1 M concentrations of deoxygenized NaOH or HCl (purged with N_2(g) for 1 hour). The pH of the solutions before and after the experiments were monitored and recorded.

Initially, a standard stock solution of approximately 2 mM (400 mg/L)-Hg was prepared using $HgCl_2$ to avoid the development of HgO(s). To study the mercury removal capacity of 1 g/L-FeS with 5 μM of Hg, five 25 mL reaction vessels containing 10 mL of 0.05 g/L-FeS and 10 mL of 5 μM-Hg(II) were placed on a reciprocal rotator to allow reaction between the two solutions which were adjusted to pH 8. Samples were taken at different sampling times after the start of the reaction: 10 minutes, 30 minutes, 1 hour, 2 hours, and 3 hours. The sampling procedure includes immediate filtration of the solution in the reaction vessel using 0.02 μm Whatman Anodisc membrane filters, followed by the storage of filtrates collected in 25 mL bottles in the anaerobic chamber. This was done to prevent changes in the Hg (II) oxidation state and pH changes before being analyzed for Hg (II) using cold vapor AAS spectroscopic analysis (CV-AAS).

The same procedure was applied with conditions containing anions and humic acid with the final reaction volume set to 20 mL, solutions adjusted to pH 8, and sampling times were 10, 30, 60, 120 and 180 minutes, respectively, after the start of the reaction. Batch adsorption experiments were conducted to investigate the mercury removal capacity of FeS at 1 μM (0.1 g/L) and 11 μM

(1 g/L) with the initial concentrations of Hg (II) set at 5 µM (1 mg/L) and 50µM (10 mg/L). Additionally, the effect of 0.1M anions (Cl^-, SO_4^{2-}, and NO_3^-) on mercury removal was investigated. Furthermore, the effect of the presence of humic acid (HA) was studied by adding concentrations of 0.1 and 1.0 mg/L of HA. A control test was done with 5 µmol Hg and different concentrations of HA (0.5, 1, 5, 10 mg/L) without FeS. NaOH solution was used to increase the pH of DDW to around 11 in order to dissolve HA without any pre-treatment. Consequently, the final HA solution was adjusted to pH 8.

Once the filtrates were collected in 25 mL bottles, the filter discs with the trapped nanoparticulate Hg-FeS complex was placed in 30 mL of 0.1 M $Na_2S_2O_3$ solution for 24 hours prior to CV-AAS Hg(II) analysis. This part of the batch experiment is described as desorption which was used to examine the stability of the Hg-contacted FeS. Behra et al. (*138*) conducted desorption experiments of Hg(II) to approximate the release of Hg(II) after the adsorption test of Hg(II) contaminated water with pyrite (*138*). The desorption experiment involved the use of 0.1 M of inorganic ligands such as NH_3 and NO_3^-as weak ligands, EDTA, SO_3^{2-}, I^-, CN^- and $S_2O_3^{2-}$ at acidic and basic pH. At pH 7.1, Behra et al. (*138*) reported a strong desorption capacity of $S_2O_3^{2-}$ (89%). Since this study was conducted at pH 8, thiosulfate ($S_2O_3^{2-}$) that had a strong desorption capacity near neutral pH was chosen as inorganic ligand for desorption experiment (*138*).

3.4. Dead-end ultrafiltration (DE/UF) system-based experiments

Experiments were conducted using a low-pressure dead-end ultrafiltration device under 1 bar N_2 to evaluate the continuous removal of Hg(II). This could be operated in non-stirred and stirred mode. Figure 3.3 shows the workflow of the experiments and the DE/UF system consisting of a reservoir which are fed with FeS-Hg mixture, followed by 0.1M thiosulfate solution, and then additional 5 µmol Hg(II) solutions into the ultrafiltration reactor with a 30 kDa RC membrane.

The gas and water flows are controlled by an adapter box which is connected to the N_2 cylinder and the permeate water is collected at the end of the UF reactor for analysis. For each condition, the adsorption and desorption experiments were conducted in 3 stages. The first stage involved allowing the components to react for 30 min in the reservoir container. In the second stage, the solution was transferred to the glass cell containing the 30 kDa membrane to filter out the Hg(II)-contacted FeS from the solution, simulating a dead-end ultrafiltration system in non-stirred mode. To test the stability of Hg(II) on FeS, the remaining Hg(II)-contacted FeS on the membrane is exposed to 0.1 M of $Na_2S_2O_3$ in the third stage (desorption). These three stages were conducted in series.

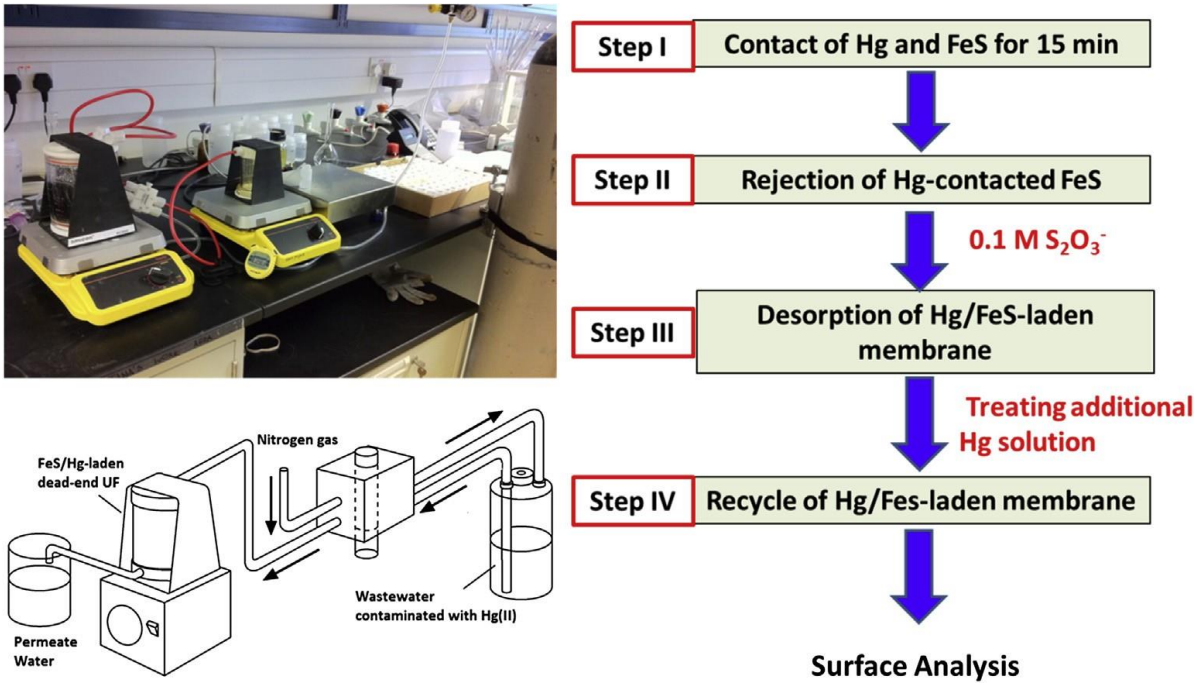

Figure 3.3: Schematic representation of FeS-supported dead-end ultrafiltration system for removal of Hg(II) (modified from (Millipore, 2004)) and flowchart of experimental procedures. Reprinted with permission from the publisher, Elsevier (*48*).

To study the additional sorption capacity of the Hg(II)-contacted FeS for the four conditions, the three stages mentioned were conducted in series and a fourth stage was included. The Hg(II)-contacted FeS retained on the UF membrane was exposed to extra volumes of 5 µmol Hg, set to pH 8 and deoxygenated by purging with N_2 (99.99%) for 30 minutes. The permeate water, produced from the second to the fourth stage of the experiments, were collected over a specific time period to obtain the flux. Then the pH measurements along with Hg analyses and Fe analyses were made. The results of these experiments were represented as normalized flux (J/J_o), Hg(II) concentration (C/C_o), pH, and Fe concentration (µg/L) in permeate water as a function of time. At the end of each experiment, the membrane was washed with DDW, and stored in the anaerobic chamber for SEM analyses. Equation 3.1 shown below was used to calculate the flux (J):

$$J = J_0(1 + kt)^{-n} \tag{3.1}$$

Where J_0 is the initial flux and J is the flux at a given time, t, with k as the empirical rate constant, and n is a coefficient that describes the fouling mechanism. There are four different n values to indicate cake formation (0.5), internal pore constriction (1.0), partial pore blocking (1.5) and complete pore blocking (2.0) (*44*).

The following procedure is an example of the experiments carried out which involves the reaction of 250 mL of 10 µM (2 ppm) Hg and 250 mL of 2g/L (22 mM) FeS set to pH 8, using 30 kDa membrane in non-stirred mode and pressure maintained at 1 bar.

Approximate forty-five vials (for absorption and desorption tests) and three 500 mL bottles (for maximum sorption recycle) were pre-weighed prior to starting the experiment. Then, the following solutions were prepared, set to pH 8, and deoxygenated by purging with N_2 (99.99%): (i) 22 µM-FeS (250 mL) and 10 µM-Hg (250 mL), which were diluted to 11 µM-FeS and 5 µM-

Hg in a final volume of 500 mL, (ii) 0.1M-$Na_2S_2O_3$ (500 mL), (iii) Two 500 mL 5 µM-Hg solutions.

The virgin membrane was washed three times with 500 mL of DDW and the initial flux of the virgin membrane was obtained prior to starting the first stage of the experiment. Then, the first stage was initiated by adding the two solutions of FeS and Hg into the reservoir container and allowed to react for 30 min. A pressure control plug was used to purge the reservoir container with N_2 to maintain anoxic conditions. Subsequently, the reacted solution was transferred to the glass cell using 1 bar of N_2 to start the second stage of the experiment and the permeate water is collected. Then, the desorption test was conducted by filling the reservoir vessel with 500 mL volume of 0.1M $Na_2S_2O_3$and then transferred to the ultrafiltration glass cell. The initial flux was measured prior to collecting the permeate water at recorded times.

Finally, the fourth stage included testing the additional sorption capacity of FeS with the reservoir vessel filled with two-500 mL volumes of 5 µM (1 ppm) Hg solutions, which was then transferred to the ultrafiltration glass container to allow contact with the retained Hg(II)-contacted FeS. The permeate water was collected at fixed times. A sample table used for the data collection of the continuous contact system experiments is shown in Table 3.1. Finally, at the end of each experiment, the membrane was washed with 500 mL of DDW, and stored in the anaerobic chamber for SEM and EDS analyses. The surface analyses of the solids retained in the membrane were used for determining surface morphology, element quantification, and analysis of the cake-layer formed on the surface of the membrane.

Table 3.1: Example of table to record data for the DE/UF experiments.

Weight Difference (g)	Flux (L/m2.hr)	Normalized Flux (F/F0)	Time (min)	Time, (cumulative)	pH	Abs (CV-AA)	Fe (ICP)
25.74	486.95	1	1	1			
23.19	478.73	0.983	0.916	1.9166			

3.5. Cross-Flow Ultrafiltration (CF/UF) system-based experiments

The setup for the cross-flow ultrafiltration system is shown in Figure 3.4. Feed solutions from the water reservoir are transferred to the CF/UF membrane via a peristaltic pump and the same workflow procedure was applied as the DE/UF experiments. All feed solutions (FeS and Hg, Sodium Thiosulfate, and additional Hg) were purged with N_2 gas to ensure anoxic conditions which avoid oxidation of FeS. The CF/UF system experiments were conducted in four steps: (i) 15-minute contact between Hg(II) and FeS in the feed water reservoir with or without the presence of 0.1 M anions/1 mg/L HA, (ii) transferring of Hg(II)-contacted FeS solution to the CF/UF system, (iii) 0.1 M thiosulfate solution fed from the feed reservoir to the CF/UF system to measure the extent of Hg release from the solids retained in the UF membrane, (iv) investigating the additional sorption capacity of retained solids in the membrane by feeding 5 μmol Hg(II) solution into the reservoir. The CF/UF system was functioned in retentate mode to circulate the Hg-loaded particles.

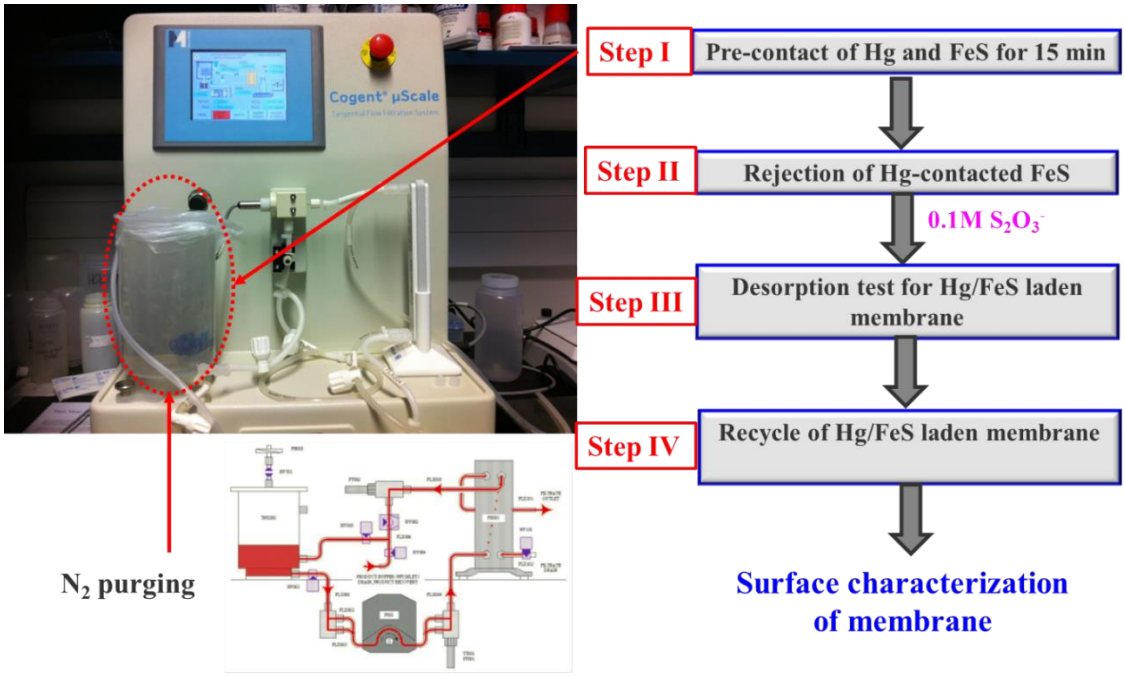

Figure 3.4: Schematic representation of FeS-supported crossflow ultrafiltration membrane system for removal of Hg(II) and flowchart of experimental procedures. Reprinted with permission from the publisher, Nova Science Publishers, Inc. (*59*).

The permeate water, obtained from each step, was collected over time to measure the flux, Hg and Fe concentrations, and pH. Equation 3.2 shows the calculation of the instantaneous permeate flux (J) over the initial (t_1) and final time (t_2) intervals where A if the membrane area (m^2) and V is the permeate volume (L) collected.

$$J = \frac{(V_2 - V_1)}{A(t_2 - t_1)} \tag{3.2}$$

3.6. Analyses of aqueous phase and solid phase samples

3.6.1. CV-AAS

The cold vapor atomic absorbance spectrometry (CV-AAS) was implemented to measure the concentration of mercury. The reagents used for CV-AAS (Varian, AA240FS) analyses are: 5 M HCl, 0.05% NaOH and 1% $NaBH_4$. Standard solutions of mercury (5, 10, 30, and 60 µg/L) were prepared from Inorganic Ventures mercury standard in nitric acid. The settings included a lamp current of 4.0 mA, 253.7 nm wavelength, slit width of 0.5 nm, with background correction switched on, carrier gas flow of 240 mL/min, 4 measurements with 4 s of measurement time, 60 s stabilization time and 60 s baseline delay time. For the Hg measurement, the average method detection limit (MDL) was 7.7 µg/L, the average recovery (accuracy) was 101.9% and the relative standard deviation (precision) was 2.6%.

3.6.2. ICP/OES

The Thermo Fisher Scientific iCAP 6000 series ICP-OES (Inductively Coupled Plasma – Optical Emission Spectrometry) equipment mode was set to identify the Fe element and the analyses were conducted using Fe standard solutions (50, 250, 500, 1000 µg/L) prepared from Inorganic Ventures iron standard in nitric acid. The average method detection limit (MDL) was 11.3 µg/L, the average recovery (accuracy) was 98.8% and the relative standard deviation (precision) was 2.85%.

3.6.3. SEM/EDS

The scanning electron microscopy (SEM) equipped with energy dispersive X-ray spectrometer (EDS) analysis was implemented to characterize the chemical composition and surface morphology of the Hg (II)-contacted FeS retained on the membrane before and after the experiments were conducted. The SEM images of the UF membrane obtained from the third

condition (11 mM FeS, 5 µM Hg, and 1 mg/L HA) were collected at a working distance of 9.8 mm under a magnification 93x and acceleration voltage of 10.0 kV for the cross-section image. The top section SEM images were collected at a working distance of 8.8 mm under a magnification 115x and acceleration voltage of 10.0 kV. The cross-section SEM image for the UF membrane collected from the experiment with 11 mM-FeS and 5 µM-Hg were collected at a working distance of 40.8 mm under a magnification 150x and acceleration voltage of 10.0 kV.

3.6.4. ATR/FTIR

The ATR-FTIR (attenuated total reflectance-Fourier transform infrared) spectroscopy was conducted on the CF/UF 1000 kDa PES membrane to determine its permeation performance before and after washing with DDW and conducting the experiments. ATR-FTIR is suited to analyze the membrane surface since the IR beam penetration depth into the sample can vary between 0.5-10 µm by adjusting the incidence angle (*139*). The ATR-FTIR spectra was recorded using the Perkin Elmer FTIR spectrophotometer model spectrum one within the range of 4000 – 450 cm^{-1} at 25^0C with a nominal incident angel of 45^0 using ZnSe crystal (25 mm x 5 mm x 2 mm) (*140-141*).

4. RESULTS*

This section presents the results of the batch tests involving Hg(II) removal from water using FeS nanoparticles in the absence and presence of anions and humic acid. Additionally, the outcomes of Hg(II) removal using FeS and dead-end ultrafiltration in non-stirred mode and stirred mode systems are discussed with the effects of the absence and presence of anions and humic acid as well as the molecular weight cut-off of the ultrafiltration membrane. Furthermore, the evaluation of Hg(II) removal using FeS and cross-flow ultrafiltration system in the absence and presence of anions are revealed in this chapter.

4.1. Hg(II) removal with FeS nanoparticles

Figure 4.1 shows the Hg(II) removed (%) and the total Fe released (μmol) in the permeate water as a function of time for experiments conducted with a 0.05 g/L of FeS and initial concentrations of Hg(II) (500, 1000, 1250 μmol). These represent Hg(II) removal results for $[Hg]_0/[FeS]_0$ molar ratios of 0.9, 1.8, and 2.2, respectively.

*Reprinted from Water Research, Vol 53, Han, D.S.; Orillano, M; Khodary, A.; Duan, Y.; Batchelor, B.; Abdel-Wahab, A.; "Reactive iron sulfide (FeS)-supported ultrafiltration for removal of mercury (Hg(II)) from water", 310-321, Copyright 2014, with permission from Elsevier and "Effects of anions on removal of mercury(II) using FeS-supported crossflow ultrafiltration" by Han, D. S.; Orillano, M.; Duan, Y.; Batchelor, B.; Park, H.; Abdel-Wahab, A.; Nidal, H..; 2017. *Nova Science Publishers, Inc.*, 129-152, Copyright 2017 by Nova Science Publishers, Inc.

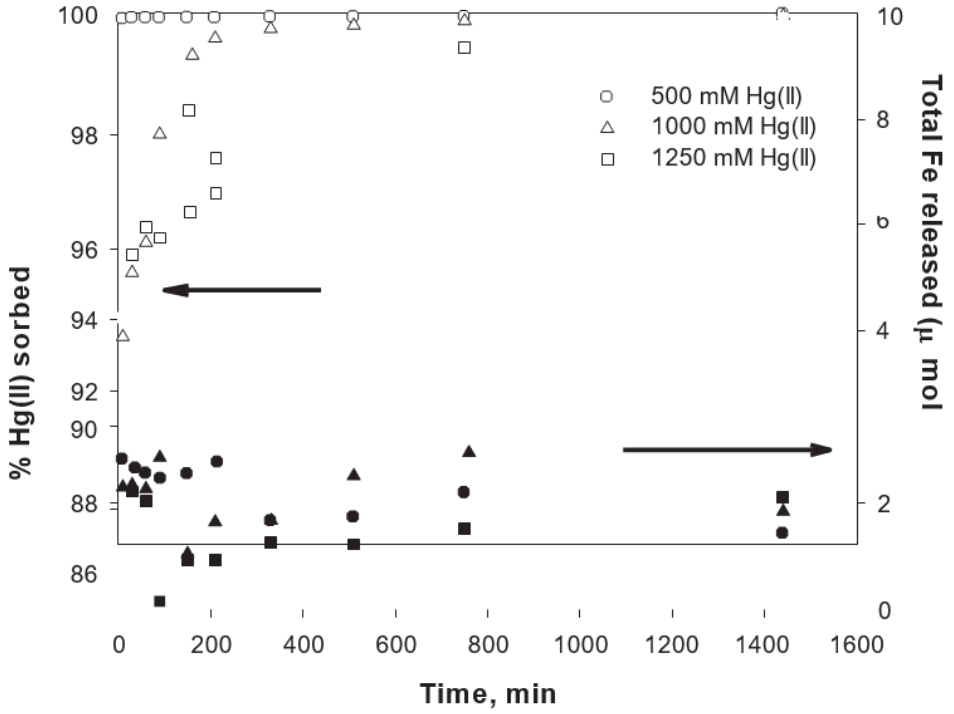

Figure 4.1: Percentage removal of Hg(II) and concentration of total Fe released as a function of time at pH 8 for three initial Hg(II) concentrations. Reprinted with permission from the publisher, Elsevier (*48*)

The results exhibit two types of behaviors for the different $[Hg]_0/[FeS]_0$ molar ratios: fast and complete removal within 10 minutes for 0.9 $[Hg]_0/[FeS]_0$ ratio and slow and gradual removal for a molar ratio of 2.2. This proves that even a small amount of FeS is efficient at removing Hg(II) from water. Such behavior could be attributed to chemical interactions between FeS surface and Hg that are slower than the initial transport of Hg(II) to the surface (*23, 39, 48, 142*). Furthermore, the concentration of total Fe in the permeate water was around 3 µmol (0.5% of the total Fe added as FeS, initially 568 µmol). This indicates that the formation of HgS and Fe(II) contributes to a small proportion of what occurs when Hg(II) is contacted with FeS for a molar ratio between 0.9 – 2.2 ($[Hg]_0/[FeS]_0$). Possible surface reactions between Hg(II) and FeS could result in the formation of surface precipitates (Eq. 4.1), discrete precipitates (Eq. 4.2) for higher molar ratios,

or surface complexes (Eq. 4.3) which are evident with molar ratios of Hg(II) to FeS below 1 or Hg(II) sorbs onto partially oxidized FeS (*23, 39, 48, 142*). However, Skyllberg and Drott (2010) reported formation of precipitates rather than surface complex formation between Hg(II) and FeS for molar ratios ($[Hg]_0/[FeS]_0$) between 0.002 to 0.012 (*39*). Different results could be attributed to the synthesis of FeS, concentration of ions implemented in the experiments, and different molar ratios of $[Hg]_0/[FeS]_0$. Thus, further studies have to be developed to conclude the formation of precipitates at specific conditions. In Eq. 4.3, $\equiv FeS_{(s)}$ signifies the charged FeS hydrolyzed over pH leading to surface charge and Hg(II) includes various types of divalent mercury complexed with other anions, if present.

$$FeS_{(s)} + xHg(II) \rightarrow \left[Fe_{(1-x)}, Hg_{(x)}\right]S_{(s)} + xFe(II) \quad (4.1)$$

$$FeS_{(s)} + Hg(II) \rightarrow HgS_{(s)} + Fe(II) \quad (4.2)$$

$$\equiv FeS_{(s)} + Hg(II) \rightarrow \equiv FeS_{(s)} - Hg(II) \quad (4.3)$$

4.1.1. Effect of anions

The extent of Hg(II) immobilization for a molar ratio of $[Hg(II)]_0/[FeS]_0$ as 0.005 in the absence and presence of 0.1 M anions (Cl^-, NO_3^-, SO_4^{2-}) at pH 8 is displayed in Figure 4.2. Desorption experiments were conducted by exposing the Hg-contacted FeS to 0.1 M Sodium Thiosulfate ($Na_2S_2O_3$) for 24 hours to examine the stability of the Hg-contacted FeS. Thiosulfate solution was chosen based on the desorption studies conducted by Behra et al. (*138*) using Hg(II) contacted pyrite and investigated the performance of several ligands (e.g. Cl^-, NO_3^-, NH_3, $S_2O_3^{2-}$, I^- etc.) at different pH ranges (*138*). Results of Behra et al. (*138*) showed the effective Hg(II) desorption from Hg contacted pyrite by $S_2O_3^{2-}$ at pH 7.1. Results of the Hg(II) released during the

desorption experiments are displayed in Figure 4.3. For a molar ratio of $[Hg(II)]_0 / [FeS]_0 = 0.005$ at initial pH 8, within 10 min, 100% Hg(II) was immobilized in the presence of anions and an average of 0.5% of Hg(II) remained in the solution after the desorption experiments indicating stable Hg(II)-contacted FeS solids. In the absence of anions, a longer time was taken to completely immobilize Hg(II) from the solution. Nearly 60 minutes was required to improve the immobilization of Hg(II) from 99% to 100%.

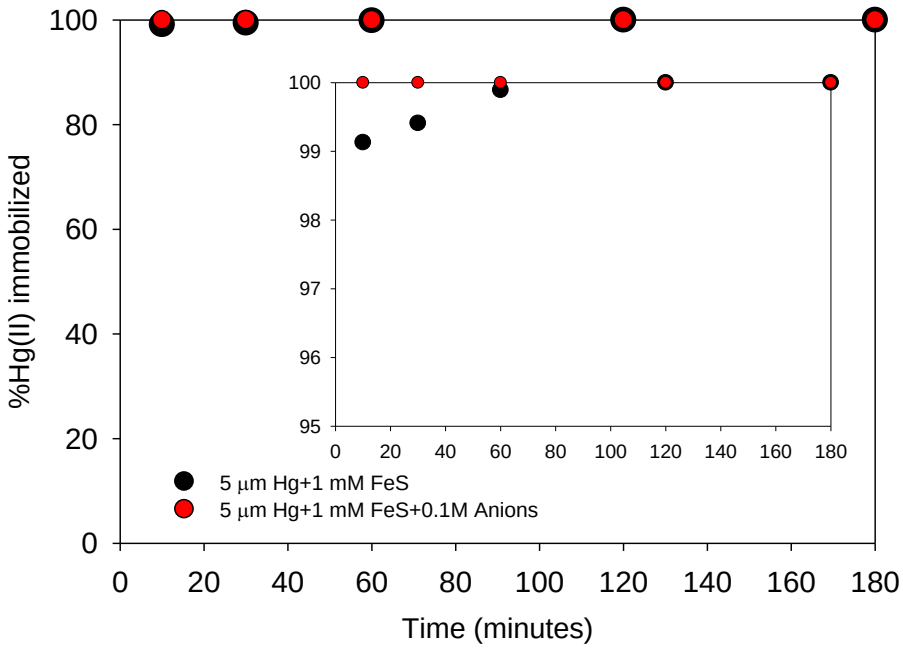

Figure 4.2: Hg(II) removal with FeS with and without the presence of 0.1 M anions at pH 8 for a molar ratio of [Hg(II)]0 /[FeS]0 = 0.005 as a function of time.

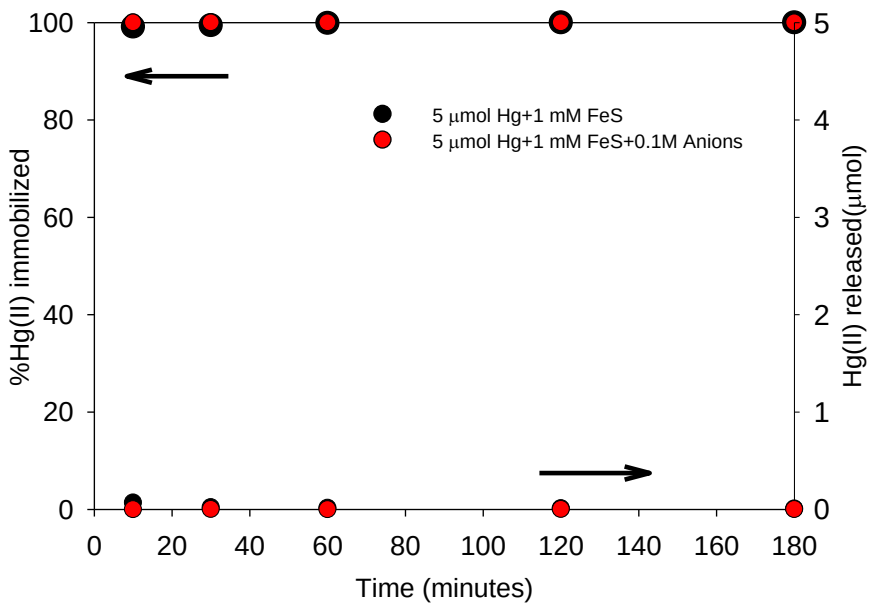

Figure 4.3:Percentage of Hg(II) immobilized and Hg(II) released as a function of time after a 24-hour exposure of Hg-contacted FeS to 0.1 M Thiosulfate solution at pH 8 for a molar ratio of $[Hg(II)]_0$ /$[FeS]_0$ = 0.005 with and without 0.1 M Anions.

These results show that the most probable sorption mechanism was the adsorption of Hg(II) on the available active sites of the FeS surface (*21-22, 40, 97*). Desorption experiments reveal that even in the presence of anions, negligible amounts of Fe(II) was released forming stable Hg(II)-contacted FeS. FeS has a highly reactive surface and its solubility and surface chemistry were reported by Wolthers et al. (*142*) .The dissolution of FeS in water can be described by Equation 4.4, where K_s^{app} is the apparent solubility constant at zero ionic strength which is calculated as shown in Equation 4.5. The speciation of sulfide species depends on solution pH as presented in Equation 4.6 (*142*).

$$FeS(s) + 2H^+ \leftrightarrow Fe^{2+} + H_2S\,(aq), K_s^{app} \tag{4.4}$$

$$K_s^{app} = \frac{\{Fe^{2+}\}\times\{H_2S\}}{\{H^+\}^2} = 10^{+4.87\pm0.27} \tag{4.5}$$

$$H_2S\ (aq) \leftrightarrow HS^- + H^+, K_1 = 10^{-6.98} \quad (4.6)$$

Furthermore, the results of the acid-base titrations conducted by Wolthers et al. (*142*) showed that the pH value of the point of zero charge of FeS (pH_{pzc}) is approximately 7.5 (*142*). Therefore, at pH 8 (> 7.5) the FeS surface becomes negatively charged and attracts Hg(II) cations. The possible reactions for the uptake of Hg(II) by FeS were presented by Jeong et al. (*21*), Skyllberg and Drott (*39*), and Gong et al. (*40*) as shown in Equations 4.7-4.12 (*21*, *39-40*):

Substitution or surface/Ion exchange:

$$FeS(s) + xHg(II) \Leftrightarrow [Fe_{1-x}, Hg_x]S(s) + xFe(II) \quad (4.7)$$

Chemical precipitation following dissolution of FeS:

$$\mathrm{FeS(s)} + \mathrm{Hg(II)} \Leftrightarrow HgS(s) + Fe(II) \quad (4.8)$$

Chemical precipitation following partial dissolution of FeS:

$$FeS(s) + H^+ \Leftrightarrow Fe(II) + HS^- \quad (4.9)$$

$$Hg(II) + HS^- \Leftrightarrow HgS(s) + H^+ \quad (4.10)$$

$$FeS(s) + Hg(II) \Leftrightarrow Fe(II) + HgS(s) \quad (4.11)$$

Surface complexation:

$$\equiv FeS + Hg(II) \Leftrightarrow \equiv FeS - Hg(II) \quad (4.12)$$

With an average of 0.5% Hg(II) released, surface complexation is more likely to have occurred. Skyllberg and Drott (*39*) confirmed that for low molar ratios of Hg(II) to FeS of less than 0.05, adsorption is the main Hg(II) removal mechanism (*39*).

Sun et al. (*24*) also reported enhance Hg(II) removal in the presence of Chloride (0-10 mM) with a molar ratio of $[Hg(II)]_0$ /$[FeS]_0$ as 0.005. The increase in ionic strength in the aqueous

solution could cause oxidation, dissolution, and other variations in the FeS surface can result in additional porous structures which provide more active sites for Hg(II) sorption (*97*). Since FeS is very reactive with oxygen, FeOOH is formed via FeS oxidation in water as shown in equation 4.13 (*22*).

$$FeS + H_2O + O_2 \leftrightarrow FeOOH + S^0 \quad (4.13)$$

Another oxidation product of FeS is $Fe(OH)_3$ as shown in equation 4.14 (*21*).

$$FeS + 3H_2O \leftrightarrow Fe(OH)_3 + S(0) + 3H^+ + 3e^- \quad (4.14)$$

Hence, FeS oxidation could produce FeOOH and $Fe(OH)_3$ and act as extra Hg(II) adsorbents (*21-22, 97*).

Hg(II) removal with FeS in the absence and presence of anions with a molar ratio of $[Hg(II)]_0 / [FeS]_0 = 0.05$ as a function of time is shown in Figure 4.4 and results of Hg(II) released after conducting the desorption experiments are included in Figure 4.5. The Hg(II) sorption rate remains the same in the absence of anions even at a relatively higher $[Hg]_0$ concentration with 100% Hg(II) immobilization within 10 minutes. However, the effect of 0.1 M anions becomes evident when the molar ratio of $[Hg(II)]_0 / [FeS]_0$ is increased from 0.005 to 0.05. Nearly 95% of Hg(II) is immobilized from 10-60 minutes, then increasing to 99% after 2 hours. A decrease in Hg(II) immobilization to 97% is observed after 3 hours. For conditions with excess FeS surface sites with only Hg(II) in the aqueous solution, complexation of Hg(II) with the reactive sites explain the decrease in dissolved Hg(II). However, the presence of anions at 0.05 molar ratio of $[Hg(II)]_0 / [FeS]_0$ introduces competition with [Hg(II)] to react with the FeS active sites. It has been reported in previous studies that Chloride significantly hinders Hg(II) adsorption by FeS (*21, 24, 40, 97*). Hence, in addition to saturation of FeS active sites with Hg(II) and anions, excess Hg(II) can form $HgCl_x^{2-x}$ (x= 1.2.3.4) with chloride which have a lower affinity to FeS compared to Hg-

OH complexes. Furthermore, following the dissolution of FeS, HgS(s) precipitation is more likely to occur. For conditions with higher $[Hg]_0$ at basic conditions, Jeong et al. (*143*) reported that a sudden increase in dissolved Hg(II) may be due to released Fe(II) precipitates coating the FeS particles which causes structural variations that prevent HgS(s) formation. This could explain the increase in dissolved Hg(II) after three hours in the presence of anions. Figure 4.5 shows that no Hg(II) release was observed during the desorption experiments indicating stable Hg-contacted FeS.

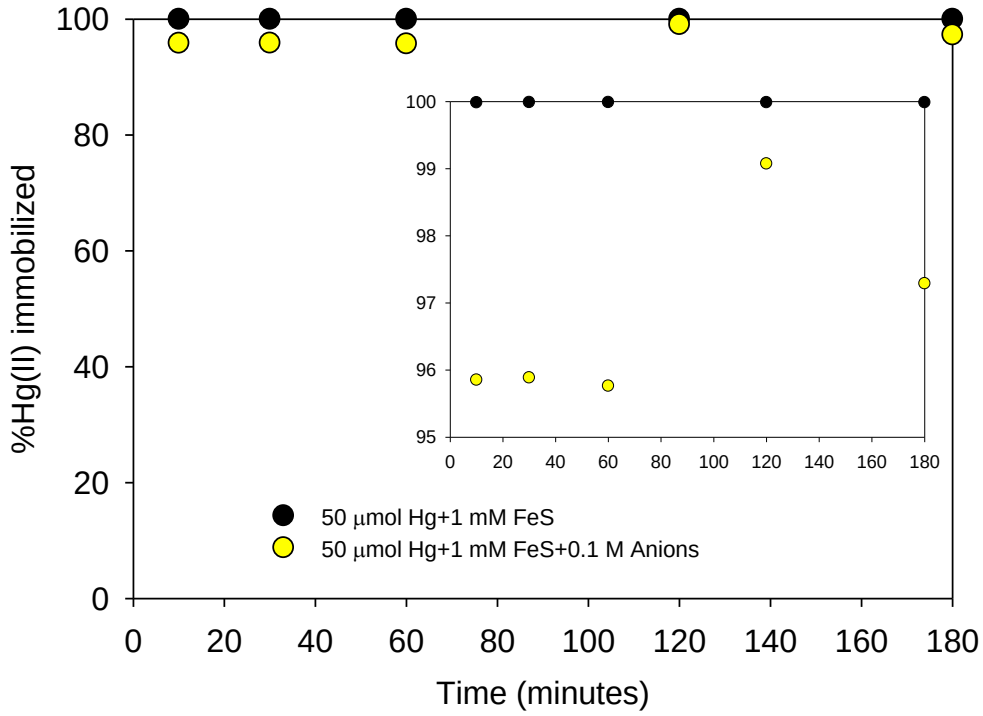

Figure 4.4: Hg(II) removal with FeS with and without the presence of 0.1 M anions at pH 8 for a molar ratio of $[Hg(II)]_0$ /$[FeS]_0$ = 0.05 as a function of time.

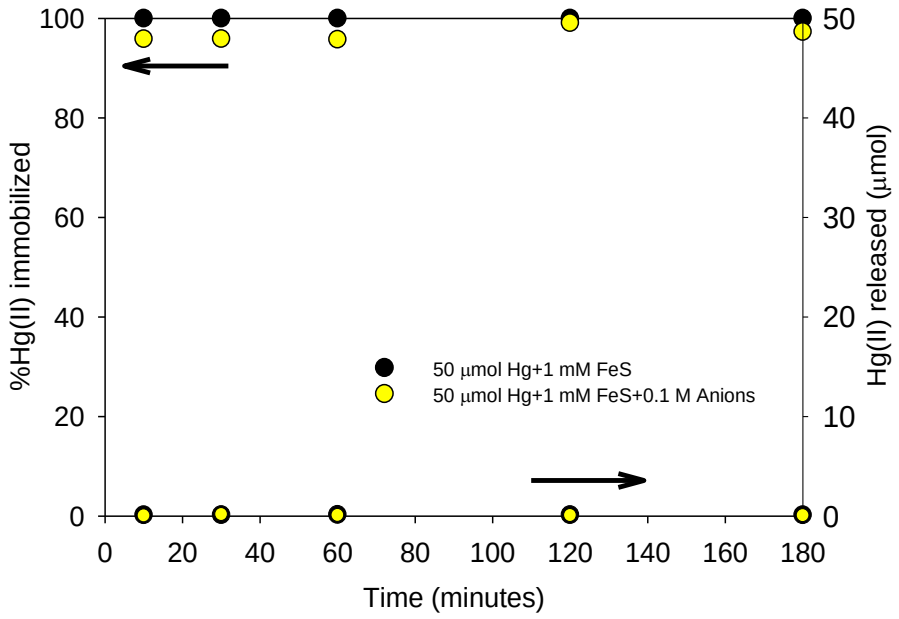

Figure 4.5: Percentage of Hg(II) immobilized and Hg(II) released as a function of time after a 24-hour exposure of Hg-contacted FeS to 0.1M Thiosulfate solution at pH 8 for a molar ratio of $[Hg(II)]_0 / [FeS]_0 = 0.05$ with and without 0.1 M Anions after desorption tests.

Gong et al. (*40*) studied the effect of Chloride ions on the sorption of Hg(II) with Carboxymethyl Cellulose (CMC) stabilized FeS. The reported effect of chloride concentration below 106 mg/L, typically present in natural fresh waters, was insignificant. Between 106 to 1775 mg/L, the adsorption capacity of CMC stabilized FeS was lowered by 14% due to the presence of Hg-Cl complexes. Beyond 1775 mg/L, Cl^- had negligible effect on Hg(II) sorption. Since the chloride concentration added in the batch experiments were 35 mg/L (0.001 M Anions), 354 mg/L (0.01 M anions), 3545 mg/L (0.1 M anions); the presence of $HgOHCl^-$ is predominant when 0.001 M anions was used, and the mercury species $HgCl_2$, $HgCl_3^-$, and $HgCl_4^{2-}$ were present when 0.01 M and 0.1 M of anions were added resulting in decreased Hg(II) uptake. The complexation between Hg(II) and Cl^- is described as follows with stability constants ranging from $10^{2\text{-}7.15}$ (*144*):

$$Hg^{2+} + Cl^- \Leftrightarrow HgCl^+ \qquad logK_1 = 7.15 \tag{4.15}$$

$$HgCl^+ + Cl^- \Leftrightarrow HgCl_2 \qquad logK_2 = 6.9 \tag{4.16}$$

$$HgCl_2^0 + Cl^- \Leftrightarrow HgCl_3^- \qquad logK_3 = 2.0 \tag{4.17}$$

$$HgCl_3^- + Cl^- \Leftrightarrow HgCl_4^{2-} \qquad logK_4 = 0.7 \tag{4.18}$$

In summary, the presence of anions such as NO_3^- (week inorganic ligand), SO_4^{2-}, and Cl^- (comparatively strong ligands) could affect Hg(II) sorption by FeS in various ways. Reduced cation (Hg(II)) sorption may occur due to ternary anion-cation-surface complex formation (*145-146*), or surface precipitation due to the competition between cation and anion for surface sites (*146-147*). Conversely, cation sorption may be enhanced in the presence of anions through electrostatic interaction (*146*, *148*).

4.1.2. Effect of Humic Acid

The influence of humic acid on Hg(II) sorption onto FeS was investigated using two different concentrations of HA (0.1 and 1 mg/L). First, control tests were conducted using 5 µM Hg with different concentrations of HA (0.5,1,5, and 10 mg/L) in the absence of FeS. Figure 4.6 shows that the presence of HA can result in 72% reduction of dissolved Hg(II) for concentrations ranging from 0.5 – 10 mg/L within 10 minutes from the start of the reaction time. However, presence of HA alone cannot completely immobilize Hg(II). HA could play a role in forming strong Hg(II)-HA complexes at low Hg(II)/HA ratios due to the strong binding of Hg-thiol bonds (*149*). Nascimento and Masini (*150*) studied the effect of HA on Hg(II) removal and demonstrated that HA was capable of removing 86% of Hg(II) from an initial concentration of 10 µM with 25 mg/L HA at pH 6. Results showed that HA had a high adsorption capacity for Hg(II) (537 ± 30 µmol/g for 25 mg/L HA) due to the strong affinity of Hg(II) to the amine, carboxylic, and phenolic groups of HA. Ravichandran (*151*) and Skyllberg (*152*) have reported possible Hg(II)-DOM

complex formations as shown below, with stability constants $10^{31.6\text{-}32.2}$ (*153*), $10^{28.5}$ (*154*), $10^{25.8\text{-}27.2}$ (*155*), and $10^{43.3\text{-}47.7}$ (*39, 151*), (*39*).

$$Hg^{2+} + RS^{-} \leftrightarrow HgRS^{+} \tag{4.19}$$

$$Hg^{2+} + 2RS^{-} = Hg(RS)_2 \tag{4.20}$$

Hg(II)-DOM complexation can involve Hg(II) bound to one or two monodentate bonded thiol group (RS^{-}) , carboxylic or phenolic acid sites, or bidentate aromatic and aliphatic thiol groups (*39, 151*). Additionally, humic acid could also enhance the photocatalytic reduction of Hg(II) to Hg(0) and subsequent re-oxidation of elemental mercury (*151*).

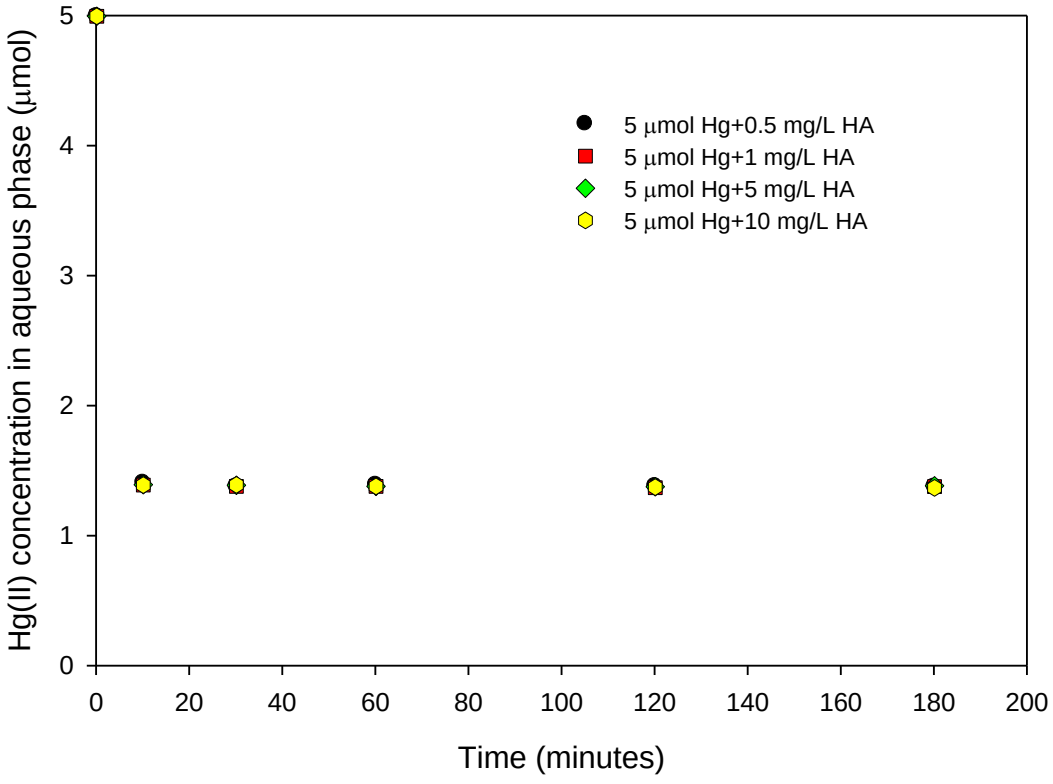

Figure 4.6: Hg(II) concentration in the aqueous phase a function of time in the presence of humic acid at different concentrations: 0.5, 1, 5, and 10 mg/L HA at pH 8.

Figure 4.7 shows the Hg(II) concentration in the aqueous solution over time in the presence of humic acid and FeS (molar ratio Hg/FeS = 0.0005) at pH 8. A combined effect of HA and FeS complexation reduced the initial concentration of Hg(II) by 85% within 10 minutes. With HA (0.1 and 1 mg/L) and 11 mM FeS, nearly 100% of Hg(II) was immobilized within one hour. The synergistic effect of Hg-HA complexation, conversion of Hg(II) to other forms of mercury, Hg-FeS complexation, and availability of FeS active sites could contribute to the reduction of dissolved Hg(II). Hence, surface complexation and cation bridging mechanisms contributed to increased adsorption of Hg(II) in the presence of HA(*150*). However, this could only be possible at low molar ratios of $[Hg]_0/[FeS]_0$ = 0.0005 when comparatively less Hg(II) is available for competition with HA and anions for FeS active sites.

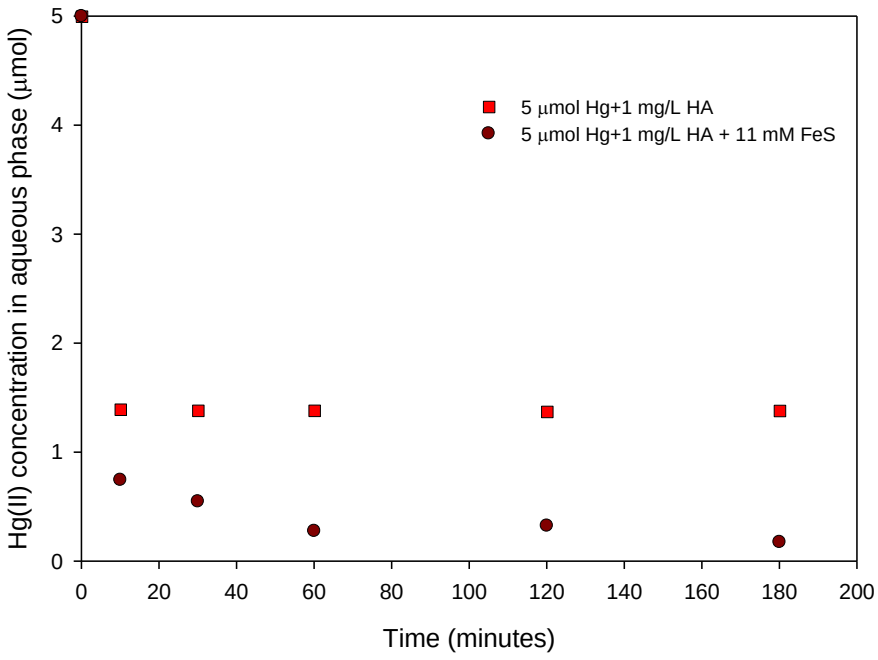

Figure 4.7:Hg(II) concentration in the aqueous phase a function of time in the presence of humic acid (1 mg/L) and 11 mM of FeS ($[Hg(II)]_0$ /$[FeS]_0$ = 0.0005) at pH 8.

On the contrary, recent studies reported by Sun et al. (*24*) reported the inhibitive effects of HA (0-20 mg/L) on the mercury adsorption of Al_2O_3-supported nanoscale FeS with a molar ratio $[Hg]_0/[FeS]_0 = 0.002$ with an initial Hg(II) concentration of 5 µmol (*24*). Hg(II) could form stable complexes with the phenolic hydroxyl groups of HA which hinder adsorption by FeS. Additionally, competition between HA and Hg(II) for active sites would occur. The mercury removal efficiency of FeS/Al_2O_3 was reduced by 20% in presence of 5 mg/L HA and 60% with 15 mg/L HA. Similarly, Gong et al. (*40*) investigated the effects of HA and DOM (1-20 mg/L) with carboxymethyl cellulose stabilized FeS (CMC-FeS) for a molar ratio of $[Hg]_0/[CMC\text{-}FeS]_0 = 1.4$. With 5.5 mg/L HA, 12% reduction in mercury removal efficiency was reported. No further reduction was observed when the concentration of HA was increased from 5.5 to 28 mg/L (*40*).

Overall, the batch experiments reveal that Hg(II) removal by FeS exhibits rapid initial removal by adsorption followed by slow surface reactions. Complete Hg(II) removal with FeS was achieved within 10 minutes in the presence of anions and 60 minutes in the presence of humic acid (HA). Desorption experiments affirm the Hg(II)-contacted FeS nanoparticles, in the presence and absence of anions and HA, were chemical stable despite a 24-hour exposure to 0.1 M sodium thiosulfate with no Hg(II) and negligible Fe released in the aqueous phase.

4.2. Removal of Hg(II) using FeS-enhanced Dead-End Ultrafiltration (DE/UF) system

Experiments were conducted using a low-pressure dead-end ultrafiltration device under 1 bar N_2 to evaluate the continuous removal of Hg(II) from water. The workflow of the experiments for the DE/UF system consist of a reservoir which is fed with FeS-Hg mixture, followed by 0.1M thiosulfate solution, and then additional Hg(II) solutions into the ultrafiltration reactor with a 30 kDa Regenerated Cellulose (RC) membrane. The gas and water flows are controlled by an adapter box which is connected to the N_2 cylinder and the permeate water is collected at the end of the UF

reactor for analyses. Based on the batch tests, 0.05 g/L FeS (568 µmol Fe) has shown to efficiently remove Hg(II) with initial concentrations from 500 – 1250 µmol. Then, experiments were conducted to evaluate the dead-end ultrafiltration system on the removal of Hg(II) using FeS with a molar ratio $[Hg]_0/[FeS]_0$ of 0.0004. An initial concentration of 5 µmol Hg was used to simulate the water environment from the industrial/mining sectors(*48*)). Then, 1 g/L FeS (11 mM Fe) was applied to fully cover the area of the UF membrane and allow further evaluation for additional removal of Hg(II) of the Hg(II)-contacted FeS particles on the membrane. A high capacity of additional Hg(II) removal is expected as more reactive sites are available from the initial 0.0004 $[Hg(II)]_0/[FeS]_0$ loading. Two modes of operations were applied, the non-stirred and the stirred mode, which can produce a shear effect at the membrane surface to reduce fouling. The DE/UF system in stirred mode is similar to the cross-flow membrane operation.

4.2.1. Stirred mode – DE/UF system

Figure 4.8 shows the results of the normalized flux and permeate water properties Hg(II) and total Fe concentration, pH) for the DE/UF system in stirred mode with a molar ratio of $[Hg]_0/[FeS]_0$ as 0.0004.

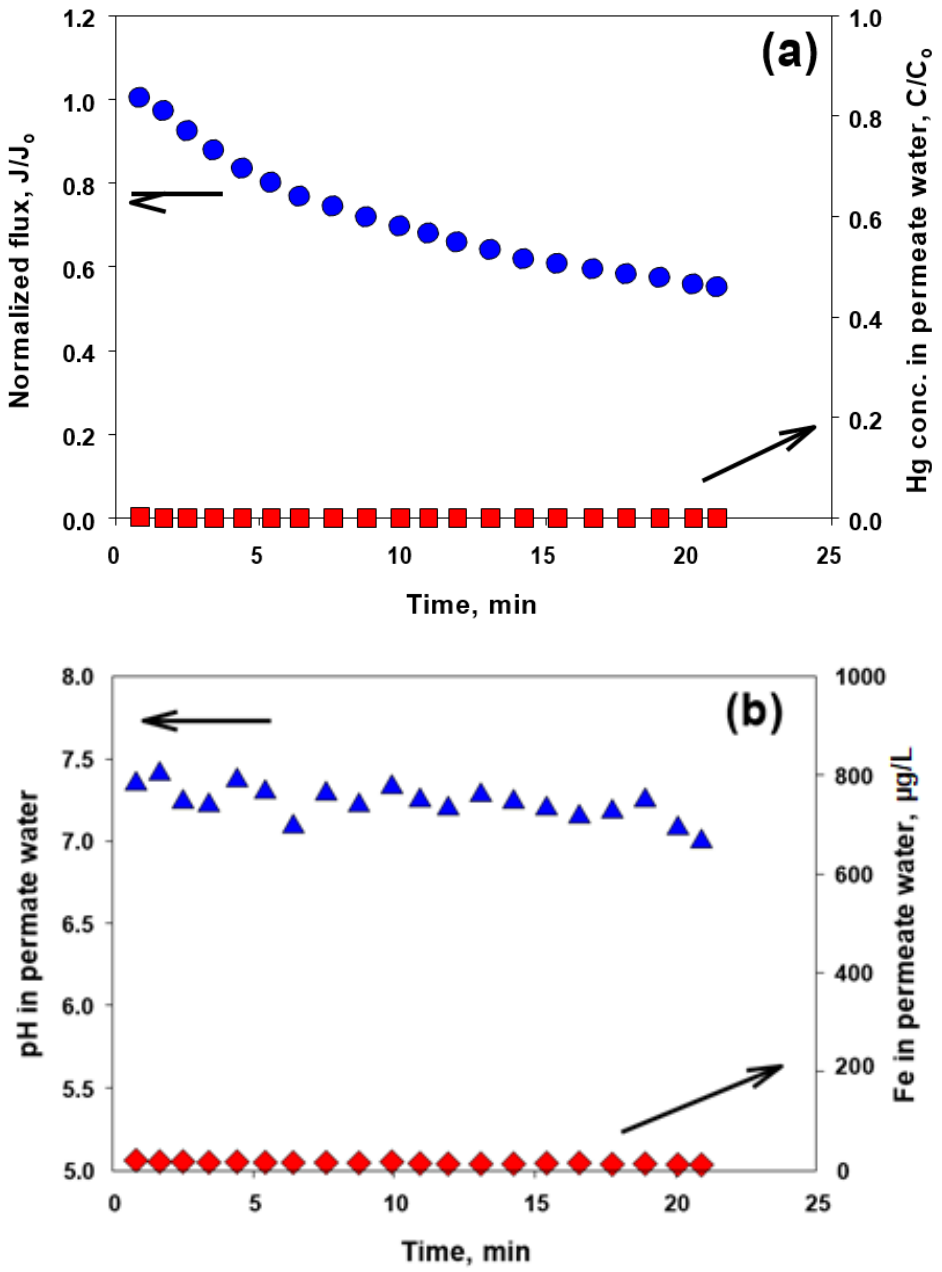

Figure 4.8: Results of the removal of Hg(II) using FeS in a stirred DE/UF system. (a) Normalized water flux and Hg(II) concentration in permeate as a function of time; (b) pH and Fe concentration in permeate water over time. Conditions: 30 kDa RC membrane, 5 mM Hg(II), 1 g/L FeS, pH 8, 1 bar transmembrane pressure, N2-purged, 15 min of pre-contact time for Hg(II) with FeS prior to feeding the solid suspension. Reprinted with permission from the publisher, Elsevier (*48*).

Results show that the flux declined to 42% of the initial value, with no Hg(II) detected, and pH varied between 7 to 7.5 while 0.4% of total Fe was released compared to the initial Fe concentration of 11 mM. This indicates that the added Hg(II) to the system was sorbed onto FeS and the Hg-contacted FeS particles were stable. The desorption experiments (step III) involved feeding 0.1 M $S_2O_3^{2-}$ solution (with no Hg or FeS) at pH 8 into the reservoir to evaluate the chemical stability of Hg(II)-contacted FeS. As shown in Figure 4.9, no Hg(II) release from the Hg(II)-FeS particle laden membrane and flux reduced by 10% in 10 minutes then steadily returned to the initial flux after 30 minutes. From an initial pH of 8, the pH range during the desorption experiment fluctuated between 7.3 and 7.7.

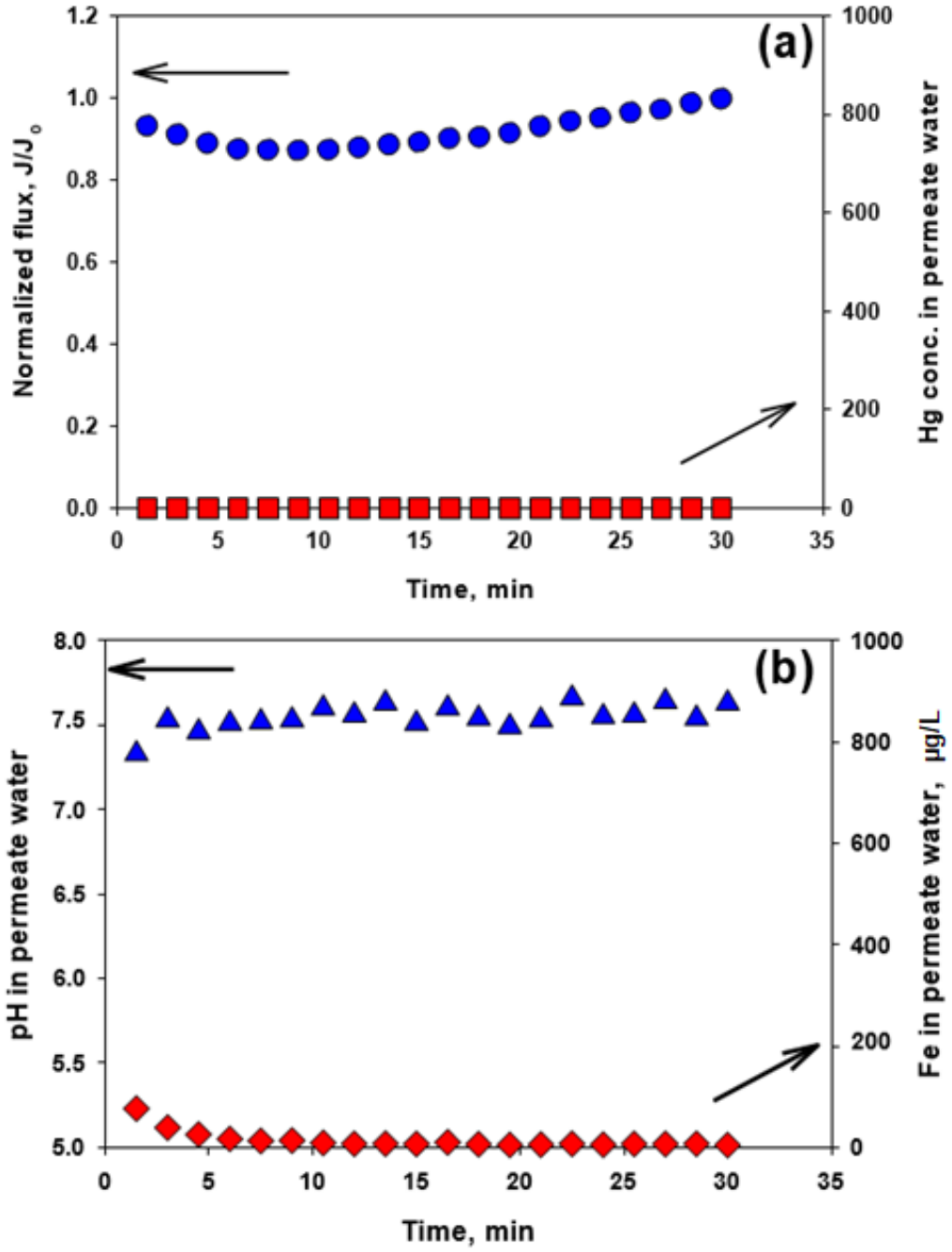

Figure 4.9: Results of Hg desorption experiments using thiosulfate feed. (a) Normalized flux and relative concentration of Hg in permeate over time; (b) pH and Fe in the permeate over time. Conditions: 0.1 M $S_2O_3^{2-}$, pH 8, 1 bar transmembrane pressure, N_2-purged, membrane previously contacted with FeS solids. Reprinted with permission from the publisher, Elsevier (*48*).

There was an observed Fe release during the first 8 minutes of the desorption experiment and then reduced to 0 after 10 minutes. This could indicate that the thiosulfate solution promoted surface precipitation causing Fe release. Then, due to the stirred mode, the shear effect caused the release Fe to form surface complexes with the Hg-FeS laden particles and reduce the cake formation. At the end of the experiment, the results prove that the Hg-contacted FeS particles on the membrane were stable and can be disposed to the environment safely with Hg(II) release being improbable.

Additional removal capacity with 250 mL of Hg(II) solution

Following the desorption test, the final step of the experiment was to evaluate the remaining Hg-contacted FeS particles for additional removal capacity by feeding the DE/UF system with around 200 - 220 mL of 5 μM Hg(II) solution at pH 8. The additional treated permeate water quality (Hg removal, pH and Fe concentration) and flux were measured in 3 batches. Figure 4.10 shows that for an additional 77.6, 63.5, and 60 L of permeate volumes per unit area of the membrane surface; the Hg(II) removal efficiencies were 100, 90, and 40%, respectively.

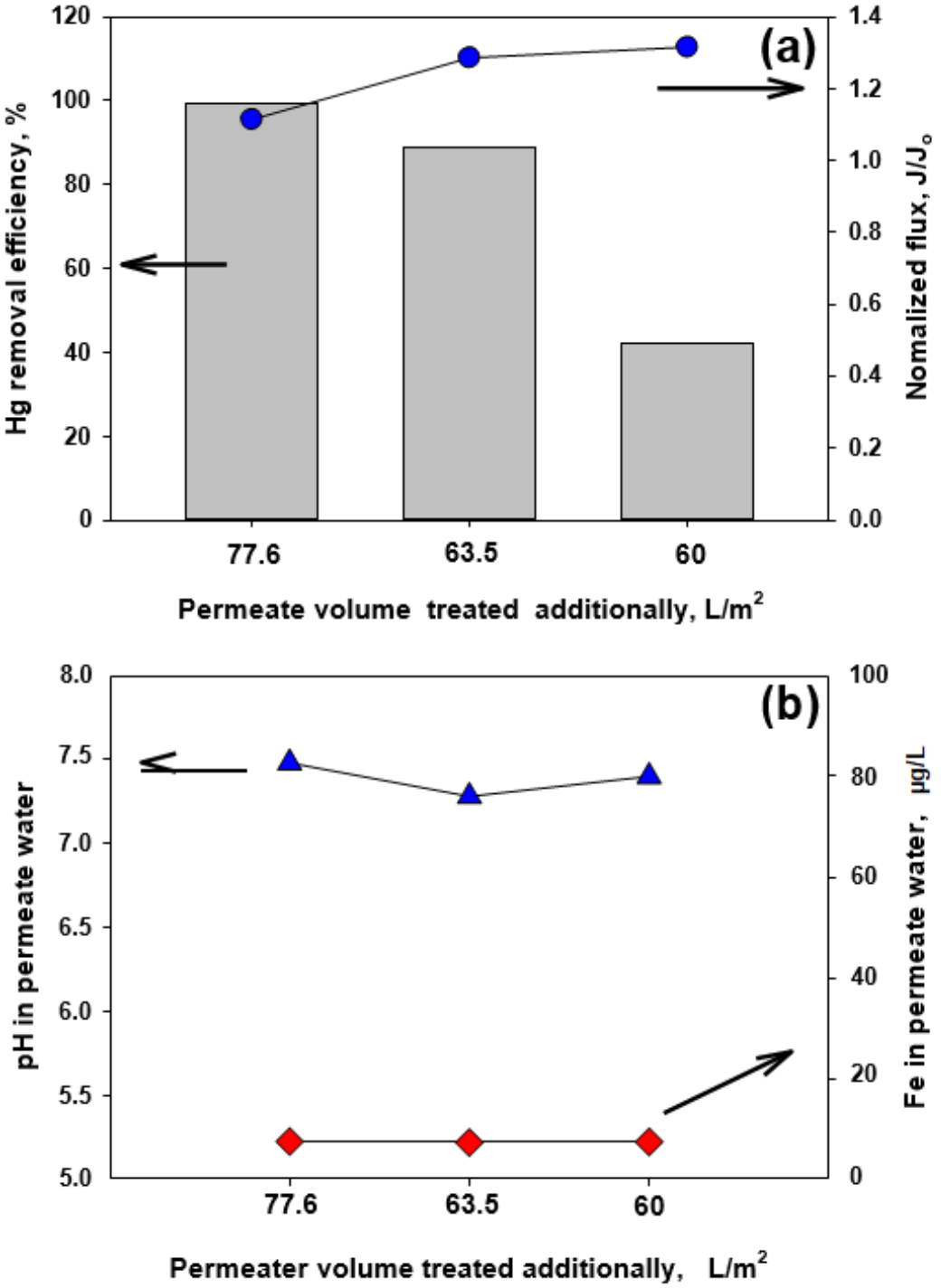

Figure 4.10: Removal of Hg(II) and relative normalized water flux and (b) pH and Fe concentration in permeate based on the additional permeate volume treated. Conditions: 5 µM Hg(II), pH 8, 1 bar transmembrane pressure, N_2 purged, membrane previously contacted with FeS solids and thiosulfate. Reprinted with permission from the publisher, Elsevier (*48*).

Hence, the Hg-contacted FeS particles could treat 79% of the additional 201 mL of 5 µM Hg(II) solution (1.05 µM Hg(II)/g FeS remaining in the permeate). However, a color change was observed on the Hg-contacted FeS particles on the membrane (from black to ocher-like color). This verifies that an alteration to the particles occurred that impacted the Hg(II) removal capacity. It is possible that a small amount of oxygen, present in the water reservoir despite N_2 purging, might have contacted with FeS via stirring. There was a 20-30% increase in flux by the end of the experiment improved by stirring, negligible pH change (between 7.3-7.5) and insignificant Fe release in the permeate water (5 µg/L Fe).

Surface characterization of stirred DE/UF membrane

Once the four-step experiments were complete, the membrane was stored in an anaerobic chamber till the surface analyses were performed. Images of the particles-laden membrane before and after drying (Figure 4.11 a and b) exhibit no change to the ocher-like color. The top and cross-sectional images of the membrane (Figure 4.11 c and d) show that it is entirely covered by a superficial FeS-Hg cake layer with rock-like shapes and particle clusters.

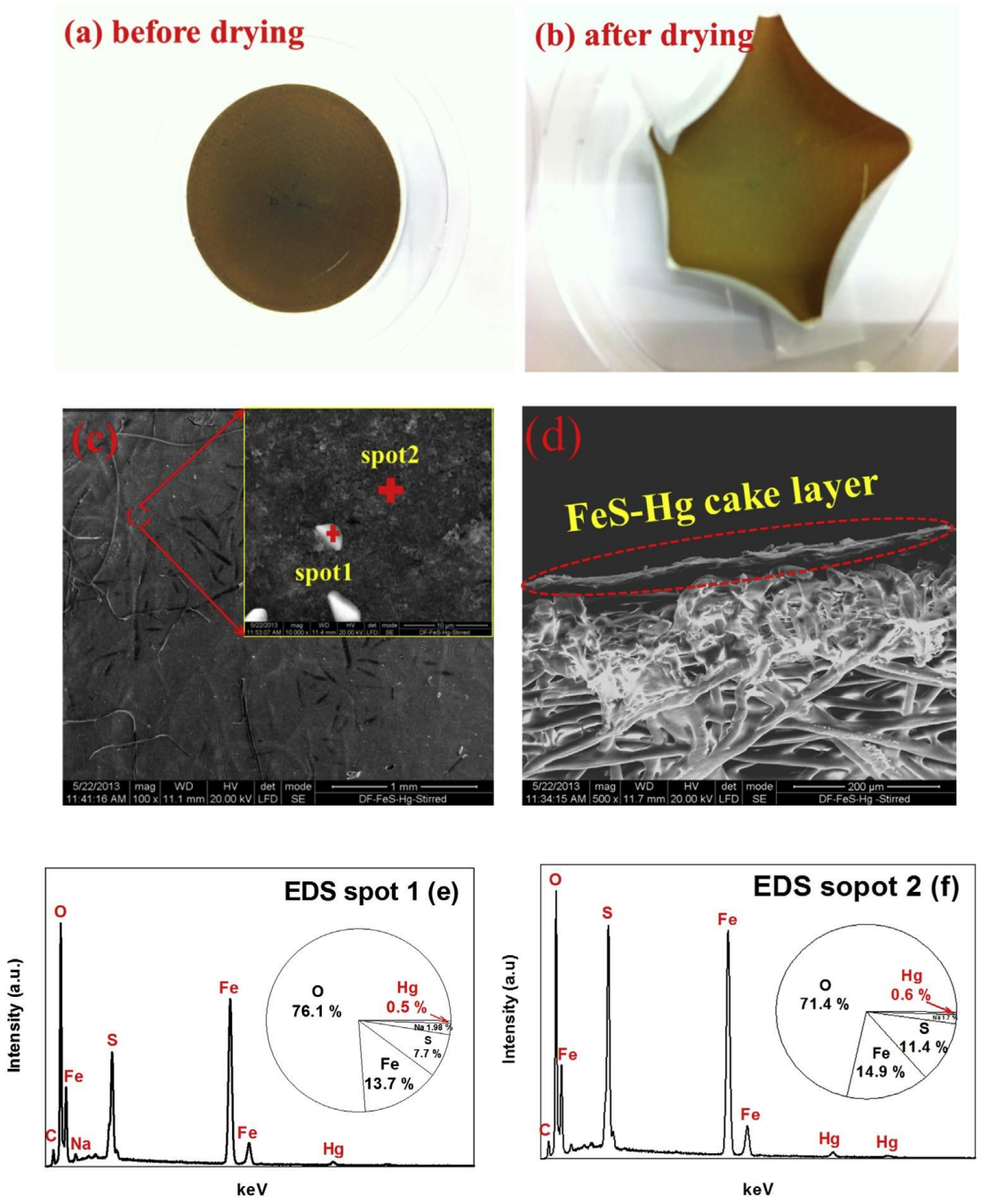

Figure 4.11: SEM/EDS analysis of membranes removed from stirred DE/UF system after step 4, photos of the membrane (a) before and (b) after drying inside the anaerobic chamber; back scattering (c) top-view and (D) cross-sectional SEM images and EDS analysis of (e) rock-like particle (spot 1) and (F) particle cluster (spot 2) on the membrane. Conditions: 11 mM FeS, 5 µM Hg(II), initial pH 8, and N2-purged. Reprinted with permission from the publisher, Elsevier (*48*).

The observed color change could lead to different morphologies after a modification occurred on the FeS particles. To determine the composition and Hg loading on rock-like and particle clusters, EDS analysis was conducted and showed that the rock-like shapes had lower Hg loading and higher elemental oxygen percentages (spot 1 with 0.5% Hg and 76% O) than the particle clusters (spot 2 with 0.6% Hg and 71% O). The possible sources of elemental oxygen found at both spots could be from the 0.1 M Thiosulfate solution and surface oxidation during the transfer and sample preparation for the SEM/EDS analyses.

4.2.2. Non-stirred mode – DE/UF system

Similar trends were observed when the non-stirred mode was applied to the DE/UF set up with the molar ratio of 0.0004 ($[Hg]_0/[FeS]_0$). Results in Figure 4.12 and Figure 4.13 show that the normalized flux decreased by 60% at the end of step II, no Hg release was observed, pH varied between 7.5 and 7.6, and negligible Fe (5 µg/L) was in the permeate.

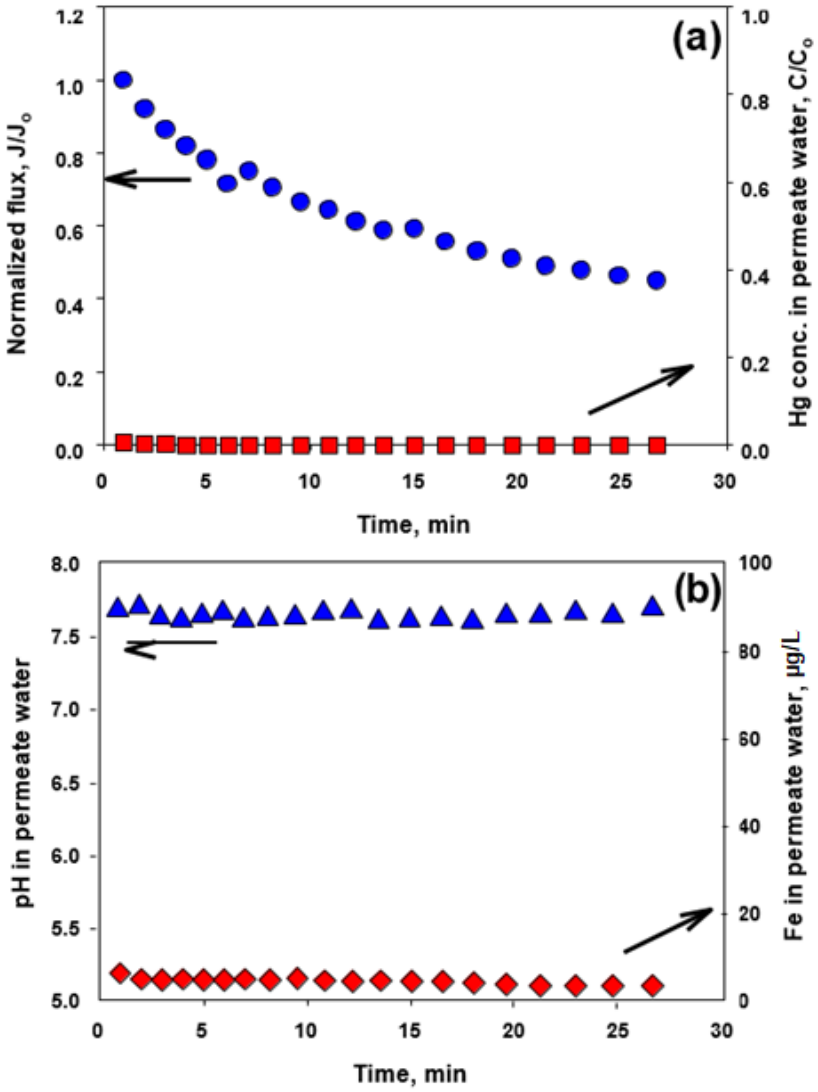

Figure 4.12: Results of Hg(II) removal from water using FeS in non-stirred DE/UF system. (a) Normalized water flux and relative Hg(II) concentration. (b) pH and Fe in the permeate over time. Conditions: 30 kDa RC membrane, 5 µM Hg(II), 11 mM FeS, pH 8, 1 bar transmembrane pressure, and N_2-purged, 15 min of pre-contact time for Hg(II) with FeS prior to feeding the solid suspension. Reprinted with permission from the publisher, Elsevier (*48*).

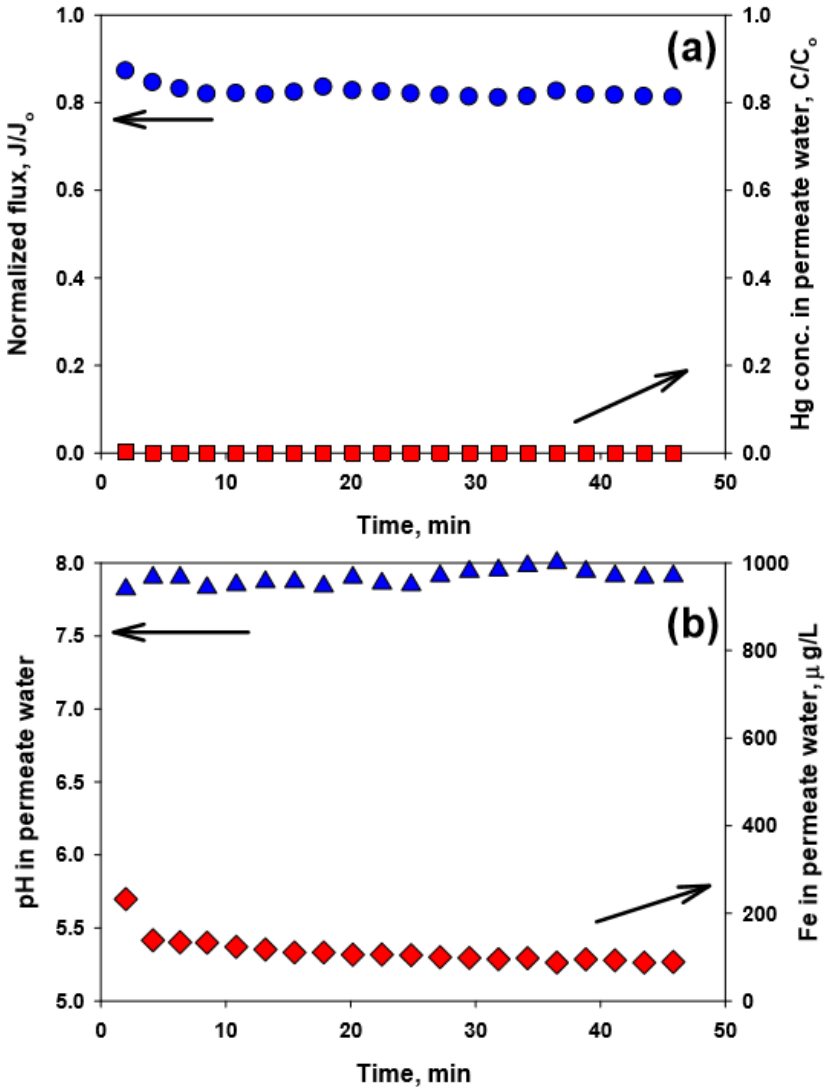

Figure 4.13: Results of Hg(II) desorption experiments using thiosulfate feed in non-stirred DE/UF system. (a) Normalized flux and relative Hg concentration in permeate; (g) pH and Fe concentration in permeate over time. Conditions: 0.1 M $S_2O_3^{2-}$, pH 8, 1 bar transmembrane pressure, N_2-purged, membrane previously contacted with FeS solids. Reprinted with permission from the publisher, Elsevier (*48*).

Figure 4.14 shows a comparison of the flux decline for the DE/UF system treating Hg(II) with FeS before and after contact (stirred and non-stirred mode). The flux decline for the FeS suspension contacted with Hg(II) was 1.3 times greater than the one with FeS alone.

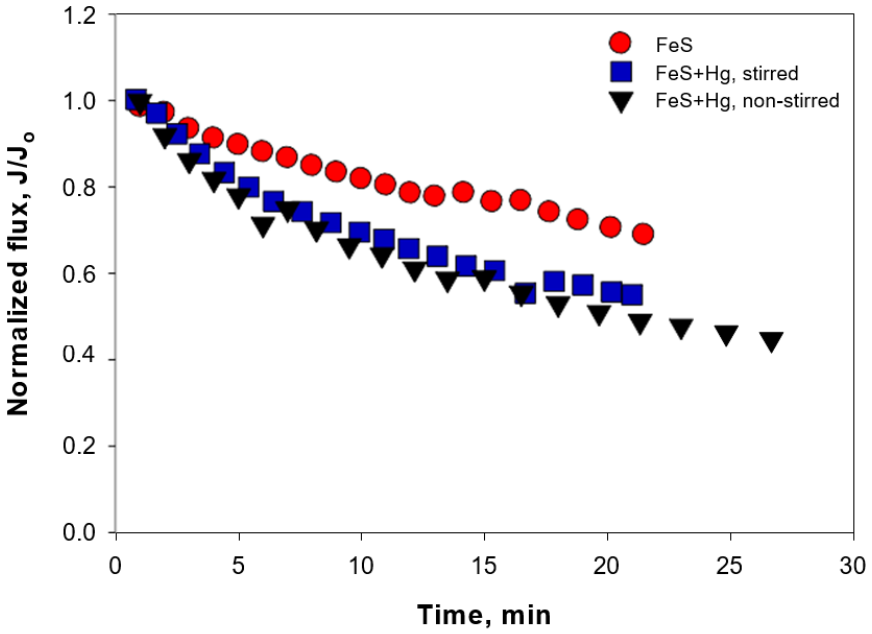

Figure 4.14: Flux decline for FeS suspension (non-stirred) and FeS suspensions after contact with Hg(II) (stirred and non- stirred). Conditions: 30 kDa DE/UF membrane, 5 mM Hg(II), 1 g/L FeS, pH 8, 1 bar transmembrane pressure, N2-purged, 15 min of pre-contact time for Hg(II) with FeS prior to feeding the solid suspension. Reprinted with permission from the publisher, Elsevier (*48*).

The stirred mode exhibited 1.03 times less flux decline than the non-stirred mode. The shear caused by stirring may have helped reduce the cake formation on the membrane surface to a limited extent. Future studies could investigate various stirring speeds that could significantly reduce flux decline. To determine the fouling mechanism causing the flux decline, a flux decline model was applied (*44*) as shown in Equation 4.21:

$$J_{DE/UF} = J_0(1 + kt)^{-n} \quad (4.21)$$

n=0.5 (cake formation), 1 (internal pore constriction), 1.5 (partial pore blocking), 2 (complete pore blocking)

Where $J_{DE/UF}$ and J_0 are the flux calculated for the DE/UF system, *t* is the time (min), *k* is an empirical rate constant, and *n* is a coefficient corresponding to the fouling mechanism. Table

4.1 displays the results of the calculated parameters with the values of *n* and the values of the model parameters obtained from nonlinear regression. The value of *n* as 0.5, with the lowest sum of squared residuals between the predictions of the flux model and experiment data, indicates that cake formation was the most probable fouling mechanism.

Table 4.1: Calculated parameters of the flux decline model for rejection of FeS and Hg(II)-contacted FeS in non-stirred and stirred mode

Samples	n=0.5	n=1.0	n=1.5	n=2.0
FeS w/o stirring	SSR=0.0016 k=0.047 ± 0.0015	0.002 0.21 ± 6E-4	0.0024 0.013 ± 4E-4	0.0027 0.009 ± 4E-4
FeS + Hg w/ stirring	0.005 0.107 ± 0.0055	0.006 0.042 ± 0.0016	0.0073 0.026 ± 0.001	0.0088 0.018 ± 8E-4
FeS + Hg w/o stirring	0.007 0.135 ± 0.008	0.008 0.05 ± 0.002	0.0126 0.135 ± 0.0079	0.0164 0.021 ± 0.0012
*SSR is sum of squared residual between experimental data and flux decline model.				

In step 3 (desorption test), analyses of the permeate thiosulfate solution displayed no Hg release, relatively constant pH between 7.7 and 8 and 0.3% of initial Fe was released (300 µg/L) within 2 minutes then eventually decreased to 0.01% (100 µg/L) after 30 minutes. In contrast to the stirring experiment, the thiosulfate permeate flux decreased to 20% within five minutes and then stabilized till the end of the experiment with no recovery to the initial flux. Additionally, no color change was observed on the retained Hg(II)-contacted FeS solids on the UF membrane. This proves that no changes occurred on the chemical properties of the FeS particles, which explains the complete treatment of an additional 220 mL of 5µM Hg(II) solution (Figure 4.15).

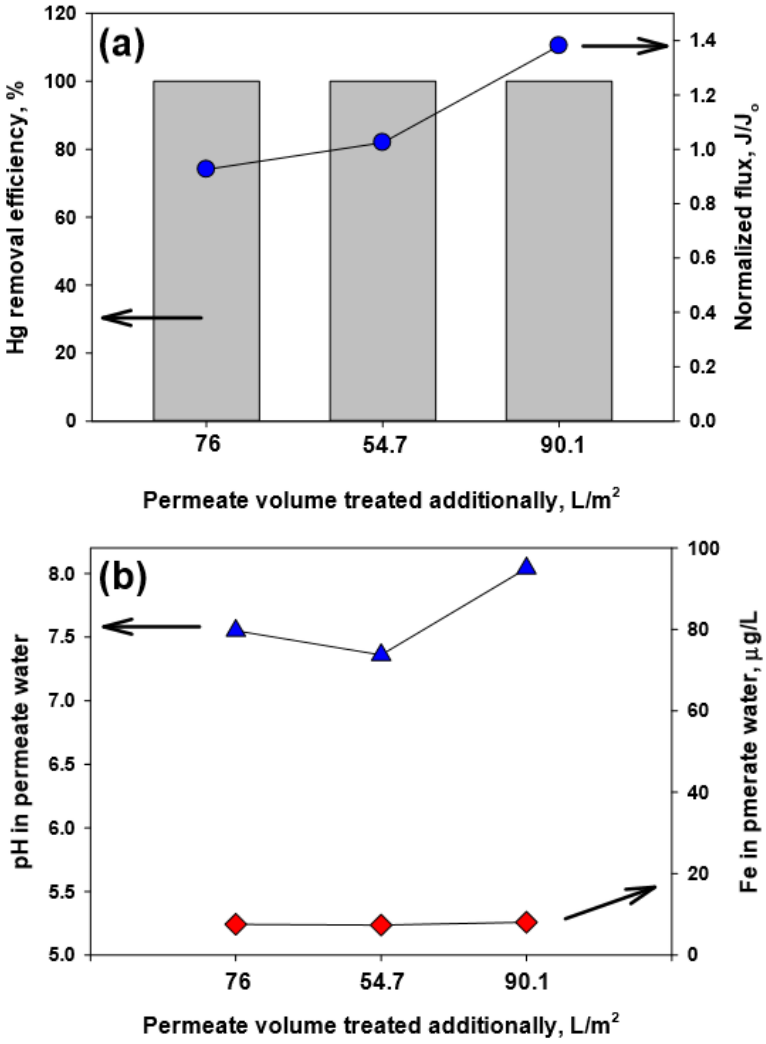

Figure 4.15: Results of the Hg-contacted FeS additional removal capacity experiments in non-stirred DE/UF system. (a) Removal of Hg(II) and normalized water flux and (b) pH and Fe concentration in permeate based on the additional permeate volume treated. Conditions: 5 µM Hg(II), pH 8, 1 bar transmembrane pressure, N_2-purged, membrane previously contacted with FeS solids and thiosulfate as described in Figure 4.13. Reprinted with permission from the publisher, Elsevier (*48*).

The flux increased to 56% by the end of step 4 (additional Hg(II) removal capacity test), pH was recovered from 7.5 to 8 and negligible Fe was found in the permeate water as shown in Figure 4.15. After step 4, the Hg-FeS laden membrane for the non-stirred experiment was collected and dried for surface analyses preparation. In contrast to the color change observed with the

membrane from the stirred experiment, images shown in Figure 4.16 a and b indicate no color change before and after the non-stirred experiment membrane was dried. Further investigation is required to clarify the mechanism that causes chemical change in the FeS particles during the stirring experiment (Figure 4.11) since it has a negative impact on the Hg(II) removal capacity.

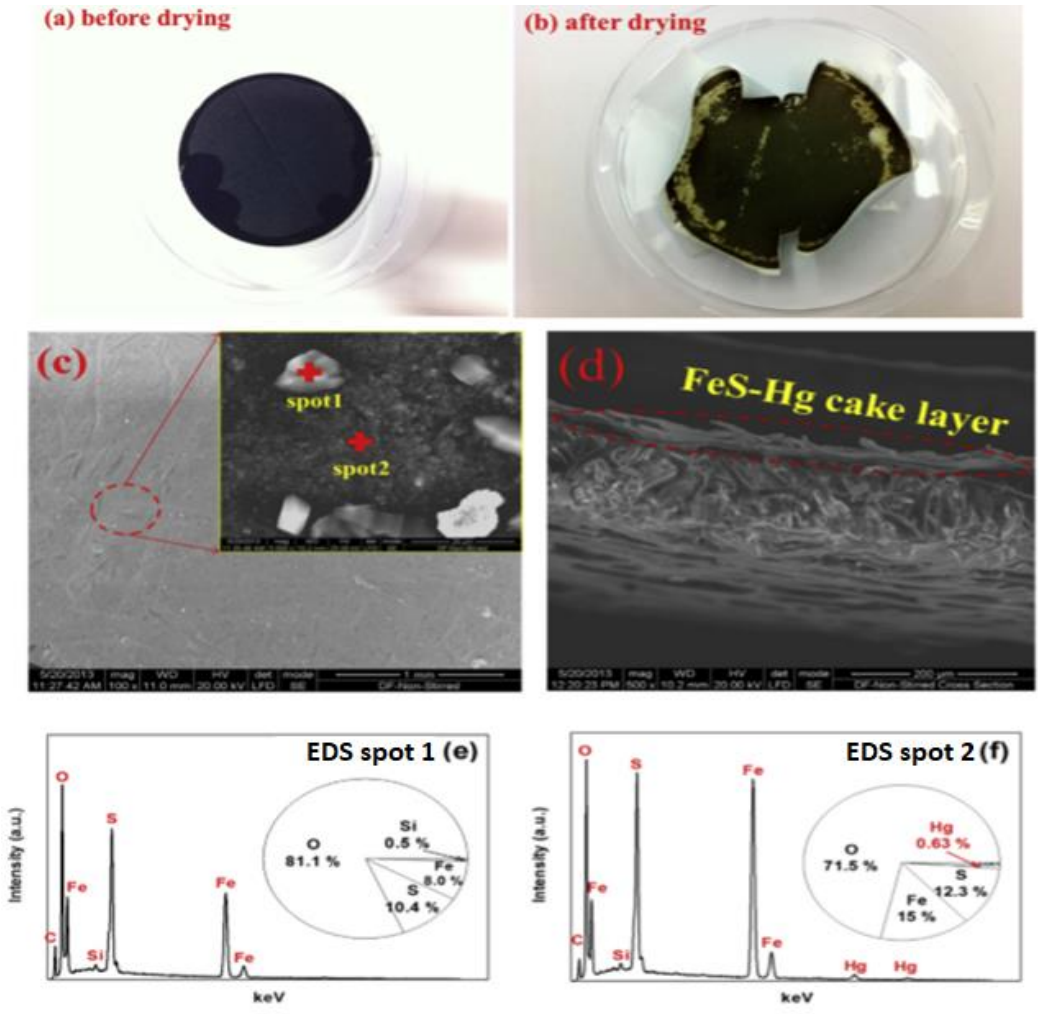

Figure 4.16: Surface analysis of 30 kDa RC UF membranes after undergoing step III experiment in non-stirred DE/UF system; Photo images of the membrane (a) before and (b) after drying inside anaerobic chamber; back scattering (c) top-view and (d) cross-sectional SEM images and EDS analysis of (e) rock-lick particle (spot 1) and (f) particle cluster (spot 2) on the membrane: 1g/L FeS, 5 µM Hg(II), initial pH 8, and N_2-purged continuous contact system. Reprinted with permission from the publisher, Elsevier (*48*).

Similar to the Hg-FeS laden membrane from the stirred experiment, the top and cross-sectional SEM images (Figure 4.16 c and d) exhibit a superficial cake-layer formation covering the membrane with rock-shape and particles clusters on the surface. The presence of rock-shape particles could originate from reactions between FeS and Hg(II) or exposing the Hg-FeS particles to slightly anoxic environments in the anaerobic chamber during drying; or transferring the membrane for surface analyses causing partial oxidation of exchanged Fe by Hg or structural Fe. This assumption is also applicable for the DE/UF stirred experiment. EDS analyses reveal the absence of Hg (probable below detectable level) and higher elemental oxygen concentration (81%) on rock-shape particles (Figure 4.16 e). Particle clusters contain 0.56% of elemental Hg and 71% elemental O (Figure 4.16 f).

Effect of anions and humic acid on DE/UF non-stirred system

As shown in the previous sections, the DE/UF system in non-stirred mode provides the most desirable results leading to complete additional Hg(II) removal capacity of the Hg-FeS laden membrane. The effect of 0.01 M anions (Cl^-, NO_3^-, and SO_4^{2-}) (i.e. $[Hg]_0/[Anion]_0$ ratio of $5x10^{-5}$) and 1 mg/L HA were investigated with the DE/UF system in non-stirred mode with 0.0004 molar ratio of $[Hg(II)]_0/[FeS]_0$, 0.1M thiosulfate solution, and 166-250 mL of 5 µM Hg(II) solution for additional treatment (as in the previous four-step experiments).

Results of the permeate water quality after step 2 (rejection of Hg-FeS solids) and step 3 (desorption tests) presented in Figure 4.17 to

Figure 4.22 show no Hg release and negligible Fe release. However, greater flux declines were observed with anions (22-56%) and humic acid (10-40%) than without anions or HA (25%)

compared to the initial flux. The permeate pH remained stable at 8.0 for the experiments without anions and humic acid and a decline to pH 7.0 was noticed in the presence of anions. These show that anions and humic acid affect the permeability of the membrane by competing with Hg or Fe for sorption sites. Anions provide a slightly acidic environment to neutralize the permeate as observed in the CF/UF system whereas humic acid has no significant effect on the pH. During the desorption tests, no Fe release was detected in the solution with or without anions. However, in the presence of humic acid, the thiosulfate permeate had 44% of the initial Fe initially and 20 minutes later, the concentration decreased to 18% then to 4% at the end of the experiment. A similar trend was observed for the CF/UF system with no anions where the Fe source in the permeate could be from HgS and $\left[Fe_{(1-x)}, Hg_{(x)}\right]S_{(s)}$ precipitation or from the release of Hg-FeS solids since Hg-HA complexes are formed. In step 4 (additional Hg(II) removal capacity tests), similar trends were observed with nearly 100% Hg(II) removal capacity, flux decline by 30-40% from the initial value, negligible Fe concentration in the permeate, and pH stabilized between 6-6.5 due to surface redox reactions and Hg-Cl or Hg-HA complex formations. It is important to note that a greater flux decline was observed for the DE/UF non-stirred experiment with humic acid (20-60%). This shows that HA has a greater impact on the membrane permeability than anions forming bigger HA-Hg complex particles that get entrained in the membrane.

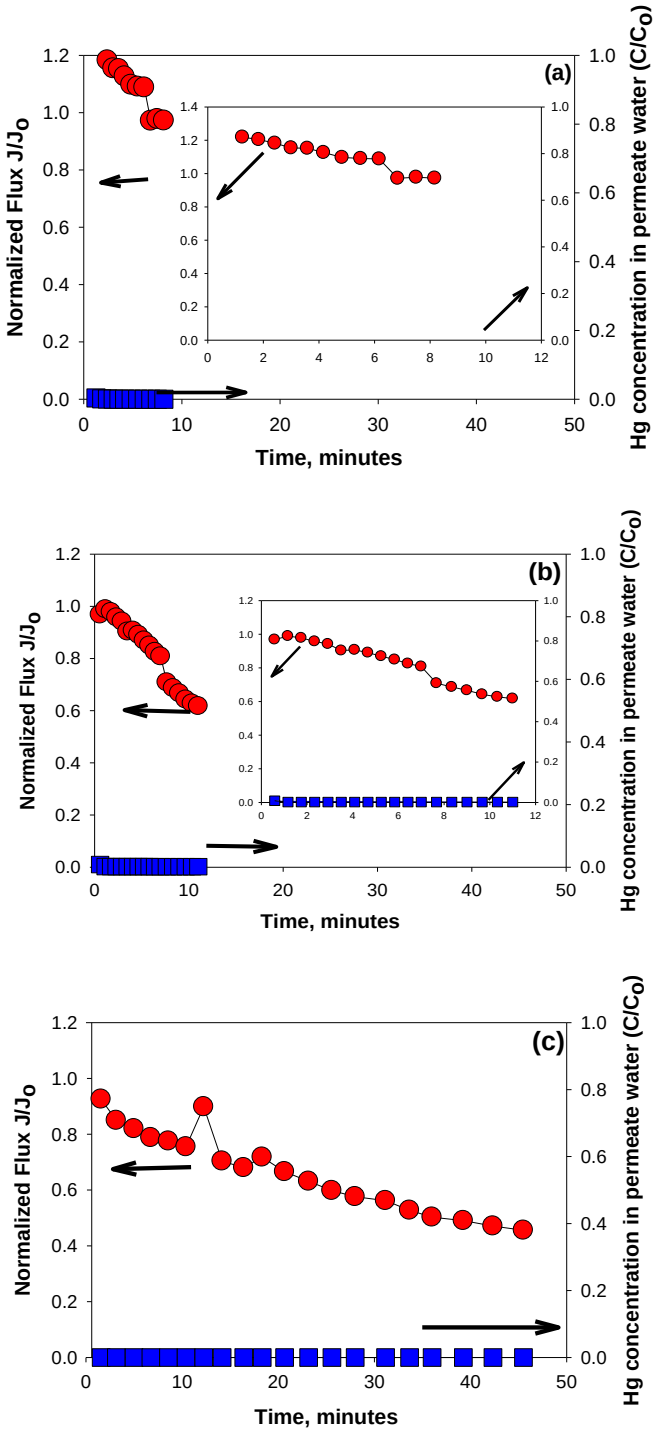

Figure 4.17: Normalized water flux and relative Hg(II) concentration in permeate water as a function of time in non-stirred DE/UF system for Hg(II) removal from water using FeS in the presence and absence of anions and HA. Conditions: pH 8, 1 bar pressure, 30 kDa RC UF membrane, 30 min. reaction time; (a) 5 µM Hg + 11.36 mM FeS, (b) 5 µM Hg + 11.36 mM FeS+ 0.01 M anions, (c) 5 µM Hg + 11.36 mM FeS + 1 mg/L HA

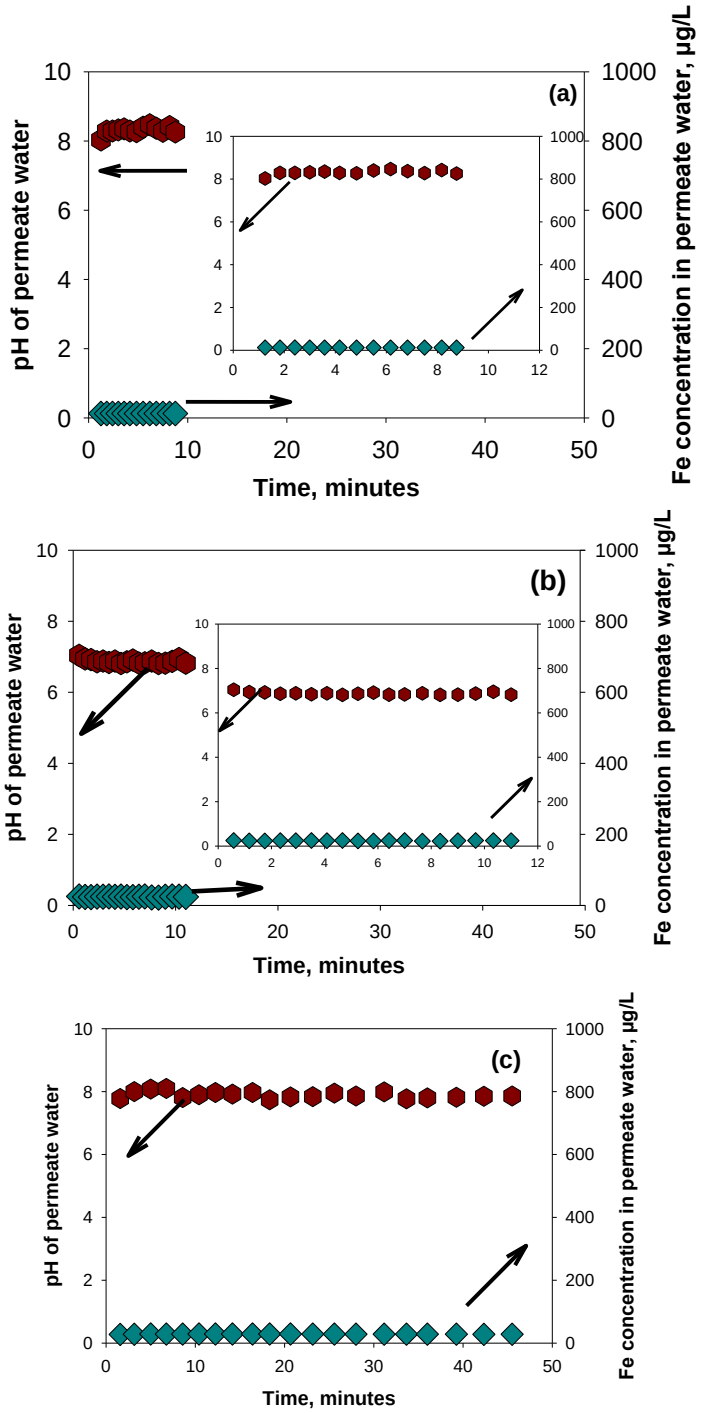

Figure 4.18: pH and Fe concentration in permeate water as a function of time in non-stirred DE/UF system. Conditions: pH 8, 1 bar pressure, 30 kDa RC UF membrane, 30 min reaction time; (a) 5 µM Hg + 11.36 mM FeS, (b) 5 µM Hg + 11.36 mM FeS+ 0.01 M anions, (c) 5 µM Hg + 11.36 mM FeS + 1 mg/L HA

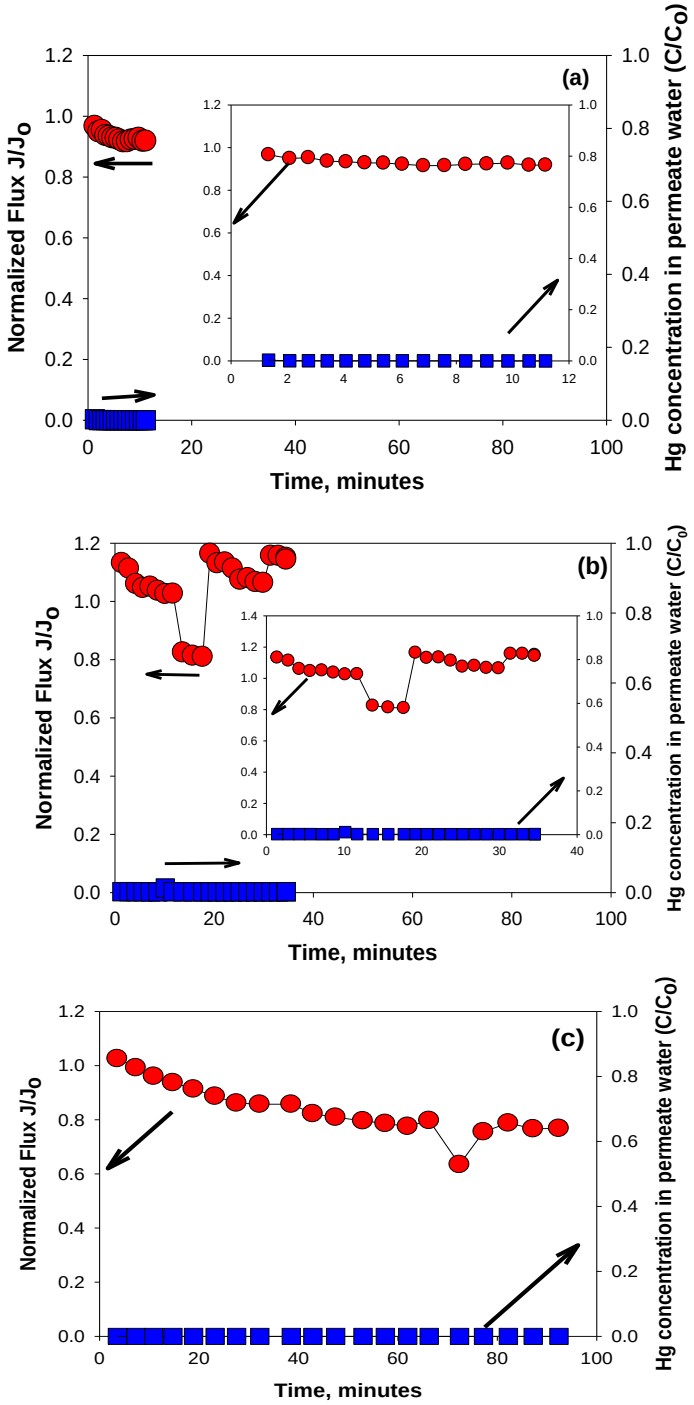

Figure 4.19: Normalized water flux and relative Hg(II) concentration in permeate water as a function of time in non-stirred DE/UF system. Conditions: pH 8, 1 bar pressure, 30 kDa RC UF membrane, 30 min reaction time; (a) 5 µM Hg + 11.36 mM FeS, (b) 5 µM Hg + 11.36 mM FeS+ 0.01 M anions, (c) 5 µM Hg + 11.36 mM FeS + 1 mg/L HA

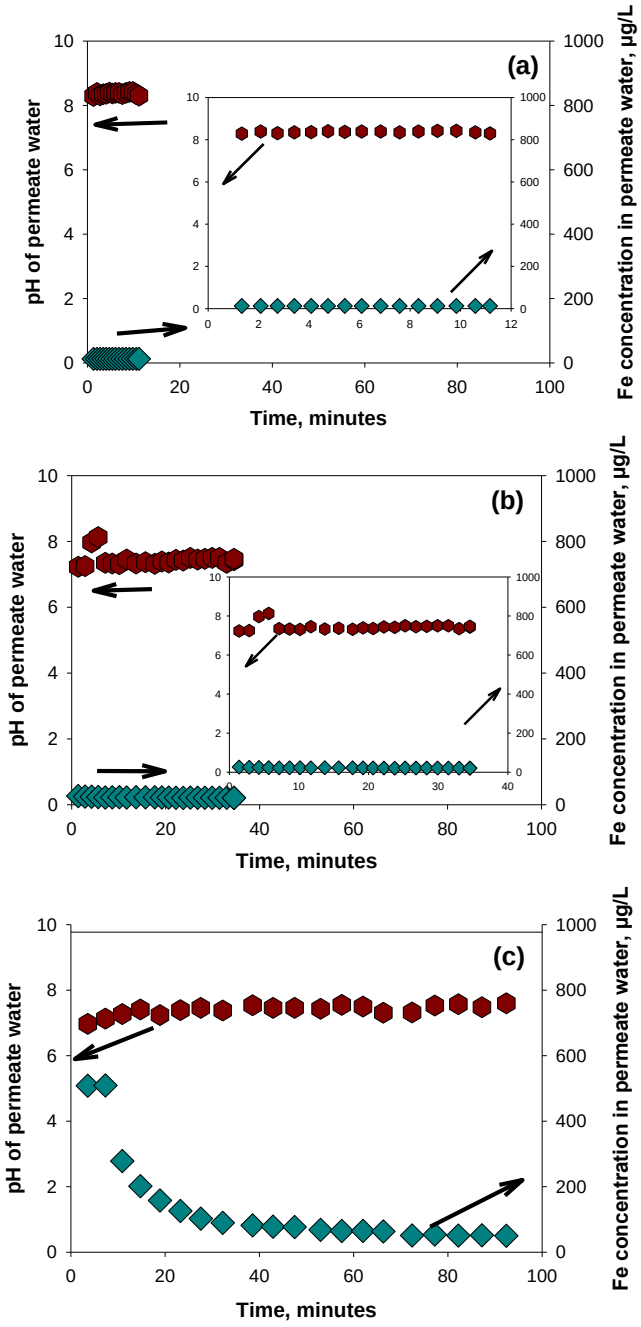

Figure 4.20: pH and Fe concentration in permeate water as a function of time from the desorption experiments in non-stirred DE/UF system. Conditions: pH 8, 1 bar pressure, 30 kDa RC UF membrane, 30 min reaction time; (a) 5 µM Hg + 11.36 mM FeS, (b) 5 µM Hg + 11.36 mM FeS+ 0.01 M anions, (c) 5 µM Hg + 11.36 mM FeS+ 1 mg/L HA

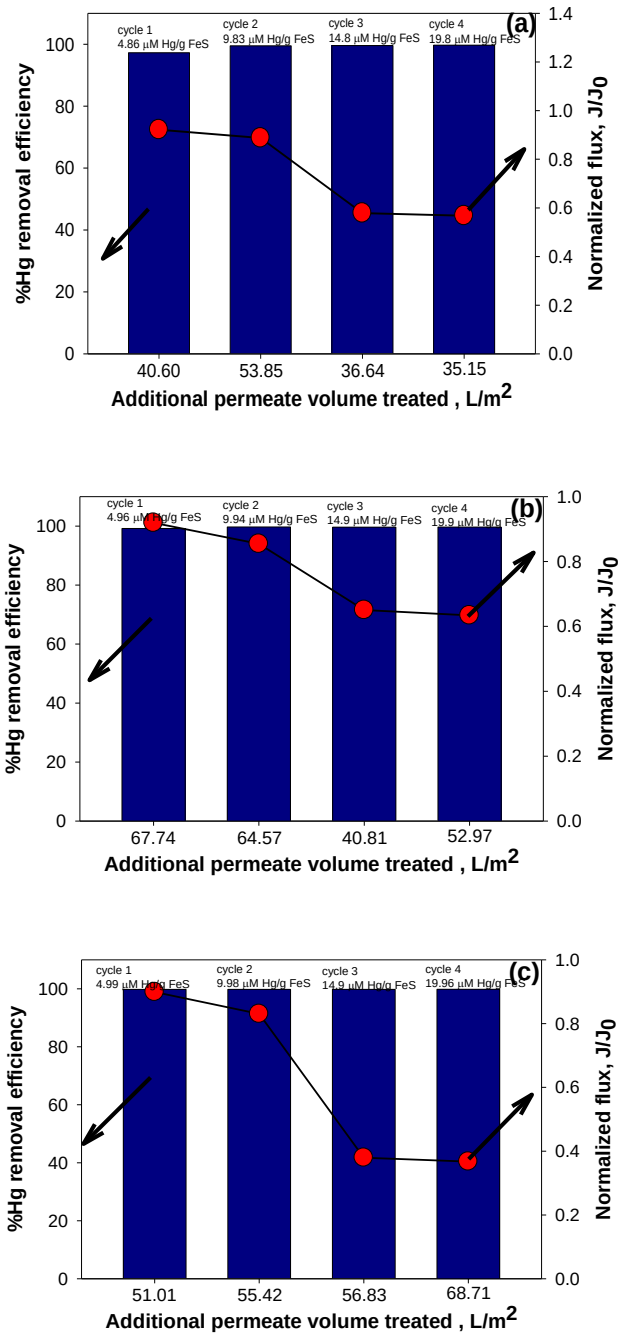

Figure 4.21: Additional sorption capacity experimental results in the form of %Hg removal and normalized flux as a function of additional treated water volume in non-stirred DE/UF system for the following conditions:(a) 5 µM Hg + 11.36 mM FeS, (b) 5 µM Hg + 11.36 mM FeS+ 0.01 M anions, (c) 5 µM Hg + 11.36 mM FeS+ 1 mg/L HA

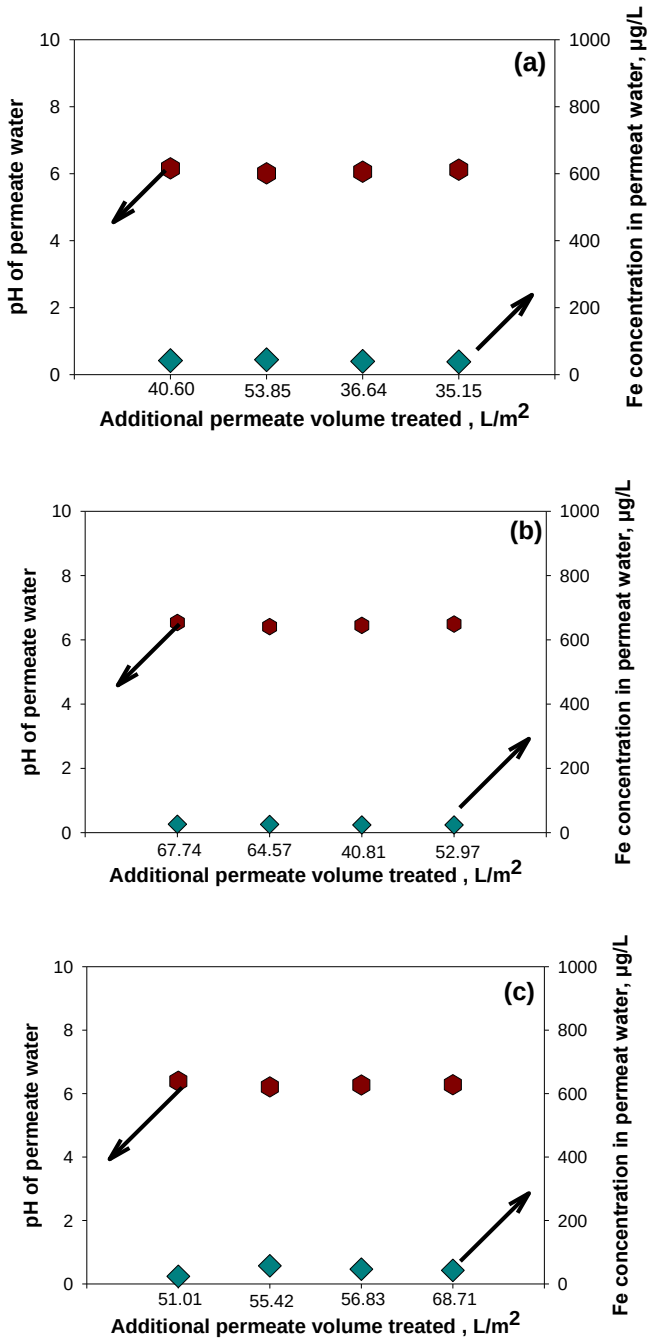

Figure 4.22: Additional sorption capacity experimental results in the form of pH and Fe concentration in permeate water as a function of additional treated water volume in non-stirred DE/UF system for the following conditions:(a) 5 µM Hg + 11.36 µM FeS, (b) 5 µM Hg + 11.36 µM FeS+ 0.01 M anions, (c) 5 µM Hg + 11.36 mM FeS+ 1 mg/L HA.

Several studies have reported enhanced Hg(II) removal with FeS in the presence of anions, most particularly Cl^- (*3, 48, 156*). Sun et al. (*3*) conducted experiments with a molar ratio of Hg: FeS of 0.002 with 0.1 M Cl^- ions. Despite the fact that Hg-Cl complex formations have a lower affinity to FeS, Cl^- ions augments ionic strength that endorses FeS structure variation which leads to accelerated oxidation or dissolution of FeS and corrosion of the surface which uncover more sulfide ions for HgS precipitation (*3, 24, 157*). Considering this study includes a low [Hg]0/[FeS]0 molar ratio of 0.0004 with 0.01 M anions, competition between Hg(II) and anions for the FeS active sites are less likely.

Duan et al. (*156*) reported the improved Hg(II) adsorption on pyrite with 10 and 20 mg/L HA using a molar ratio of Hg(II) to sand coated-FeS_2 of 0.0005 (*156*). The results were attributed to the Hg-HA complexation with the reduced sulfur reactive groups of HA (thiol R-SH and disulphide R-SS-R, and disulfane R-SSH) and other functional groups (*153*). Furthermore, reactions between Hg(II) and soluble HA could produce Hg-HA solid phase and larger complexes that can be rejected by the UF membrane filter in addition to being adsorbed onto FeS particles(*156*). The formation of larger complexes causing reduction in membrane permeability could explain the reduced flux of the permeate in step IV. Another study conducted by Park et. al. (*158*) included enhanced Cd(II) adsorption on activated biochar from pH 3.5-8.0 with a ratio of Cd(II) to biochar of 0.04 (2 mg/L Cd(II), 0.05g/L biochar), 10 mg/L HA and 0.001 M Cl^- (*158*). At higher pH, Cd(II) adsorption decreased due to the surface charge variation of the adsorbed HA (*158*). HA-biochar surface complexation produced a slightly negative shift of zeta potential values which lead to an overall negative surface charge. Furthermore, HA was found to reduce aggregation of the biochar particles which increased the number of sorption sites. Consequently,

electrostatic interactions of Cd(II) and formation of tertiary biochar-HA-Cd complexes become more apparent. This could explain the similar trend in this study with increased Hg(II) removal by FeS in the presence of anions with a low molar ratio of Hg to FeS of 0.0004. However, with higher molar ratios, Sun et al. (*24*), whose experiments included a molar ratio of $[Hg]_0/[FeS]_0$ of 0.02 with 0.02 g/L HA, and Skyllberg and Drott (*39*) reported inhibitive effects of HA due to the formation of stable coordination compounds of Fe(II) with HA reactive groups (hydroxyl-, phenoxyl, and carboxyl-) which competed with Hg(II) for FeS sorption sites. Additionally, HA-Hg complexation restrains Hg(II) adsorption on FeS (*39, 97*).

Surface characterization of Hg+FeS and Anion/HA membrane using SEM/EDS analyses

SEM images of the membrane from the DE/UF non-stirred mode with only FeS and Hg after step 4 showed a non-uniform rock-filled morphology (Figure 4.23). EDS analyses display the rock like particle (spot1) with lower Hg concentration and elemental oxygen (0.69% Hg, 46.91% O) compared to the flatter surface (spot 2) with 1.02% Hg and 47.68% O. SEM images of the membrane from the setup with anions displayed smaller rock-shape formations on the

membrane (

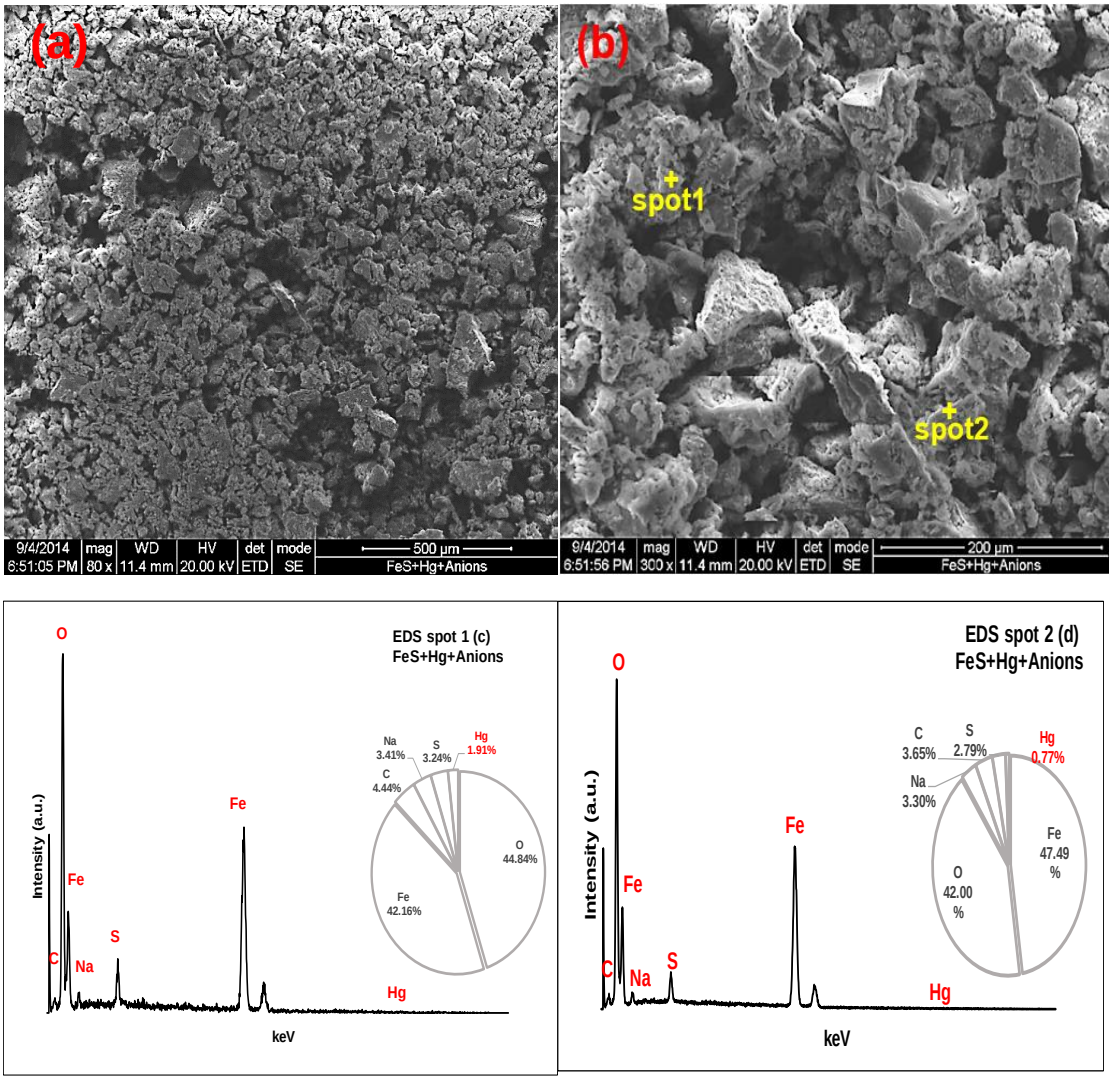

Figure 4.24) with two spots showing 0.77% and 1.91% Hg. In the presence of humic acid, the SEM images of the membrane's surface exhibited flat surfaces and larger rock-like particles (Figure 4.25). The flat surface (spot 1) had a higher Hg concentration (2.06% Hg) compared to the rock-like particle (0.81%Hg). Hence, based on the EDS analyses, the Hg loading on the membrane

was higher in the presence of humic acid (17-35%) and anions (12-25%) compared to the set up with only FeS and Hg(II).

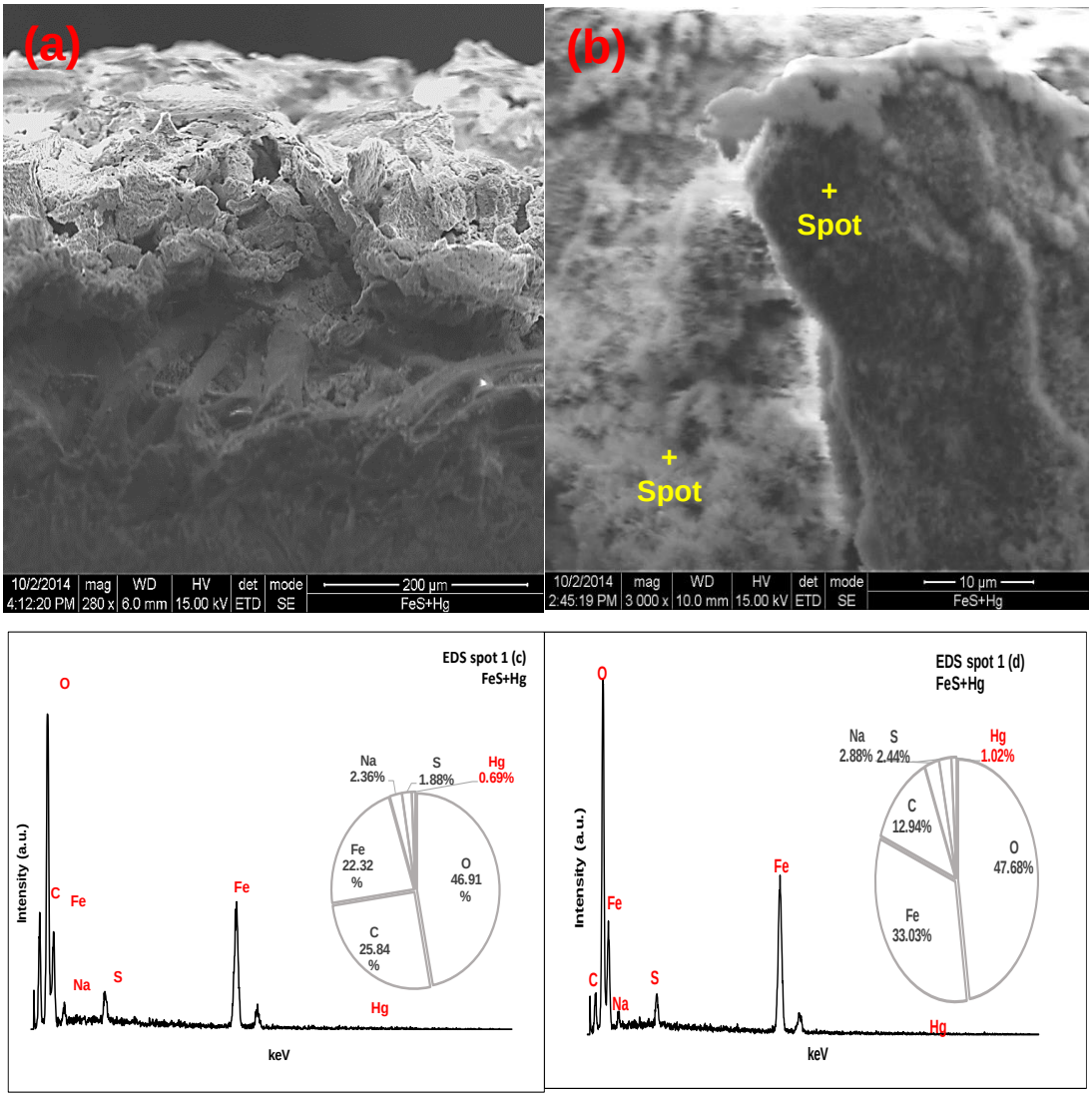

Figure 4.23: Surface analysis of 30 kDa RC UF membrane after undergoing step IV experiment in non-stirred DE/UF system. (a) cross-sectional view and (b) magnified view to 100 µm SEM images and EDS analyses of (c) rock-shape particle on the membrane and (d) flat surface on the membrane:5 µM Hg + 11 mM FeS.

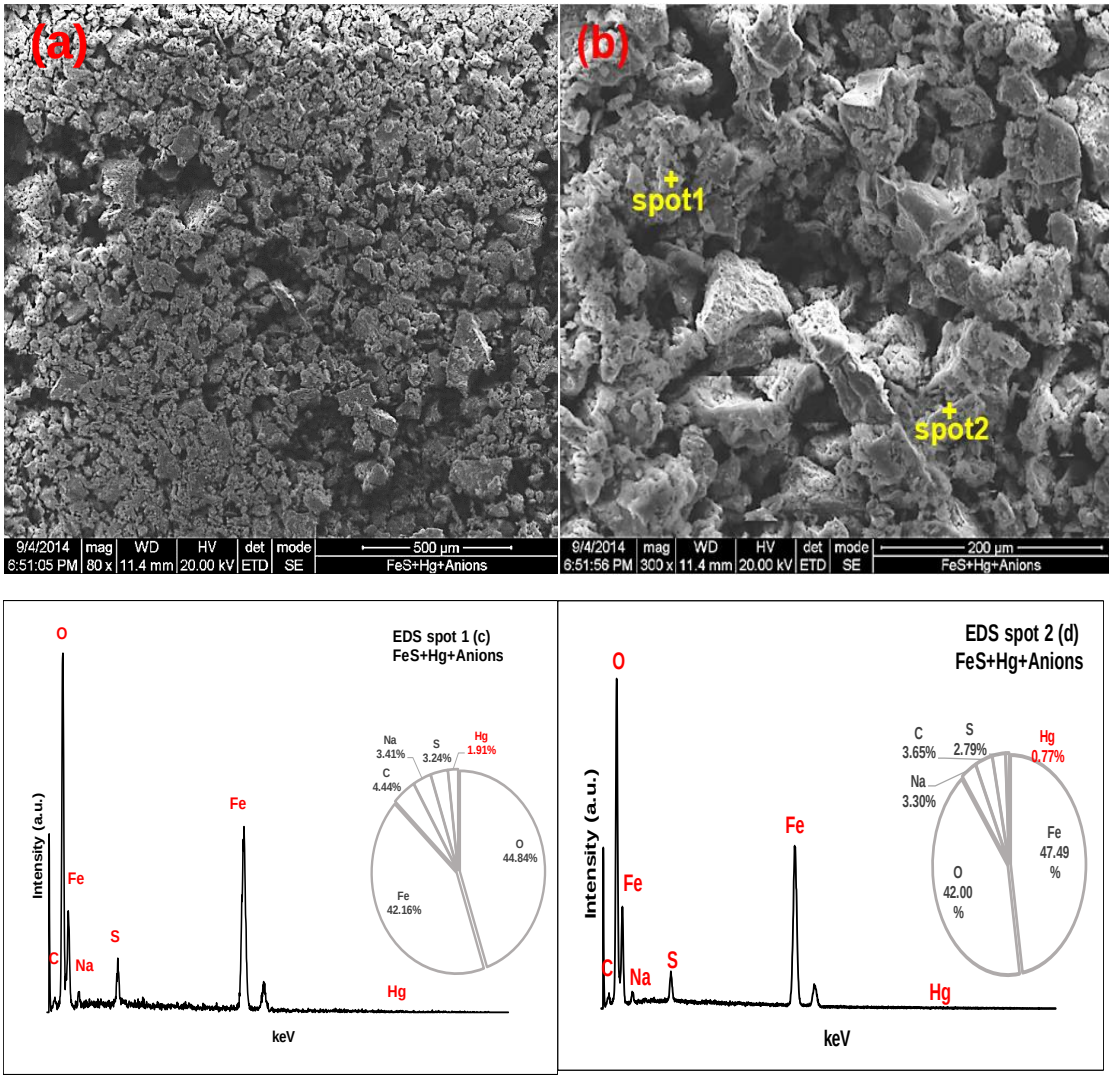

Figure 4.24: Surface analysis of 30 kDa RC UF membrane after undergoing step IV experiment in non-stirred DE/UF system. (a) top-view and (b) magnified view to 200 µm SEM images and EDS analyses of (c) particle cluster (spot 1) and rock-shape particle (spot 2) on the membrane: 5 µM Hg + 11 mM FeS+ 0.01 M anions.

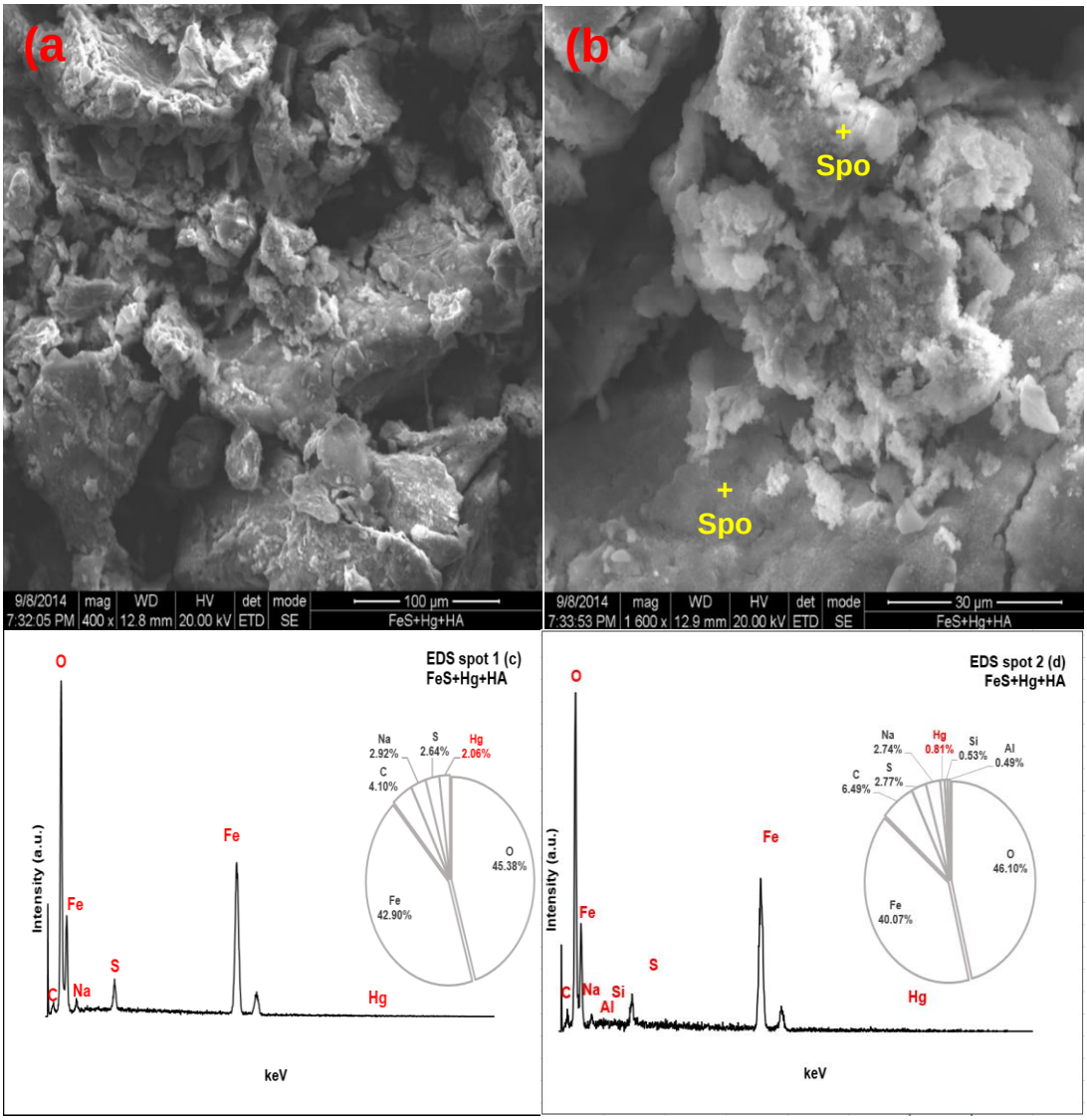

Figure 4.25: Surface analysis of 30 kDa RC UF membrane after undergoing step IV experiment in non-stirred DE/UF system. (a) top-view and (b) magnified view to 100 µm SEM images and EDS analyses of (c) flat surface (spot 1) and (d) rock-shape particle (spot 2) on the membrane: 5 µM Hg + 11 mM FeS + 1 mg/L HA.

Effect of MWCO (30, 100, and 300 kDa) on DE/UF non-stirred system

The MWCO pore size plays an important role in the fouling regime of the UF membrane. In this study, 30, 100, and 300 kDa MWCO were evaluated to treat 0.0004 molar ratio of $[Hg]_0/[FeS]_0$ using Regenerated Cellulose (RC) membrane in the four-step process. Figure 4.26 - Figure 4.29 show similar trends for the three MWCO pore size membranes achieving nearly complete Hg(II) removal of the additional feed with no Fe concentration in the permeate and pH stabilized between 6.2-6.5. However, in step 4, a recovery in flux has been observed using 100 kDa and 300 kDa similar to the DE/UF stirred system using 30 kDa. Similar trends have been reported by Peeva et al. (*159*) who studied the effects of MWCO (5 to 300 kDa) on fouling behavior and treatability of HA solutions through PES membranes. Results showed that higher MWCO displayed better treatability despite greater flux decline during the ultrafiltration experiments (*159*). Additionally, Qu et al. (*160*) reported that hydrophilic (cellulose acetate) membranes experience less adsorptive fouling, slower flux decline, and better fouling reversibility compared to hydrophobic (polyethersulfone) membranes when treating extracellular organic matter solution using 10, 100 and 300 kDa MWCO pore sizes (*160*). Membranes with larger pores involved remarkable flux recovery and scarcer adsorptive fouling despite greater flux decline (*160*). Hence, further studies could investigate the removal of Hg(II) applying DE/UF non-stirred system with 100 kDa and 300 kDa with a hydrophilic membrane.

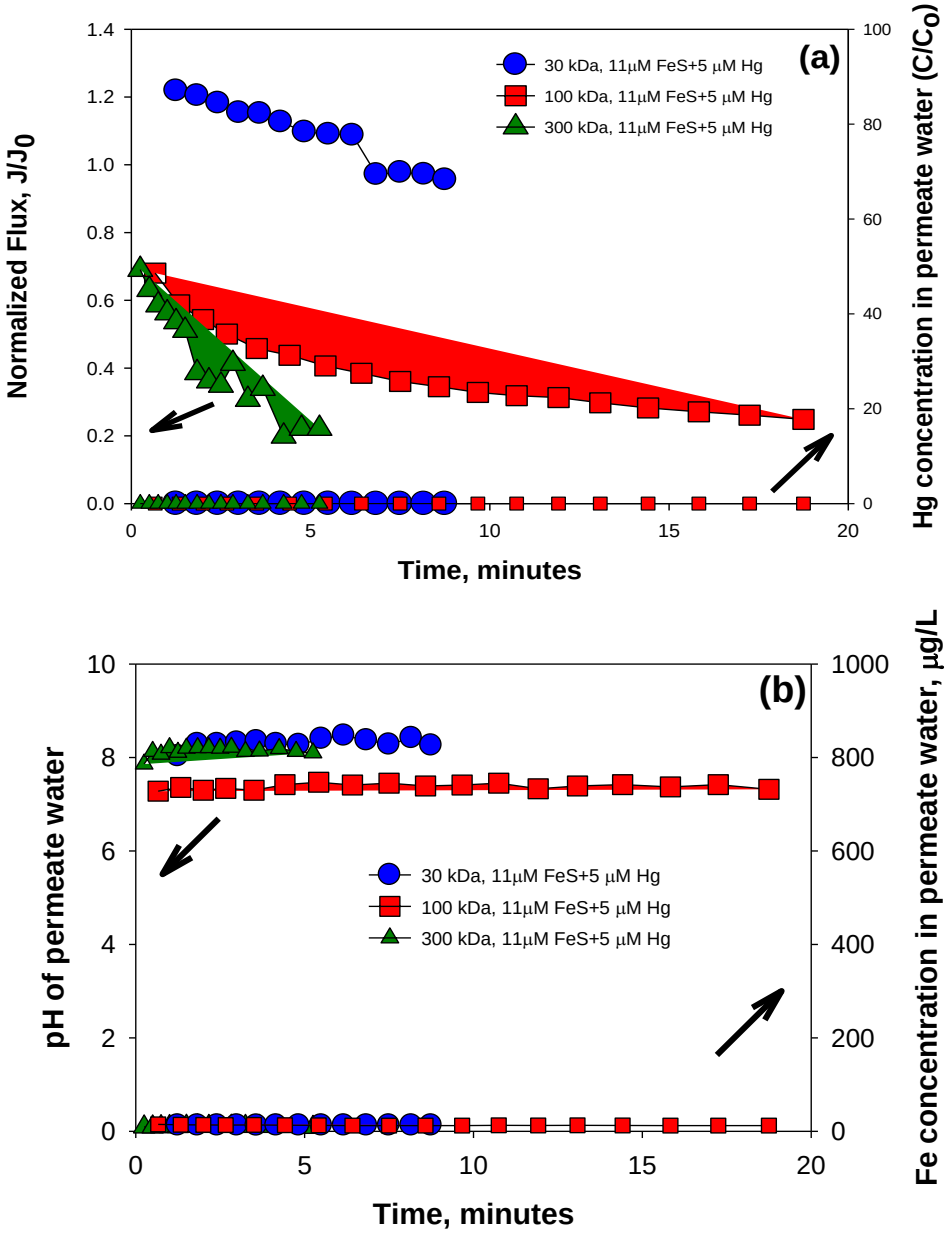

Figure 4.26: Adsorption experimental results using 30 (blue), 100(red), and 300 (green)kDa RC UF membrane: (a) Normalized water flux and relative Hg(II) concentration in permeate water as a function of time, (b) pH and Fe concentration in permeate water as a function of time.

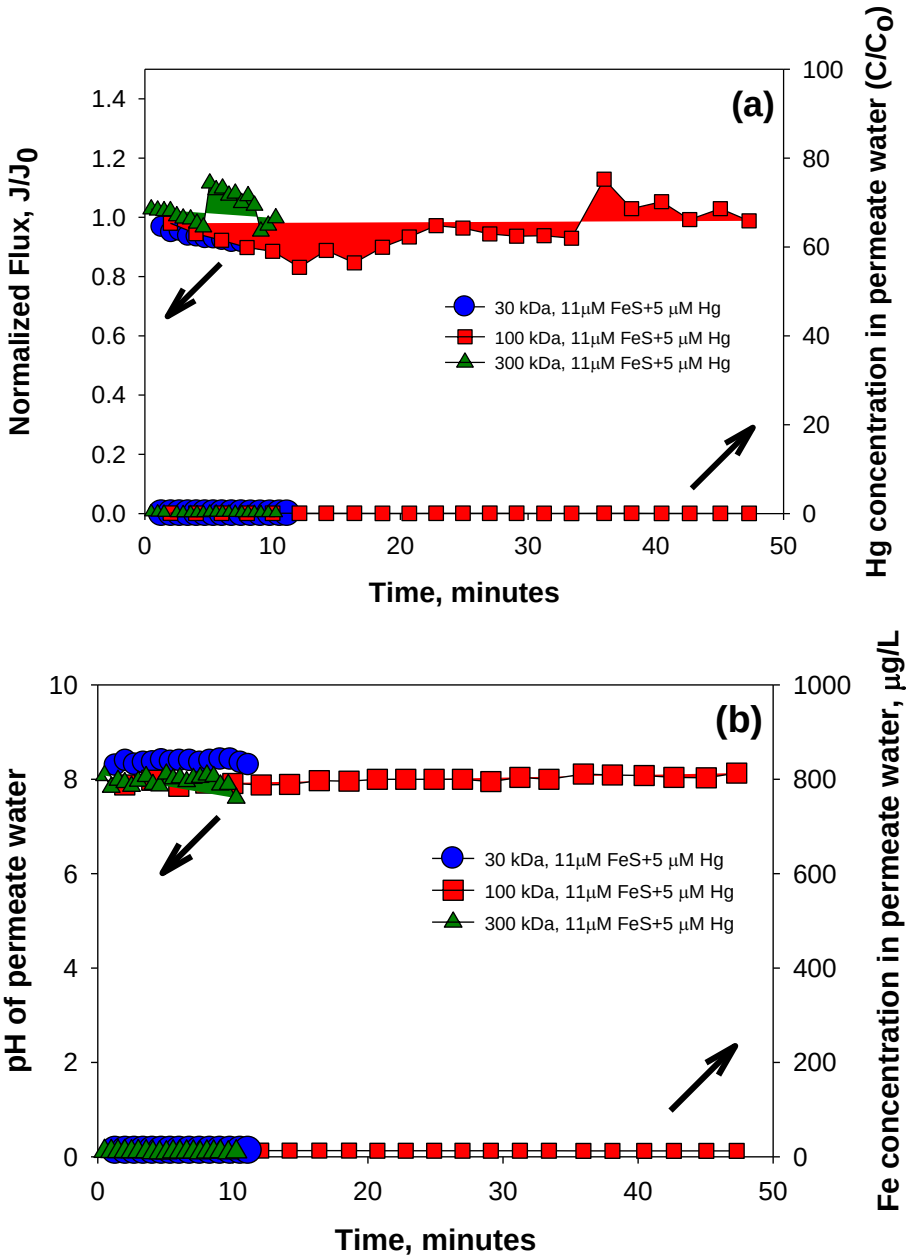

Figure 4.27: Desorption experimental results using 30 (blue), 100 (red), and 300 (green) kDa RC UF membrane: (a) Normalized water flux and relative Hg(II) concentration in permeate water as a function of time, (b) pH and Fe concentration in permeate water as a function of time in non-stirred DE/UF system.

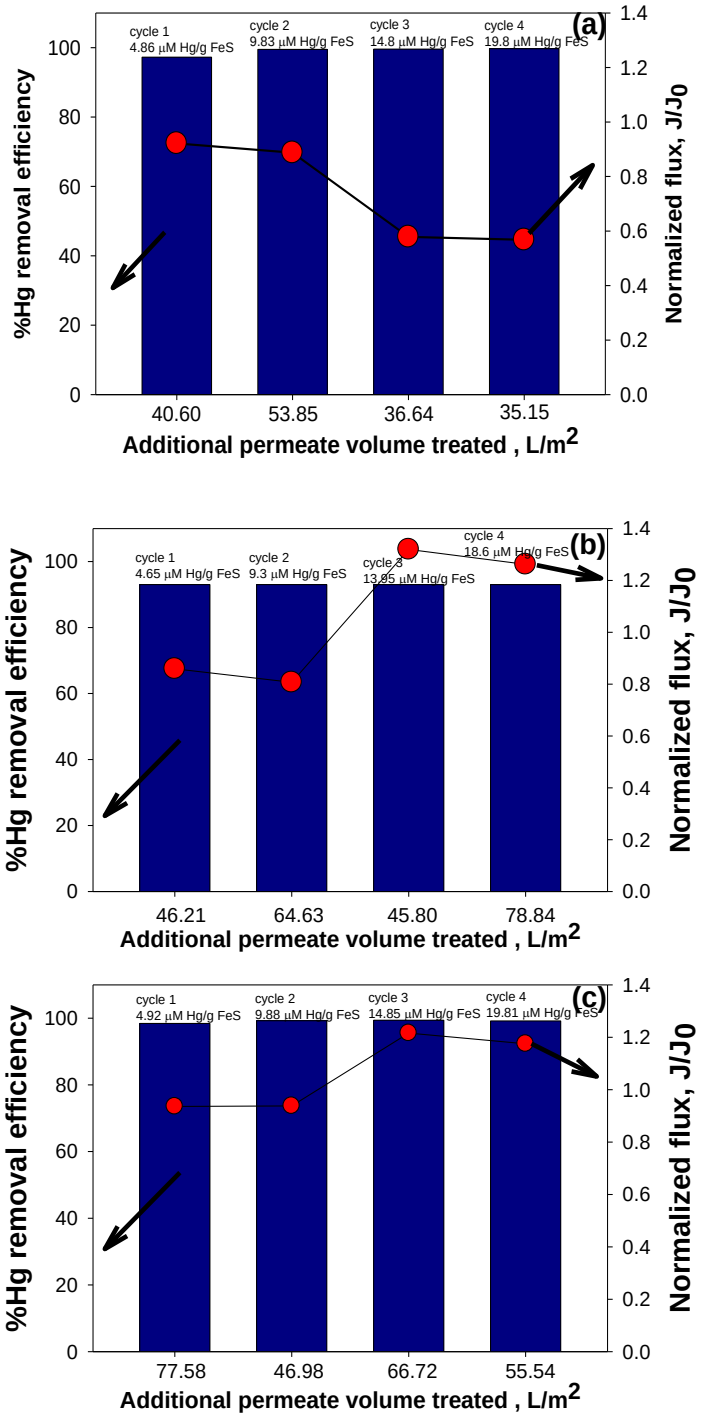

Figure 4.28: Additional sorption capacity experimental results using 11.36 µM FeS+ 5µM Hg with (a) 30, (b) 100, and (c) 300 kDa RC UF membrane represented as %Hg removal and normalized flux as a function of additional treated water volume in non-stirred DE/UF system.

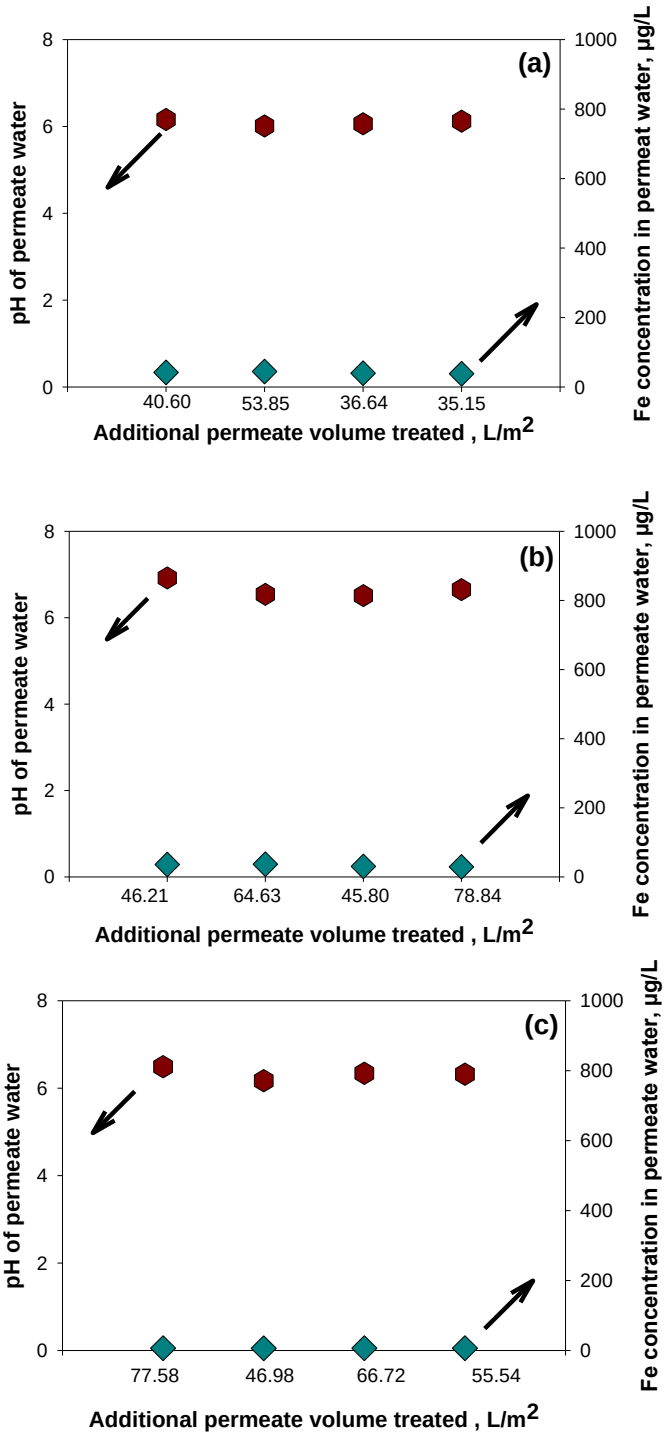

Figure 4.29: Additional sorption capacity results using 11.36 µM FeS+ 5µM Hg with (a) 30, (b) 100, and (c) 300 kDa RC UF membrane represented as pH and Fe concentration in permeate water as a function of additional treated water volume in non-stirred DE/UF system.

4.3. Removal of Hg(II) using FeS-enhanced Cross-Flow Ultrafiltration (CF/UF) system

In addition to a dead-end ultrafiltration system, another continuous contact system was developed using a cross flow ultrafiltration device and retentate recycle (*59, 161*). The cross-flow ultrafiltration system includes a water reservoir where feed solutions are transferred to the CF/UF membrane via a peristaltic pump and the same workflow procedure was applied as the DE/UF experiments.

Based on the previous experiments, it is evident that 1 g/L (11 mM) of FeS is sufficient to remove a wide range of Hg(II) concentrations (500, 1000, 1250 µmol). Hence, for the CF/UF system, the experimental conditions involved 0.1 g/L (1 mM) FeS to evaluate if this even smaller quantity can achieve the desired treatment through a 1000 kDa Biomax (PES) UF membrane (molar ratio $[Hg]_0/[FeS]_0 = 0.004$); 5 µM Hg(II) solution, 0.1M thiosulfate solution for desorption tests, and additional quantity of 5 µM Hg(II) solution. Furthermore, the effect of anions was investigated using 0.01 M anions (Cl^-, NO_3^-, and SO_4^{2-}). To predict the most probable chemical species formed in 5 µM Hg(II) and 0.01 M anions, the MINTEQ chemical equilibrium program was used and revealed that Hg-Cl complexes are present at pH below 8.0 and $Hg(OH)_2$, HgClOH (aq), and $Hg(OH)_3^-$ exist at pH above 8.0 (Figure 4.30). Therefore, this study is expected to involve Hg-Cl complexes in the reaction with FeS.

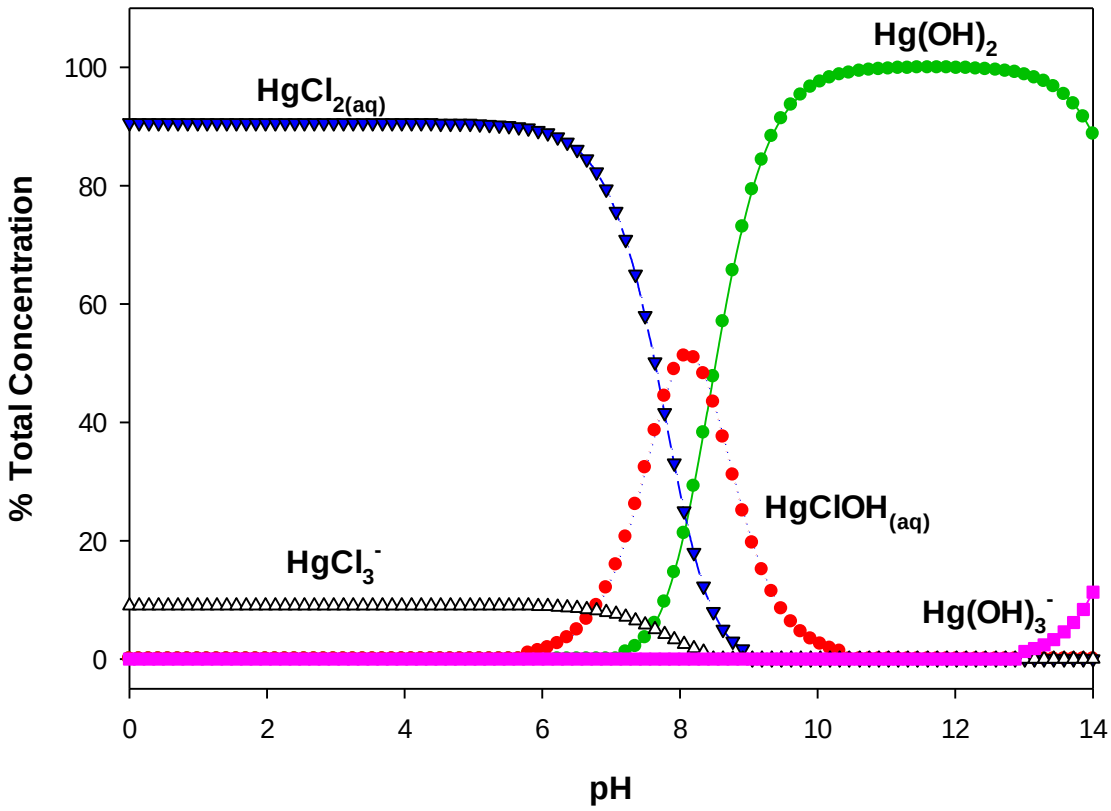

Figure 4.30: Hg(II) speciation as function of pH in the presence of anions, calculated by MINEQL+ Chemical Equilibrium Program with assumption of no solid formation: 25ºC, 5 µM Hg(II), 10 mM anions (Cl^-, NO_3^-, SO_4^{2-}). Reprinted with permission from the publisher, Nova Science Publishes, Inc. (*59*).

The instantaneous permeate flux in the cross-flow ultrafiltration system was calculated at time intervals t_1 and t_2(hr) where A is the effective membrane area (m^2), V is the collected permeate volume (L) as shown in Equation 4.22 below (*161*).

$$J_{CF/UF} = \frac{V_2 - V_1}{A(t_2 - t_1)}; \quad (4.22)$$

Figure 4.31 shows the analyses of the permeate water quality for the CF/UF system in the absence and presence of 0.01 M anions. A noticeable decrease in flux was observed for the experiments without anion and with anions by 36% and 50%, respectively. Hg concentration (C/C_0) for the setup without anions was 0.4 and steadily decreased to 0.2 within 10 minutes (Figure 4.31 a). Hg detected in the presence of anions was considerably less with Hg concentration (C/C_0) reaching 0 from 0.18 in 10 minutes (Figure 4.31 b). pH of the permeate water without anions fluctuated between 6.6-7.3 while the permeate with anions had a lower steady pH at 6.5 (Figure 4.31 c and d). This could be the result of surface redox reactions with Hg(II) reduction to Hg(I) and Fe (II) oxidation to Fe(III) or S(II) to S(0) along with the release of two protons as shown in Equations 4.23-4.25 below (*162*).

$$\equiv Fe^{2+} + Hg \cdots anions \leftrightarrow \equiv Fe^{3+} + Hg(I) \quad (4.23)$$

$$\equiv Fe^{3+} + H_2O \leftrightarrow \equiv FeOH^{2+} + H^+ \quad (4.24)$$

$$\equiv FeOH^{2+} + 2H_2O \leftrightarrow \equiv Fe(OH)_3 + 2H^+ \quad (4.25)$$

Furthermore, since Hg-Cl complexes are more likely to form, adsorption and reduction reactions would not release OH^- ions. Hence, a decrease in pH trend is more probable in the presence of anions. As for x permeate could be from HgS and $\left[Fe_{(1-x)}, Hg_{(x)}\right]S_{(s)}$ precipitation or from the release of Hg-FeS solids. In the presence of anions, the decrease of Fe concentration in the permeate could indicate a different type of mechanism of Hg(II) removal with Fe-anion complex formation.

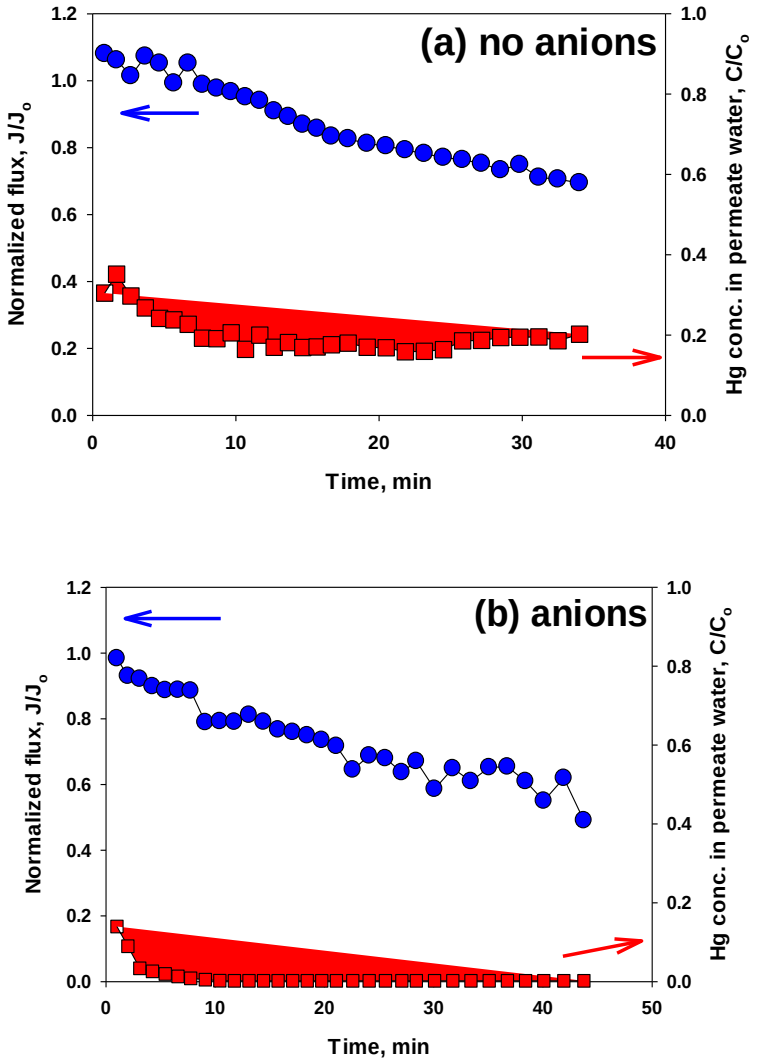

Figure 4.31: (a and b) Variation of normalized water flux and Hg(II) concentration in permeate water during treatment of Hg(II)-FeS suspension using CF/UF-cycling mode (c and d) corresponding pH and Fe concentration in permeate water: 1000 kDa MWCO Biomax UF membrane, 5 µM Hg(II), 0.1 g/L FeS, pH 8, 5 psi (initial flux of deionized water = 230 L/m^2·hr), 10 mM anion mixture (Cl^-, NO_3^-, SO_4^{2-})and N_2-purged continuous contact system. Reprinted with permission from the publisher, Nova Science Publishes, Inc. (*59*).

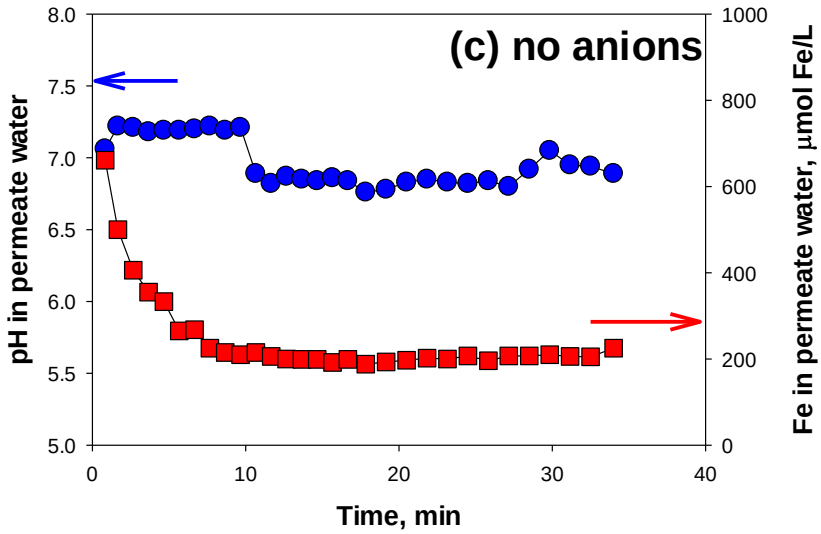

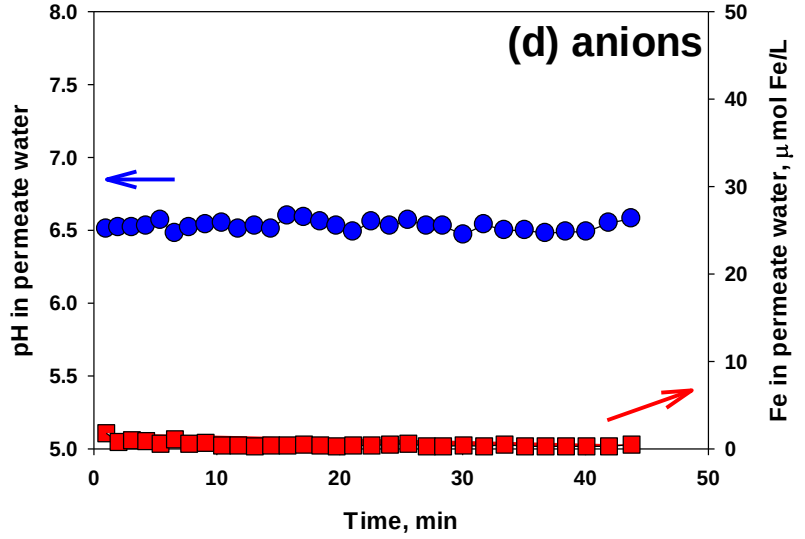

Figure 4.31 Continued

In step 3 (desorption tests), the Hg-contacted FeS in the CF/UF membrane was exposed to 0.1 M thiosulfate solution to evaluate how strong Hg(II) is bonded to the FeS solid phase and can be disposed safely to the environment. Results show no Hg and negligible Fe in the thiosulfate permeate as shown in Figure 4.32. However, more flux decline and pH variation (7.2-8) were observed in the presence of anions. These could be caused by reduced permeability of the

membrane due to increased interaction of anions inside the pores and the release of negatively charged thiosulfate interacting with the anions.

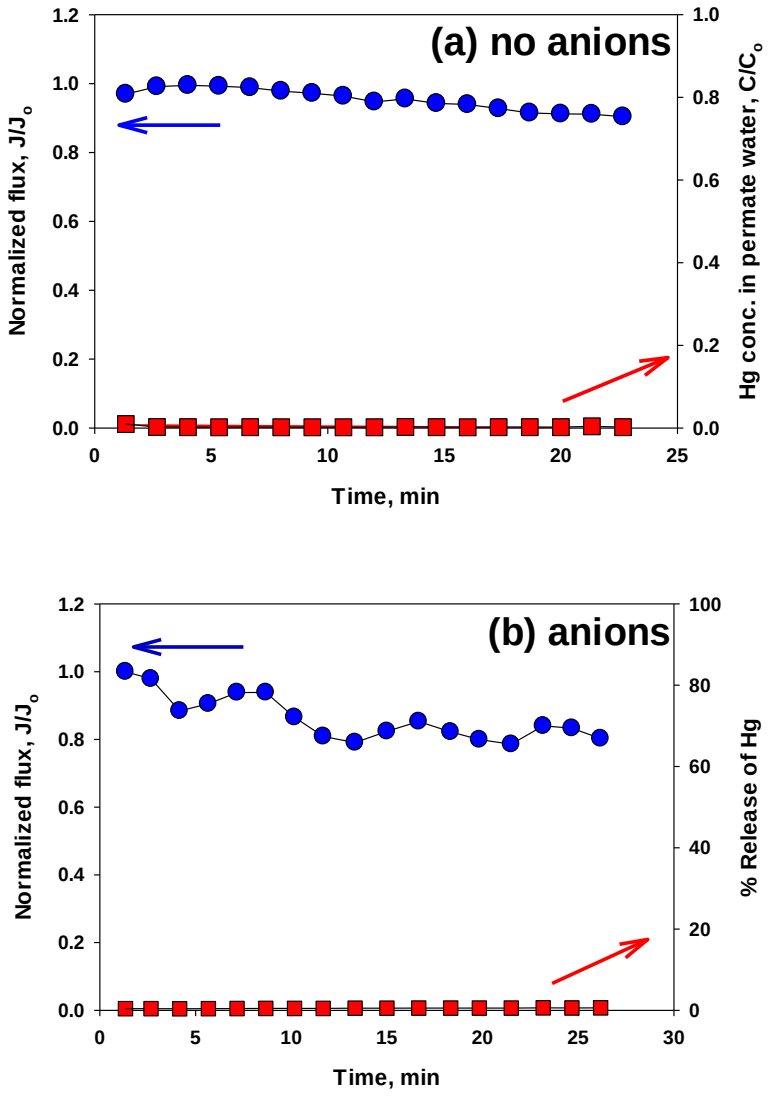

Figure 4.32 (a and b) Normalized flux and Hg concentration during contact of Hg/FeS-laden UF membrane by thiosulfate solution; (c and d) the corresponding pH and Fe concentration in permeate water in CF/UF system: 1000 kDa MWCO Biomax UF membrane, 5 µM Hg(II), 0.1 g/L FeS, pH 8, 0.1M $S_2O_3^-$, 5 psi (initial flux of deionized water = 230 L/m^2·hr), and N_2-purged continuous contact system. Reprinted with permission from the publisher, Nova Science Publishes, Inc. (*59*).

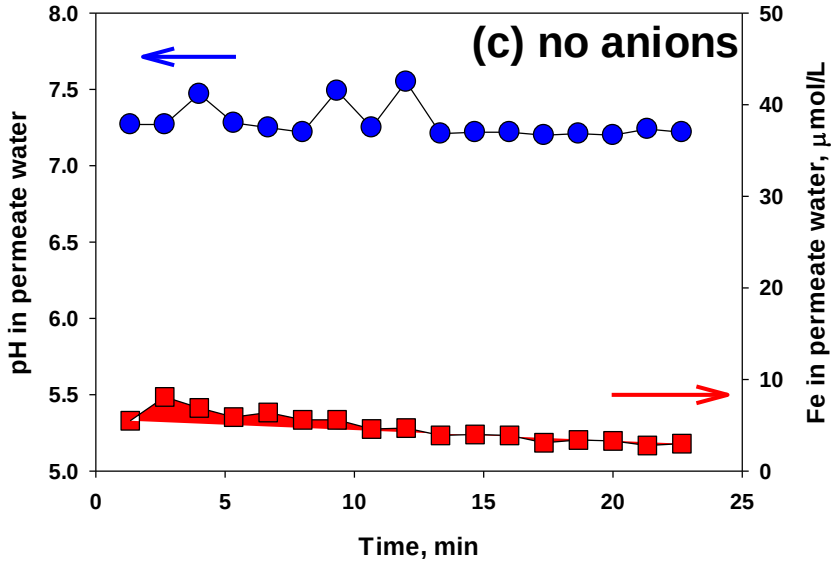

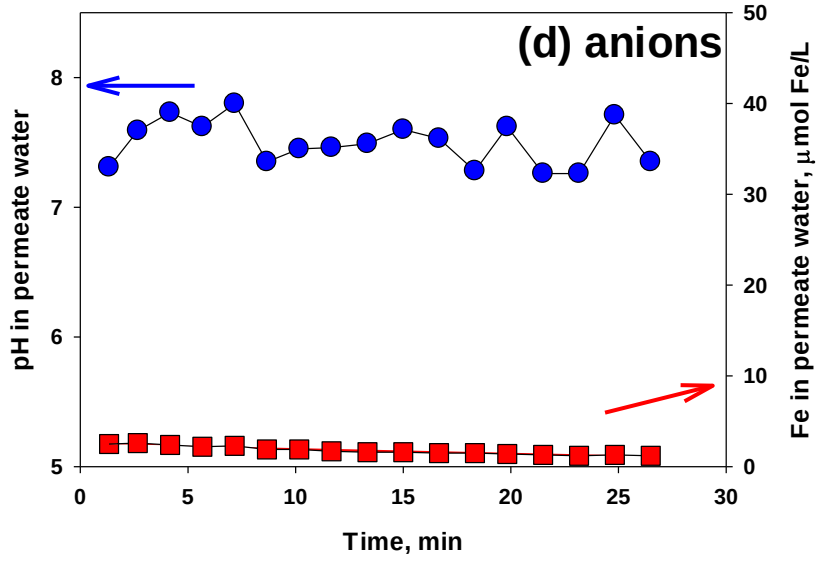

Figure 4.32 Continued

After the desorption tests, additional quantity of 5 μmol of Hg(II) solution was fed through the Hg-FeS laden CF/UF membrane for additional Hg(II) removal capacity evaluation (step 4). As shown in Figure 4.33, Hg(II) removal in the absence of anions decreased from 80% to 15% with 586 L Hg(II) solution; and a more drastic decrease in Hg(II) removal was observed in the presence of anions from 100% to 5 % with 362 L of Hg(II) solution. Though the flux remained relatively stable, the decrease in Hg(II) removal could be attributed to anions competing with Hg(II) for sorption sites and Hg-Cl complexes having less affinity to FeS. In both systems, pH remained within 7.3-7.5 and no Fe release was detected. These trends were also observed in the DE/UF system in stirred mode where the solid phase's color change indicated chemical alteration of FeS and contributed to the decreased Hg(II) removal performance. Thus far, the optimum system for the additional Hg(II) removal with a molar ratio of [Hg]0/[FeS]0 0.0004-0.004 is the DE/UF system in non-stirred mode where 100% Hg(II) removal was achieved with no chemical changes in FeS observed.

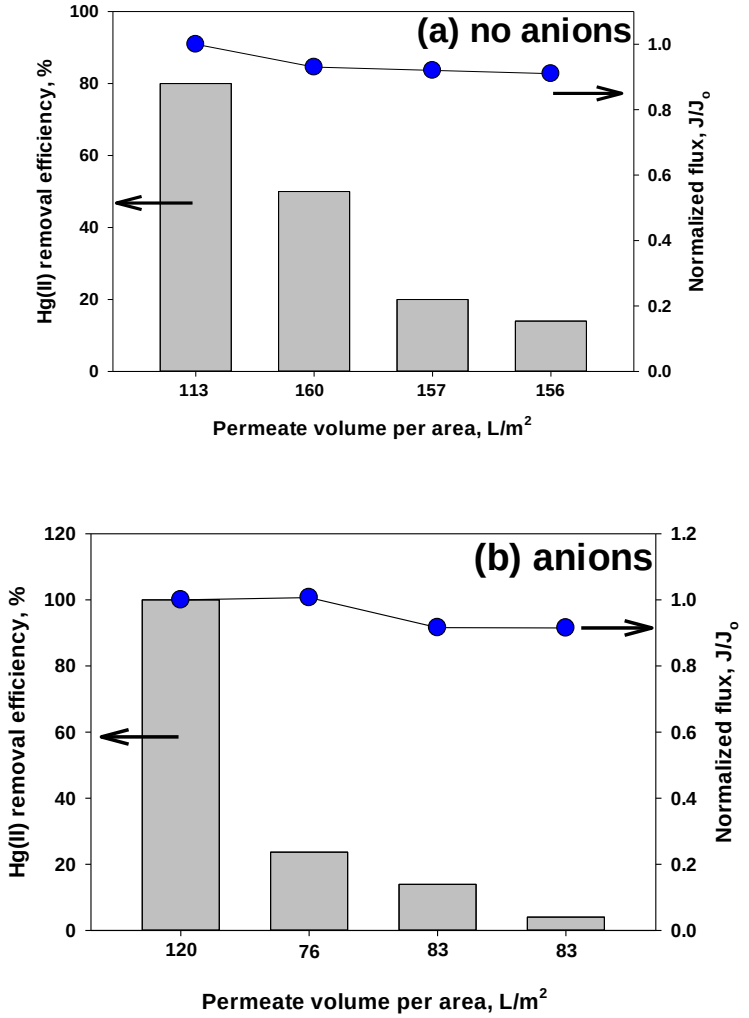

Figure 4.33: Hg(II) removal efficiency (%) and normalized water flux using a Hg/FeS-laden membrane in the CF/UF system. Conditions: 30 kDa MWCO DE/UF membrane, 1 mg/L Hg(II), 0.1 g/L FeS, pH 8, 250 kPa (initial flux of deionized water at 515 L/m^2.hr) and N_2 purged continuous contact system. Reprinted with permission from the publisher, Nova Science Publishes, Inc. (*59*).

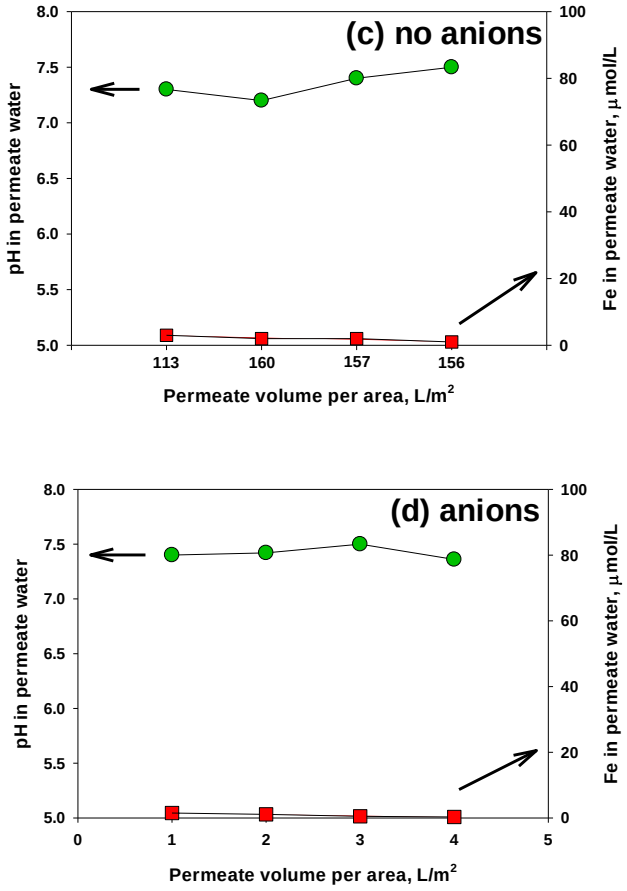

Figure 4.33 Continued**.**

Surface characterization of Hg/FeS Laden Cross-flow Ultrafiltration membrane

Figure 4.34 a and b display the cross-section and top images of the CF/UF membrane. Two spots - flat layer and particle cluster - were magnified as shown in Figure 4.34 c and d. This indicates that the solids were irregularly deposited as clusters and the membrane layer appears like a sieve. To determine if all areas are involved in Hg(II) removal, both spots were analyzed by EDS (Figure 4.34 e and f). Results display Fe, S, O, and Hg presence on spot A (flat surface) and no Fe or Hg on spot B (cluster).

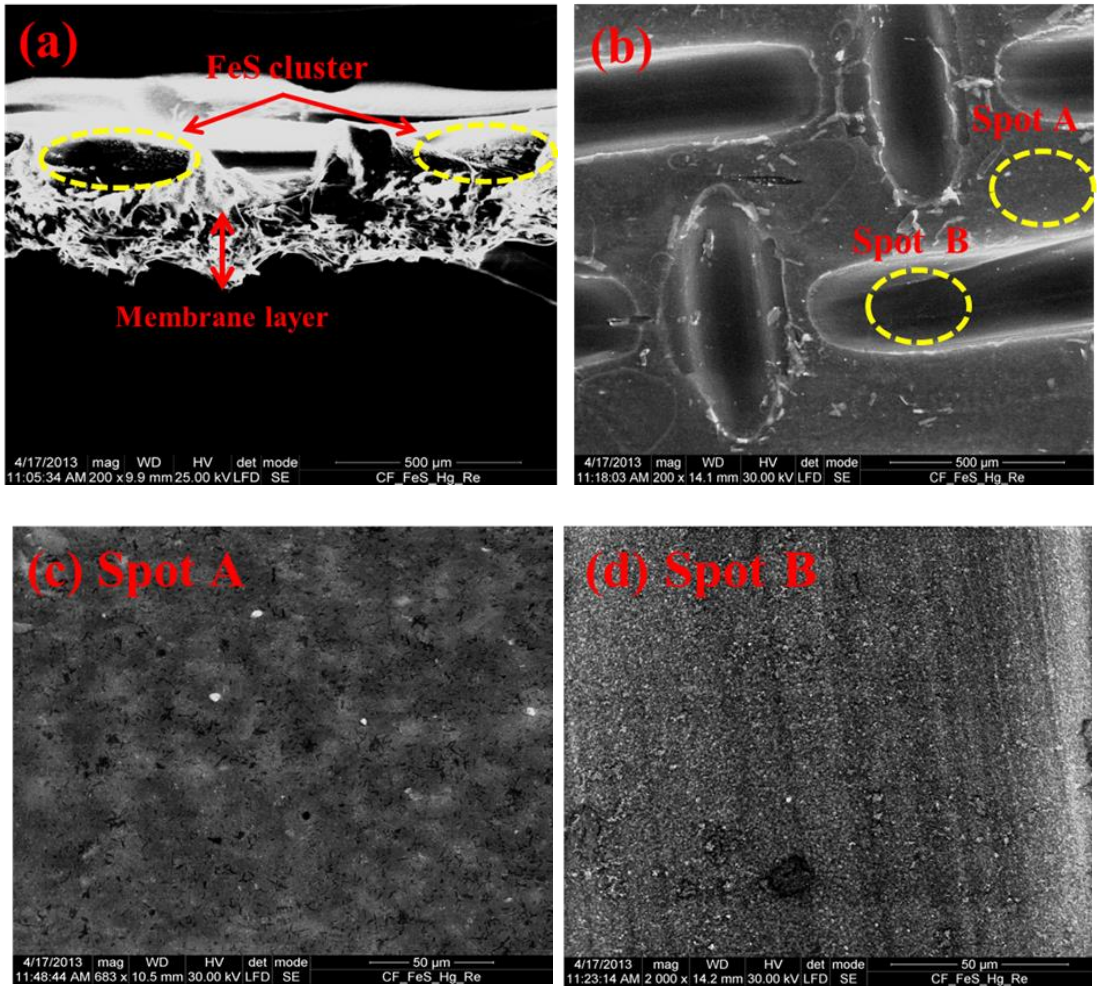

Figure 4.34: SEM/EDS analysis of PES membranes removed from CF/UF system after step IV; (a) cross-section and (b) top-view SEM images, and the magnified images (c, d) and back scattering EDS results (e, f) of spot A and spot B on the top-view image. Conditions: 1 g/L FeS, 5 µM Hg(II), initial pH 8, and N_2-purged continuous contact system. Reprinted with permission from the publisher, Nova Science Publishes, Inc. (*59*).

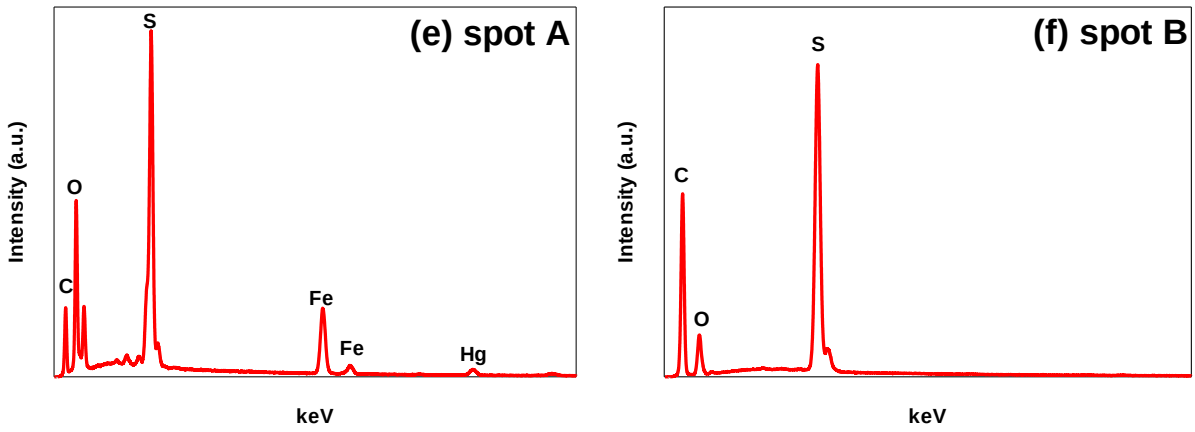

Figure 4.34 Continued.

To further evaluate the effect of the treatment on the CF/UF membrane, ATR/FTIR analysis was conducted on the CF/UF membrane in four phases: (i) prior to starting the experiments, (ii) after being washed with DDW, (iii) after FeS+Hg tests, and (iv) after the FeS+Hg+anions tests. The main characteristic of the CF/UF membrane is the polyethersulfone (PES) structure that shows C=C bond peaks at 1578 and 1485 cm^{-1}. Hence, the extent of variation in these IR peaks pre and post experiments can be used to evaluate the changes occurring on the membrane during the CF/UF treatment process.

Comparing the FTIR results of the membrane before and after washing, the lumped band 3323 cm^{-1} for O-H vanished (Figure 4.35). The strength of the O-H band from the H_2O hydrogen bridges, relates to the diffusion and sorption properties of the membrane (*139-140*). Nevertheless, the free H_2O molecule band at 3650 cm^{-1} was still present in all four phases of the membrane which indicates trapped water molecules in the polymers of the membrane. After the Hg+FeS tests, the C=C bond at 1485 cm^{-1} and bands below 1250 cm^{-1} diminished but did not vanish. This proves that FeS did not develop an impenetrable layer throughout the membrane.

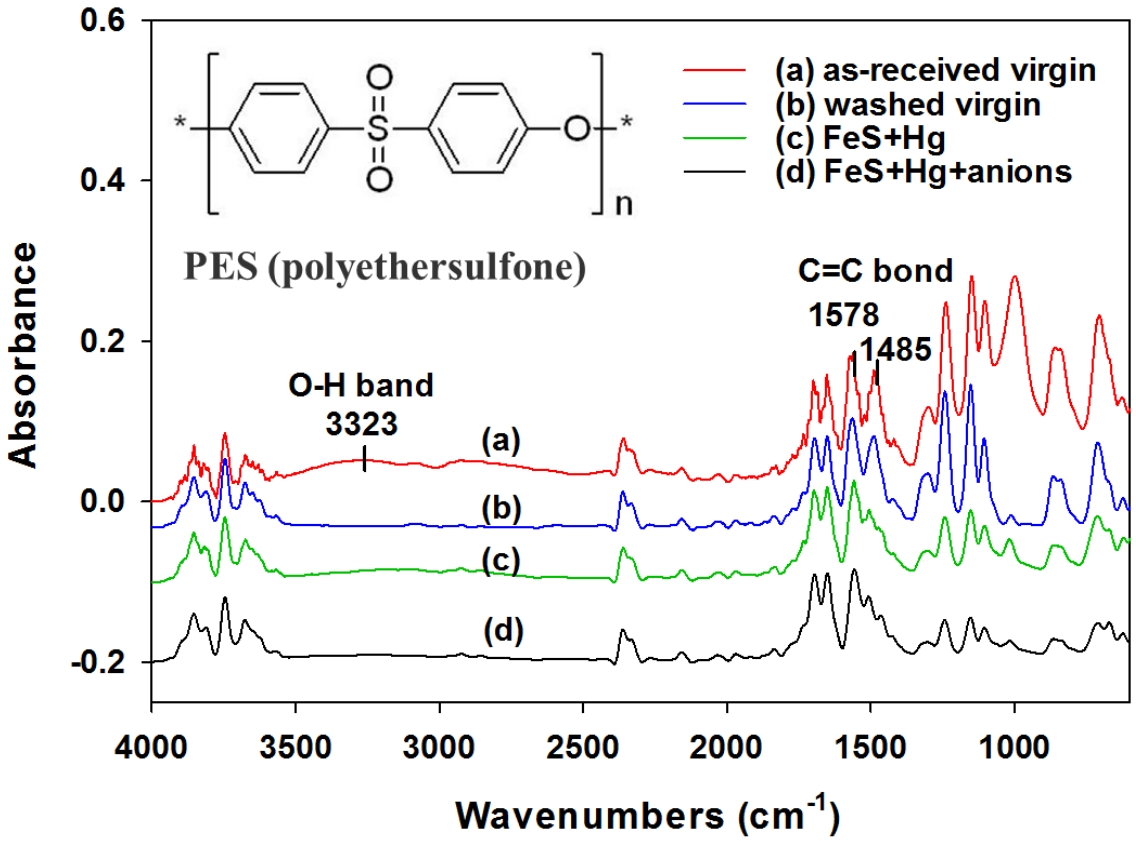

Figure 4.35: ATR/FT-IR results of the PES membranes removed from CF/UF system before and after treating with Hg(II) or mixture of Hg(II) and anions (Cl-, NO3-, SO42-). Reprinted with permission from the publisher, Nova Science Publishes, Inc. (*59*).

5. RECOMMENDATIONS FOR FUTURE WORK

Further studies could investigate the performance of the DE/UF and CF/UF system with higher molar ratios of $[Hg]_0/[FeS]_0$, include more anions (phosphate, iodide, etc.) and natural organic matter (fulvic acids and humins) into the experimental conditions, conduct desorption experiments using CN^- and I^- and compare the results to the performance of $S_2O_3^{2}$. Since FeS nanoparticles have a tendency to aggregate which affects sorption capacity, the application of stabilized FeS nanoparticles (CMC, gelatin, starch, Al_2O_3 etc.) can be applied to the DE/UF system and CF/UF set up (*3, 24, 40*). Additionally, the design parameters for the scale-up of this FeS enhanced ultrafiltration system can be established by conducting cross-flow ultrafiltration experiments at different operation modes. Non-stirred dead-end ultrafiltration mode was applied for constant pressure experiments. Further experimental conditions could include different operational modes such as the constant flux mode (*52*), and using different membrane material: (i) hydrophilic (regenerated cellulose, polyethersulfone, polynvinylidene fluoride), and (ii) hydrophobic (polypropylene) membranes which were found to be more susceptible to fouling compared to hydrophilic membranes (*52, 160, 163*). Additionally, fouling control measures can be studied such as running modes, rinsing, chemical cleaning, and air scouring (*49*).

Maurer-Jones et al. (*164*) assessed the toxicity of various engineered nanoparticles and the environmental implications of the eventual release of such substances into the ecosystem. Deonarine and Hsu-Kim (*165*) suggested that HgS nanoparticles are formed from precipitation reactions in water containing natural organic matter and exist in surface waters. These HgS nanoparticles present in the aquatic environment are known to influence the reactivity and

bioavailability of mercury in the environment (*164-165*). Therefore, there is a need to investigate the environmental effect of nanoparticulate FeS and Hg-S complexes once disposed.

6. CONCLUSION

Batch tests reveal that at lower molar ratios, Hg(II) removal from water was enhanced in the presence of anions through electrostatic interaction, and complete Hg(II) removal was obtained within 10 minutes. Similarly, surface complexation and cation bridging mechanisms contributed to increased adsorption of Hg(II) in the presence of HA for low molar ratios of $[Hg]_0/[FeS]_0$ = 0.0005. This is attributed to less Hg(II) is available for competition with HA for FeS active sites. The effect of anions become more evident at high molar ratios $[Hg]_0/[FeS]_0$ = 0.05 as Hg(II) removal with FeS is slightly reduced due to competition for FeS active sites and HgCl complexes have a lower affinity to FeS compared to Hg-OH complexes. Nevertheless, complete Hg(II) removal was achieved after 60 min. Desorption tests show that no Hg release was detected after 24 hours with 0.1 M thiosulfate solution.

FeS nanoparticles-supported dead-end (non-stirred and stirred mode) and crossflow ultrafiltration systems were developed. Results have successfully proven that these systems can remove Hg(II) from water using molar ratios of $[Hg]_0/[FeS]_0$ as 0.0004 (DE/UF) and 0.004 (CF/UF) in the presence of 0.01 M anions (Cl^-, NO_3^-, and SO_4^{2-}) or 1 mg/L HA at pH 8 with 30 kDa RC UF membrane (DE/UF) and 1000 kDa biomax PES UF membrane (CF/UF). Adsorption experiments affirm that FeS is a good scavenger for Hg(II). The effect of anions causes a slightly acidic environment due to surface redox reactions during the adsorption tests. In the CF/UF system, the presence of anions revealed 57% of initial Fe in the permeate then reduced to 18% after 10 minutes indicating Fe release from HgS and $\left[Fe_{(1-x)}, Hg_{(x)}\right]S_{(s)}$ precipitation or release from Hg-FeS solids and Fe-anion complex formation.

Desorption tests using 0.1M sodium thiosulfate ($Na_2S_2O_3$) solution demonstrated that the final Hg(II)-contacted FeS solids on the membrane in all the experimental conditions in both ultrafiltration systems were chemically stable because no Hg release was detected. Furthermore, no Fe(II) release was observed in the presence of anions in both DE/UF and CF/UF systems due to Fe-anion complex formation. However, initial Fe release was observed in the DE/UF non-stirred and stirred systems in the absence and presence of humic acid (HA) as surface redox reactions were promoted by the thiosulfate solution.

Additional Hg(II) removal capacity tests using 5µM Hg(II) solutions) revealed that the Hg-contacted FeS nanoparticles could be reused for supplementary treatment. The DE/UF non-stirred system achieved complete additional Hg(II) removal in the absence and presence of anions and HA. This proves that at a low $[Hg]_0/[FeS]_0$ ratio of 0.0004, the Cl^- ions and HA enhanced the Hg(II) removal from the permeate. Conversely, decreased additional Hg(II) removal capacity was observed for Hg(II)-contacted FeS in DE/UF stirred mode and CF/UF systems after the 1st regeneration cycle. This could be due to the shear effect (in the DE/UF stirred system) and tangential flow (in the CF/UF system) promoting oxidation or chemical variation on the Hg(II) contacted-FeS. Hence, caution must be taken to avoid changes to the FeS particles.

Surface analyses of the Hg(II) contacted FeS nanoparticles, conducted after step 4 (additional Hg(II) removal tests), exhibit non-uniform rock-like morphologies with a reversible cake layer formed at the surface of the membrane. Hg loading on the membrane was higher in the presence of HA (17-35%) and anions (12-25%) compared to experiments with FeS and Hg(II) alone. For the CF/UF system, ATR/FTIR analysis provided evidence that the membrane surface was fully covered with Hg-contacted FeS without forming an impenetrable coating on the UF membrane. However, both anions and HA have shown to negatively impact the permeability of

the membrane resulting in greater flux decline which entails frequent maintenance operations on a commercial scale. HA demonstrated a greater impact on the membrane permeability compared to anions due to the formation of larger Hg-HA that could also be adsorbed by the UF membrane filter in addition to the FeS particles

Compared to the DE/UF non-stirred mode, the DE/UF stirred mode exhibited flux recovery as the shear effect reduced the cake formation on the membrane. The effect of MWCO in the DE/UF (non-stirred) system influences flux recovery which was observed for 100 kDa and 300 kDa compared to 30 kDa during the additional Hg(II) removal capacity experiments. Despite initial flux decline, membranes with larger pores exhibit remarkable flux recovery and scarcer adsorptive fouling which results in less maintenance costs.

Overall, these findings present fundamental data that could be applied in the advancement of Hg(II)-contaminated water treatment in dead-end or cross flow ultrafiltration using low cost FeS adsorbents to achieve the target of 10 µg/L total mercury in wastewater and 1µg/L inorganic mercury in drinking water (*3, 48, 161*). With the specified experimental conditions, the DE/UF and CF/UF system produced stable Hg-contacted FeS particles that can be reused and eventually disposed safely in the environment. Consequently, this study can serve as a guideline for continuous treatment of other toxic inorganic chemicals (Pb^{2+}, Co^{2+}, As^{3+}, Cd^{2+}, Zn^{2+} etc.).

REFERENCES

1. Mekonnen, M. M.; Hoekstra, A. Y., Four billion people facing severe water scarcity. *Science Advances* **2016,** *2* (2).

2. Carolin, C. F.; Kumar, P. S.; Saravanan, A.; Joshiba, G. J.; Naushad, M., Efficient techniques for the removal of toxic heavy metals from aquatic environment: A review. *Journal of Environmental Chemical Engineering* **2017,** *5* (3), 2782-2799.

3. Sun, Y.; Liu, Y.; Lou, Z.; Yang, K.; Lv, D.; Zhou, J.; Baig, S. A.; Xu, X., Enhanced performance for Hg(II) removal using biomaterial (CMC/gelatin/starch) stabilized FeS nanoparticles: Stabilization effects and removal mechanism. *Chemical Engineering Journal* **2018,** *344*, 616-624.

4. Chen, C. Y.; Driscoll, C. T.; Eagles-Smith, C. A.; Eckley, C. S.; Gay, D. A.; Hsu-Kim, H.; Keane, S. E.; Kirk, J. L.; Mason, R. P.; Obrist, D.; Selin, H.; Selin, N. E.; Thompson, M. R., A Critical Time for Mercury Science to Inform Global Policy. *Environmental Science & Technology* **2018,** *52* (17), 9556-9561.

5. Yu, J.-G.; Yue, B.-Y.; Wu, X.-W.; Liu, Q.; Jiao, F.-P.; Jiang, X.-Y.; Chen, X.-Q., Removal of mercury by adsorption: a review. *Environmental Science & Pollution Research* **2016,** *23* (6), 5056-5076.

6. Outridge, P. M.; Mason, R. P.; Wang, F.; Guerrero, S.; Heimbürger-Boavida, L. E., Updated Global and Oceanic Mercury Budgets for the United Nations Global Mercury Assessment 2018. *Environmental Science & Technology* **2018,** *52* (20), 11466-11477.

7. Mekonnen, M. M.; Gerbens-Leenes, P. W.; Hoekstra, A. Y., The consumptive water footprint of electricity and heat: a global assessment. 2015; Vol. 1, pp 285-297.

8. Obrist, D.; Kirk, J. L.; Zhang, L.; Sunderland, E. M.; Jiskra, M.; Selin, N. E., A review of global environmental mercury processes in response to human and natural perturbations: Changes of emissions, climate, and land use. *Ambio* **2018,** *47* (2), 116-140.

9. UNEP; GESAMP/WG37, Mercury in the Aquatic Environment: Sources, Releases, Transport and Monitoring. **2011**.

10. U.S Department of the Interior, U. S. G. S., Methylmercury. 2013.

11. Kudo, A.; Fujikawa, Y.; Miyahara, S.; Zheng, J.; Takigami, H.; Sugahara, M.; Muramatsu, T., Lessons from Minamata mercury pollution, Japan—after a continuous 22 years of observation. *Water Science and Technology* **1998,** *38* (7), 187-193.

12. Tsubaki, T.; Irukayama, K., *Minamata disease. Methylmercury poisoning in Minamata and Niigata, Japan*. North-Holland Publishing Company, PO Box 211, Amsterdam, The Netherlands.: 1977.

13. Amin-Zaki, L.; Elhassani, S.; Majeed, M. A.; Clarkson, T. W.; Doherty, R. A.; Greenwood, M., Intra-uterine methylmercury poisoning in Iraq. *Pediatrics* **1974,** *54* (5), 587-595.

14. Xu, J.; Cao, Z.; Zhang, Y.; Yuan, Z.; Lou, Z.; Xu, X.; Wang, X., A review of functionalized carbon nanotubes and graphene for heavy metal adsorption from water: Preparation, application, and mechanism. *Chemosphere* **2018,** *195*, 351-364.

15. Vikrant, K.; Kim, K.-H., Nanomaterials for the adsorptive treatment of Hg(II) ions from water. *Chemical Engineering Journal* **2019,** *358*, 264-282.

16. Otto, M.; Bajpai, S., Treatment technologies for mercury in soil, waste, and water. *Remediation Journal* **2007,** *18* (1), 21-28.

17. Fu, F.; Wang, Q., Removal of heavy metal ions from wastewaters: A review. *Journal of Environmental Management* **2011,** *92* (3), 407-418.

18. Niu, Y.; Qu, R.; Chen, H.; Mu, L.; Liu, X.; Wang, T.; Zhang, Y.; Sun, C., Synthesis of silica gel supported salicylaldehyde modified PAMAM dendrimers for the effective removal of Hg(II) from aqueous solution. *Journal of Hazardous Materials* **2014,** *278*, 267-278.

19. Brown, J. R.; Bancroft, G. M.; Fyfe, W. S.; McLean, R. A., Mercury removal from water by iron sulfide minerals. An electron spectroscopy for chemical analysis (ESCA) study. *Environmental Science & Technology* **1979,** *13* (9), 1142-1144.

20. Wolfenden, S.; Charnock, J. M.; Hilton, J.; Livens, F. R.; Vaughan, D. J., Sulfide species as a sink for mercury in lake sediments. *Environmental science & technology* **2005,** *39* (17), 6644-6648.

21. Jeong, H.; Klaue, B.; Blum, J. D.; Hayes, K. F., Sorption of mercuric ion by synthetic nanocrystalline mackinawite (FeS). *Environmental science & technology* **2007,** *41* (22), 7699-705.

22. Liu, J.; Valsaraj, K. T.; Devai, I.; DeLaune, R. D., Immobilization of aqueous Hg(II) by mackinawite (FeS). *Journal of Hazardous Materials* **2008,** *157* (2–3), 432-440.

23. Jeong, H. Y.; Sun, K.; Hayes, K. F., Microscopic and spectroscopic characterization of Hg (II) immobilization by mackinawite (FeS). *Environmental science & technology* **2010,** *44* (19), 7476-7483.

24. Sun, Y.; Lou, Z.; Yu, J.; Zhou, X.; Lv, D.; Zhou, J.; Baig, S. A.; Xu, X., Immobilization of mercury (II) from aqueous solution using Al2O3-supported nanoscale FeS. *Chemical Engineering Journal* **2017,** *323*, 483-491.

25. Morse, J. W.; Arakaki, T., Adsorption and coprecipitation of divalent metals with mackinawite (FeS). *Geochimica et Cosmochimica Acta* **1993,** *57* (15), 3635-3640.

26. Rickard, D.; Schoonen, M. A.; Luther, G. In *Chemistry of iron sulfides in sedimentary environments*, ACS Symposium Series, ACS Publications: 1995; pp 168-193.

27. Han, D. S. Sorption of Arsenic, Mercury, Selenium onto Nanostructured Adsorbent Media and Stabilization via Surface Reactions. Doctoral Thesis, Texas A&M University, 2009.

28. Benning, L. G.; Wilkin, R. T.; Barnes, H., Reaction pathways in the Fe–S system below 100 C. *Chemical Geology* **2000,** *167* (1), 25-51.

29. Gong, Y.; Tang, J.; Zhao, D., Application of iron sulfide particles for groundwater and soil remediation: A review. *Water Research* **2016,** *89*, 309-320.

30. Han, D. S.; Batchelor, B.; Abdel-Wahab, A., Sorption of selenium (IV) and selenium (VI) to mackinawite (FeS): Effect of contact time, extent of removal, sorption envelopes. *Journal of hazardous materials* **2011,** *186* (1), 451-457.

31. Mullet, M.; Boursiquot, S.; Ehrhardt, J.-J., Removal of hexavalent chromium from solutions by mackinawite, tetragonal FeS. *Colloids and Surfaces A: Physicochemical and Engineering Aspects* **2004,** *244* (1), 77-85.

32. Gallegos, T. J.; Hyun, S. P.; Hayes, K. F., Spectroscopic investigation of the uptake of arsenite from solution by synthetic mackinawite. *Environmental science & technology* **2007,** *41* (22), 7781-7786.

33. Livens, F. R.; Jones, M. J.; Hynes, A. J.; Charnock, J. M.; Mosselmans, J. F. W.; Hennig, C.; Steele, H.; Collison, D.; Vaughan, D. J.; Pattrick, R. A., X-ray absorption spectroscopy studies of reactions of technetium, uranium and neptunium with mackinawite. *Journal of environmental radioactivity* **2004,** *74* (1), 211-219.

34. Parkman, R.; Charnock, J.; Bryan, N.; Livens, F.; Vaughan, D., Reactions of copper and cadmium ions in aqueous solution with goethite, lepidocrocite, mackinawite, and pyrite. *American Mineralogist* **1999,** *84*, 407-419.

35. Arakaki, T.; Morse, J. W., Coprecipitation and adsorption of Mn(II) with mackinawite (FeS) under conditions similar to those found in anoxic sediments. *Geochimica et Cosmochimica Acta* **1993,** *57* (1), 9-14.

36. Jeong, H. Y.; Klaue, B.; Blum, J. D.; Hayes, K. F., Sorption of mercuric ion by synthetic nanocrystalline mackinawite (FeS). *Environmental Science & Technology* **2007,** *41* (22), 7699-7705.

37. Pacheco, S.; Medina, M.; Valencia, F.; Tapia, J., Removal of Inorganic Mercury from Polluted Water Using Structured Nanoparticles. *Journal of Environmental Engineering* **2006,** *132* (3), 342-349.

38. Skubal, L. R.; Meshkov, N. K., Reduction and removal of mercury from water using arginine-modified TiO2. *Journal of Photochemistry and Photobiology A: Chemistry* **2002,** *148* (1–3), 211-214.

39. Skyllberg, U.; Drott, A., Competition between disordered iron sulfide and natural organic matter associated thiols for mercury (II)□ An EXAFS study. *Environmental science & technology* **2010,** *44* (4), 1254-1259.

40. Gong, Y.; Liu, Y.; Xiong, Z.; Zhao, D., Immobilization of Mercury by Carboxymethyl Cellulose Stabilized Iron Sulfide Nanoparticles: Reaction Mechanisms and Effects of Stabilizer and Water Chemistry. *Environmental Science & Technology* **2014,** *48* (7), 3986-3994.

41. Lisha, K.; Pradeep, A.; Pradeep, T., Towards a practical solution for removing inorganic mercury from drinking water using gold nanoparticles. *Gold Bulletin* **2009,** *42* (2).

42. Savage, N.; Diallo, M. S., Nanomaterials and Water Purification: Opportunities and Challenges. *Journal of Nanoparticle Research* **2005,** *7* (4), 331-342.

43. Liu, J.; Dai, C.; Hu, Y., Aqueous aggregation behavior of citric acid coated magnetite nanoparticles: Effects of pH, cations, anions, and humic acid. *Environmental Research* **2018,** *161*, 49-60.

44. Jawor, A.; Hoek, E. M. V., Removing Cadmium Ions from Water via Nanoparticle-Enhanced Ultrafiltration. *Environmental Science & Technology* **2010,** *44* (7), 2570-2576.

45. Dou, B.; Chen, H., Removal of toxic mercury(II) from aquatic solutions by synthesized TiO2 nanoparticles. *Desalination* **2011,** *269* (1–3), 260-265.

46. Sheela, T., Nayaka, Y.A., Viswanatha, R., Basavanna, S., Venkatesha, T.G., Kinetics and thermodynamics studies on the adsorption of Zn(II), Cd(II), and Hg(II) from aqueous solution using zinc oxide nanoparticles. *Powder Technology* **2012,** *217*, 163-170.

47. Liu, J.; Valsaraj, K. T.; Devai, I.; DeLaune, R., Immobilization of aqueous Hg (II) by mackinawite (FeS). *Journal of hazardous materials* **2008,** *157* (2), 432-440.

48. Han, D. S.; Orillano, M.; Khodary, A.; Duan, Y.; Batchelor, B.; Abdel-Wahab, A., Reactive iron sulfide (FeS)-supported ultrafiltration for removal of mercury (Hg(II)) from water. *Water Research* **2014,** *53* (0), 310-321.

49. Gao, W.; Liang, H.; Ma, J.; Han, M.; Chen, Z.-l.; Han, Z.-s.; Li, G.-b., Membrane fouling control in ultrafiltration technology for drinking water production: A review. *Desalination* **2011,** *272* (1–3), 1-8.

50. Cui, X.; Choo, K.-H., Natural Organic Matter Removal and Fouling Control in Low-Pressure Membrane Filtration for Water Treatment. *Environmental Engineering Research* **2014,** *19* (1), 1-8.

51. Sablani, S. S.; Goosen, M. F. A.; Al-Belushi, R.; Wilf, M., Concentration polarization in ultrafiltration and reverse osmosis: a critical review. *Desalination* **2001,** *141* (3), 269-289.

52. Lee, E. K.; Chen, V.; Fane, A., Natural organic matter (NOM) fouling in low pressure membrane filtration—effect of membranes and operation modes. *Desalination* **2008,** *218* (1), 257-270.

53. Bourgeous, K. N.; Darby, J. L.; Tchobanoglous, G., Ultrafiltration of wastewater: effects of particles, mode of operation, and backwash effectiveness. *Water Research* **2001,** *35* (1), 77-90.

54. Lanteri, Y.; Fievet, P.; Magnenet, C.; Déon, S.; Szymczyk, A., Electrokinetic characterisation of particle deposits from streaming potential coupled with permeate flux measurements during dead-end filtration. *Journal of Membrane Science* **2011,** *378* (1–2), 224-232.

55. Mendret, J.; Guigui, C.; Schmitz, P.; Cabassud, C., In situ dynamic characterisation of fouling under different pressure conditions during dead-end filtration: compressibility properties of particle cakes. *Journal of Membrane Science* **2009,** *333* (1), 20-29.

56. Xiao, K.; Shen, Y.; Huang, X., An analytical model for membrane fouling evolution associated with gel layer growth during constant pressure stirred dead-end filtration. *Journal of Membrane Science* **2013,** *427* (0), 139-149.

57. Kim, J.; DiGiano, F. A., Fouling models for low-pressure membrane systems. *Separation and Purification Technology* **2009,** *68* (3), 293-304.

58. Van den Berg, G. B.; Smolders, C. A., Flux decline in ultrafiltration processes. *Desalination* **1990,** *77*, 101-133.

59. Han, D. S.; Orillano, M.; Duan, Y.; Batchelor, B.; Park, H.; Abdel-Wahab, A.; Nidal, H., *Effect of anions on removal of mercury(II) using fes-supported crossflow ultrafiltration*. Nova Science Publishers, Inc.: USA, 2017; p 129-152.

60. Titretir Duran, S.; Karagözler, A. E., Comparison of plain and indoline modified mercury film electrodes for determination of lead, cadmium and copper in urine samples by anodic stripping voltammetry. *Polymer Bulletin* **2018**.

61. Beckers, F.; Rinklebe, J. In *Cycling of mercury in the environment: Sources, fate, and human health implications: A review*, United States, 2017; Taylor & Francis: United States, 2017; p 693.

62. Okpala, C. O. R.; Sardo, G.; Vitale, S.; Bono, G.; Arukwe, A., Hazardous properties and toxicological update of mercury: From fish food to human health safety perspective. *Critical Reviews in Food Science and Nutrition* **2018,** *58* (12), 1986-2001.

63. Risher, J. F.; Amler, S. N., Mercury Exposure: Evaluation and Intervention: The Inappropriate Use of Chelating Agents in the Diagnosis and Treatment of Putative Mercury Poisoning. *NeuroToxicology* **2005,** *26* (4), 691-699.

64. Morel, F. M.; Kraepiel, A. M.; Amyot, M., The chemical cycle and bioaccumulation of mercury. *Annual review of ecology and systematics* **1998,** *29* (1), 543-566.

65. Nriagu, J. O., *The biogeochemistry of mercury in the environment*. Elsevier/North-Holland Biomedical Press.: 1979.

66. Davis, S. N.; DeWiest, R., Hydrogeology, 463. John Wiley, New York: 1966.

67. Allard, B.; Arsenie, I., Abiotic reduction of mercury by humic substances in aquatic system — an important process for the mercury cycle. *Water Air & Soil Pollution* **1991,** *56* (1), 457-464.

68. Gilmour, J., Inorganic complexes of divalent mercury in natural water systems. *Environmental letters* **1971,** *2* (3), 143-152.

69. Hahne, H.; Kroontje, W., Significance of pH and chloride concentration on behavior of heavy metal pollutants: mercury (II), cadmium (II), zinc (II), and lead (II). *Journal of Environmental Quality* **1973,** *2* (4), 444-450.

70. Gu, B.; Bian, Y.; Miller, C. L.; Dong, W.; Jiang, X.; Liang, L., Mercury reduction and complexation by natural organic matter in anoxic environments. *Proceedings of the National Academy of Sciences* **2011,** *108* (4), 1479-1483.

71. Miskimmin, B. M.; Rudd, J. W.; Kelly, C. A., Influence of dissolved organic carbon, pH, and microbial respiration rates on mercury methylation and demethylation in lake water. *Canadian Journal of Fisheries and Aquatic Sciences* **1992,** *49* (1), 17-22.

72. Schaefer, J. K.; Morel, F. M., High methylation rates of mercury bound to cysteine by Geobacter sulfurreducens. *Nature geoscience* **2009,** *2* (2), 123-126.

73. Bradl, H. B., Adsorption of heavy metal ions on soils and soils constituents. *Journal of Colloid and Interface Science* **2004,** *277* (1), 1-18.

74. Apak, R., Adsorption of heavy metal ions on soil surfaces and similar substances. In *Encyclopedia of Surface and Colloid Science, Dekker Encylopedias*, 2nd ed.; Hubbard, A. T., Ed. New York, 2002; pp 385-417.

75. Sposito, G., *The surface chemistry of soils*. Oxford University Press: 1984.

76. McBride, M. B., *Environmental chemistry of soils*. Oxford university press: 1994.

77. Jal, P. K.; Patel, S.; Mishra, B. K., Chemical modification of silica surface by immobilization of functional groups for extractive concentration of metal ions. *Talanta* **2004,** *62* (5), 1005-1028.

78. Al-Qodah, Z.; Al-Shannag, M., Heavy metal ions removal from wastewater using electrocoagulation processes: A comprehensive review. *Separation Science and Technology* **2017,** *52* (17), 2649-2676.

79. Nanseu-Njiki, C. P.; Tchamango, S. R.; Ngom, P. C.; Darchen, A.; Ngameni, E., Mercury(II) removal from water by electrocoagulation using aluminium and iron electrodes. *Journal of Hazardous Materials* **2009,** *168* (2–3), 1430-1436.

80. Igiri, B. E.; Okoduwa, S. I. R.; Idoko, G. O.; Akabuogu, E. P.; Adeyi, A. O.; Ejiogu, I. K., Toxicity and Bioremediation of Heavy Metals Contaminated Ecosystem from Tannery Wastewater: A Review. *Journal of Toxicology* **2018,** *2018*, 16.

81. López-Muñoz, M. J.; Aguado, J.; Arencibia, A.; Pascual, R., Mercury removal from aqueous solutions of HgCl2 by heterogeneous photocatalysis with TiO2. *Applied Catalysis B: Environmental* **2011,** *104* (3), 220-228.

82. Byrne, H. E.; Mazyck, D. W., Removal of trace level aqueous mercury by adsorption and photocatalysis on silica–titania composites. *Journal of Hazardous Materials* **2009,** *170* (2), 915-919.

83. Fan, L.; Zhou, A.; Zhong, L.; Liu, Y., Photoinduced reduction of high concentration Hg(II) to Hg2Cl2 from acid wastewater with the presence of fulvic acid under anaerobic conditions. *Chemosphere* **2018,** *198*, 13-20.

84. Mathews, T. J.; Looney, B. B.; Bryan, A. L.; Smith, J. G.; Miller, C. L.; Southworth, G. R.; Peterson, M. J., The effects of a stannous chloride-based water treatment system in a mercury contaminated stream. *Chemosphere* **2015,** *138*, 190-196.

85. Looney, B.; Denham, M.; Vangelas, K.; Bloom, N., Removal of Mercury from Low-Concentration Aqueous Streams Using Chemical Reduction and Air Stripping. *Journal of Environmental Engineering* **2003,** *129* (9), 819-825.

86. Schindler, P.; Fürst, B.; Dick, R.; Wolf, P., Ligand properties of surface silanol groups. I. surface complex formation with Fe^{3+}, Cu^{2+}, Cd^{2+}, and Pb^{2+}. *Journal of Colloid and Interface Science* **1976,** *55* (2), 469-475.

87. Reed, B. E.; Cline, S. R., Retention and release of lead by a very fine sandy loam. I. Isotherm modeling. *Separation Science and technology* **1994,** *29* (12), 1529-1551.

88. Crawford, R. J.; Dann, J.; Harding, I. H.; Mainwaring, D. E., Coprecipitation of Oxide and Related Surfaces. Taylor & Francis: 2002.

89. Sposito, G.; Davis, J.; Hayes, K. In *Geochemical processes at mineral surfaces*, ACS Symposium Series, 1986; p 216.

90. Dubey, S.; Banerjee, S.; Upadhyay, S. N.; Sharma, Y. C., Application of common nano-materials for removal of selected metallic species from water and wastewaters: A critical review. *Journal of Molecular Liquids* **2017,** *240*, 656-677.

91. Arshadi, M.; Abdolmaleki, M. K.; Mousavinia, F.; Foroughifard, S.; Karimzadeh, A., Nano modification of NZVI with an aquatic plant Azolla filiculoides to remove Pb(II) and Hg(II) from water: Aging time and mechanism study. *Journal of Colloid and Interface Science* **2017,** *486*, 296-308.

92. Liu, T.; Wang, Z.-L.; Yan, X.; Zhang, B., Removal of mercury (II) and chromium (VI) from wastewater using a new and effective composite: Pumice-supported nanoscale zero-valent iron. *Chemical Engineering Journal* **2014,** *245*, 34-40.

93. Guo, X.; Yang, Z.; Dong, H.; Guan, X.; Ren, Q.; Lv, X.; Jin, X., Simple combination of oxidants with zero-valent-iron (ZVI) achieved very rapid and highly efficient removal of heavy metals from water. *Water Research* **2016,** *88*, 671-680.

94. Mattigod, S. V.; Fryxell, G. E.; Feng, X.; Parker, K. E.; Piers, E. M., Removal of Mercury from Aqueous Streams of Fossil Fuel Power Plants Using Novel Functionalized Nanoporous Sorbents. In *Coal Combustion Byproducts and Environmental Issues*, Sajwan, K.; Twardowska, I.; Punshon, T.; Alva, A., Eds. Springer New York: 2006; pp 99-104.

95. Mattigod, S. V.; Feng, X.; Fryxell, G. E.; Liu, J. U. N.; Gong, M., Separation of Complexed Mercury from Aqueous Wastes Using Self-Assembled Mercaptan on Mesoporous Silica. *Separation Science and Technology* **1999,** *34* (12), 2329-2345.

96. Kurniawan, T. S., Mika; Sillanpaa, Markus; , Nanoadsorbents for Remediation of Aquatic Environment: Local and Practical Solutions for Global Water Pollution Problems. *Critical Reviews in Environmental Science and Technology* **2012,** *42* (12), 1233-1295.

97. Sun, Y.; Lv, D.; Zhou, J.; Zhou, X.; Lou, Z.; Baig, S. A.; Xu, X., Adsorption of mercury (II) from aqueous solutions using FeS and pyrite: A comparative study. *Chemosphere* **2017,** *185*, 452-461.

98. Vunain, E.; Mishra, A. K.; Mamba, B. B., Dendrimers, mesoporous silicas and chitosan-based nanosorbents for the removal of heavy-metal ions: A review. *International Journal of Biological Macromolecules* **2016,** *86*, 570-586.

99. Shekhawat, A.; Kahu, S.; Saravanan, D.; Jugade, R., Removal of Cd(II) and Hg(II) from effluents by ionic solid impregnated chitosan. *International Journal of Biological Macromolecules* **2017,** *104*, 1556-1568.

100. Song, S.-T.; Saman, N.; Johari, K.; Mat, H., Surface chemistry modifications of rice husk toward enhancement of Hg(II) adsorption from aqueous solution. *Clean Technologies & Environmental Policy* **2014,** *16* (8), 1747-1755.

101. Arshadi, M.; Faraji, A. R.; Amiri, M. J., Modification of aluminum–silicate nanoparticles by melamine-based dendrimer l-cysteine methyl esters for adsorptive characteristic of Hg(II) ions from the synthetic and Persian Gulf water. *Chemical Engineering Journal* **2015,** *266*, 345-355.

102. Xu, D.; Wu, W. D.; Qi, H.-J.; Yang, R.-X.; Deng, W.-Q., Sulfur rich microporous polymer enables rapid and efficient removal of mercury(II) from water. *Chemosphere* **2018,** *196*, 174-181.

103. Rathore, E.; Biswas, K., Selective and ppb level removal of Hg(ii) from water: synergistic role of graphene oxide and SnS2. *Journal of Materials Chemistry A* **2018,** *6* (27), 13142-13152.

104. Guo, Y.; Wang, Z.; Zhou, X.; Bai, R., Removal of mercury (II) from aqueous solution with three commercial raw activated carbons. *Research on Chemical Intermediates* **2017,** *43* (4), 2273-2297.

105. Attari, M.; Bukhari, S. S.; Kazemian, H.; Rohani, S., A low-cost adsorbent from coal fly ash for mercury removal from industrial wastewater. *Journal of Environmental Chemical Engineering* **2017,** *5* (1), 391-399.

106. Sun, X.; Qu, R.; Sun, C.; Zhang, Y.; Sun, S.; Ji, C.; Yin, P., Sol–Gel Preparation and Hg(II) Adsorption Properties of Silica-Gel Supported Low Generation Polyamidoamine Dendrimers Polymer Adsorbents. *Industrial & Engineering Chemistry Research* **2014,** *53* (8), 2878-2888.

107. Tawabini, B.; Al-Khaldi, S.; Atieh, M.; Khaled, M., Removal of mercury from water by multi-walled carbon nanotubes. *Water Science & Technology* **2010,** *61* (3), 591-598.

108. Shadbad, M.; Mohebbi, A.; Soltani, A., Mercury(II) removal from aqueous solutions by adsorption on multi-walled carbon nanotubes. *Korean Journal of Chemical Engineering* **2011,** *28* (4), 1029-1034.

109. El-Sheikh, A. H.; Al-Degs, Y. S.; Al-As'ad, R. M.; Sweileh, J. A., Effect of oxidation and geometrical dimensions of carbon nanotubes on Hg(II) sorption and preconcentration from real waters. *Desalination* **2011,** *270* (1–3), 214-220.

110. Shang, S.; Yang, X.; Tao, X.-m., Easy synthesis of carbon nanotubes with polypyrrole nanotubes as the carbon precursor. *Polymer* **2009,** *50* (13), 2815-2818.

111. Hadavifar, M.; Bahramifar, N.; Younesi, H.; Li, Q., Adsorption of mercury ions from synthetic and real wastewater aqueous solution by functionalized multi-walled carbon nanotube with both amino and thiolated groups. *Chemical Engineering Journal* **2014,** *237*, 217-228.

112. Liu, J.-f.; Zhao, Z.-s.; Jiang, G.-b., Coating Fe3O4 Magnetic Nanoparticles with Humic Acid for High Efficient Removal of Heavy Metals in Water. *Environmental Science & Technology* **2008,** *42* (18), 6949-6954.

113. Lisha, K. P.; Maliyekkal, S. M.; Pradeep, T., Manganese dioxide nanowhiskers: A potential adsorbent for the removal of Hg(II) from water. *Chemical Engineering Journal* **2010,** *160* (2), 432-439.

114. Hakami, O.; Zhang, Y.; Banks, C. J., Thiol-functionalised mesoporous silica-coated magnetite nanoparticles for high efficiency removal and recovery of Hg from water. *Water research* **2012,** *46* (3913-3922).

115. Sagle, A.; Freeman, B., Fundamentals of membranes for water treatment. *the future of desalination in Texas* **2004,** *2*, 137-154.

116. Urgun-Demirtas, M. B., Paul L., Gillenwater, Patricia S.; Negri, M. Cristina; Xiong, Hui; Snyder, Seth W., Achieving very low mercury levels in refinery wastewater by membrane filtration. *Journal of Hazardous Materials* **2012,** *215–216* (0), 98-107.

117. U.S. EPA Office of Water, Development Document for Final Effluent Limitations Guidelines and Standards for Commercial Hazardous Waste Combustors. EPA 821-R-99-020. 2000.

118. Zeng, J.; Guo, Q.; Ou-Yang, Z.; Zhou, H.; Chen, H., Chromium (VI) removal from aqueous solutions by polyelectrolyte-enhanced ultrafiltration with polyquaternium. *Asia-Pacific Journal of Chemical Engineering* **2013**.

119. Diallo, M. S.; Christie, S.; Swaminathan, P.; Johnson, J. H.; Goddard, W. A., Dendrimer Enhanced Ultrafiltration. 1. Recovery of Cu(II) from Aqueous Solutions Using PAMAM Dendrimers with Ethylene Diamine Core and Terminal NH2 Groups. *Environmental Science & Technology* **2005,** *39* (5), 1366-1377.

120. Jana, S.; Saikia, A.; Purkait, M. K.; Mohanty, K., Chitosan based ceramic ultrafiltration membrane: Preparation, characterization and application to remove Hg(II) and As(III) using polymer enhanced ultrafiltration. *Chemical Engineering Journal* **2011,** *170* (1), 209-219.

121. Zeng, J.; Ye, H.; Hu, Z., Application of the hybrid complexation–ultrafiltration process for metal ion removal from aqueous solutions. *Journal of Hazardous Materials* **2009,** *161* (2–3), 1491-1498.

122. U.S. Environmental Protection Agency, O. o. S. R. a. T. I., Treatment Technologies for Mercury in Soil, Waste, and Water. *EPA-542-R-07-003* **2007**.

123. De Jong, G.; Rekers, C., The Akzo process for the removal of mercury from waste water. *Journal of Chromatography A* **1974,** *102*, 443-450.

124. Chemie, A. Z., The Akzo Imac TMR process for the removal of mercury from waste water. *Akzo Zout Chemie, Hengelo* **1975**.

125. Atwood, D. A.; Zaman, M. K., Mercury Removal from Water. In *Recent Developments in Mercury Science*, Atwood, D., Ed. Springer Berlin Heidelberg: 2006; Vol. 120, pp 163-182.

126. Dąbrowski, A.; Hubicki, Z.; Podkościelny, P.; Robens, E., Selective removal of the heavy metal ions from waters and industrial wastewaters by ion-exchange method. *Chemosphere* **2004,** *56* (2), 91-106.

127. Zhao, X.; Zhao, G.; Wang, J.; Yun, G., Selective extraction of trace mercury and cadmium from drinking water sources. *Water environment research* **2005**, 212-218.

128. Kang, S.-Y.; Lee, J.-U.; Moon, S.-H.; Kim, K.-W., Competitive adsorption characteristics of Co2+, Ni2+, and Cr3+ by IRN-77 cation exchange resin in synthesized wastewater. *Chemosphere* **2004,** *56* (2), 141-147.

129. Nanseu-Njiki, C. P.; Tchamango, S. R.; Ngom, P. C.; Darchen, A.; Ngameni, E., Mercury(II) removal from water by electrocoagulation using aluminium and iron electrodes. *Journal of Hazardous Materials* **2009,** *168* (2), 1430-1436.

130. Chaturvedi, S. I., Mercury Removal Using Al – Al Electrodes by Electrocoagulation. *International Journal of Modern Engineering Research (IJMER)* **2013,** *3* (1), 109-115.

131. Daniel, R. H., V.; Krupadam, R.; Anjaneyulu, Y., Removal of Mercury from Pharmaceutical Wastewaters Using Electrocoagulation. *A Cleaner Technology Option, IUP Journal of Environmental Sciences* **2010,** (4), 7-15.

132. Murthy, Z. P., S. , Electrocoagulative treatment of mercury containing aqueous solutions. *Water Science and Technology* **2012,** (65), 1468-1474.

133. Vasudevan, S. L., J.; Sozhan, G., Optimization of electrocoagulation process for the simultaneous removal of mercury, lead, and nickel from contaminated water. *Environmental Science and Pollution Research* **2012,** (19), 2734–2744.

134. Essa, A.; Macaskie, L.; Brown, N., Mechanisms of mercury bioremediation. *Biochemical Society Transactions* **2002,** *30* (4), 672-673.

135. EPA, U., Treatment technologies for mercury in soil, waste, and water (EPA-542-R-07-003). 2007.

136. Wagner-Döbler, I.; von Canstein, H.; Li, Y.; Timmis, K. N.; Deckwer, W.-D., Removal of Mercury from Chemical Wastewater by Microoganisms in Technical Scale. *Environmental Science & Technology* **2000,** *34* (21), 4628-4634.

137. Hayes, K. F.; Adriaens, P.; Demond, A. H.; Olson, T.; Abriola, L. M. *Reduced Iron Sulfide Systems for Removal of Heavy Metal Ions from Groundwater*; DTIC Document: 2009.

138. Behra, P.; Bonnissel-Gissinger, P.; Alnot, M.; Revel, R.; Ehrhardt, J. J., XPS and XAS study of the sorption of Hg (II) onto pyrite. *Langmuir* **2001,** *17* (13), 3970-3979.

139. Dias, C. R.; Rosa, M. J.; de Pinho, M. N., Structure of water in asymmetric cellulose ester membranes — and ATR-FTIR study. *Journal of Membrane Science* **1998,** *138* (2), 259-267.

140. Belfer, S.; Fainchtain, R.; Purinson, Y.; Kedem, O., Surface characterization by FTIR-ATR spectroscopy of polyethersulfone membranes-unmodified, modified and protein fouled. *Journal of Membrane Science* **2000,** *172* (1), 113-124.

141. Abdel-Karim, A.; Gad-Allah, T. A.; El-Kalliny, A. S.; Ahmed, S. I. A.; Souaya, E. R.; Badawy, M. I.; Ulbricht, M., Fabrication of modified polyethersulfone membranes for wastewater treatment by submerged membrane bioreactor. *Separation and Purification Technology* **2017,** *175*, 36-46.

142. Wolthers, M.; Charlet, L.; van Der Linde, P. R.; Rickard, D.; van Der Weijden, C. H., Surface chemistry of disordered mackinawite (FeS). *Geochimica et Cosmochimica Acta* **2005,** *69* (14), 3469-3481.

143. Jeong, H. Y.; Lee, J. H.; Hayes, K. F., Characterization of synthetic nanocrystalline mackinawite: crystal structure, particle size, and specific surface area. *Geochimica et cosmochimica acta* **2008,** *72* (2), 493-505.

144. Smith, R. M.; Martell, A. E.; Motekaitis, R. J., *NIST critically selected stability constants of metal complexes database*. National Institute of Standards & Technology: 1998.

145. Lamy, I.; Djafer, M.; Terce, M., Influence of oxalic acid on the adsorption of cadmium at the goethite surface. *Water, Air, and Soil Pollution* **1991,** *57* (1), 457-465.

146. Collins, C. R.; Ragnarsdottir, K. V.; Sherman, D. M., Effect of inorganic and organic ligands on the mechanism of cadmium sorption to goethite. *Geochimica et Cosmochimica Acta* **1999,** *63* (19–20), 2989-3002.

147. Hawke, D.; Carpenter, P. D.; Hunter, K. A., Competitive adsorption of phosphate on goethite in marine electrolytes. *Environmental science & technology* **1989,** *23* (2), 187-191.

148. Diaz-Barrientos, E.; Madrid, L.; Contreras, M.; Morillo, E., Simultaneous adsorption of zinc and phosphate on synthetic lepidocrocite. *Soil Research* **1990,** *28* (4), 549-557.

149. Nagy, K. L.; Manceau, A.; Gasper, J. D.; Ryan, J. N.; Aiken, G. R., *Metallothionein-Like Multinuclear Clusters of Mercury(II) and Sulfur in Peat*.

150. do Nascimento, F. H.; Masini, J. C., Influence of humic acid on adsorption of Hg(II) by vermiculite. *Journal of Environmental Management* **2014,** *143* (0), 1-7.

151. Ravichandran, M., Interactions between mercury and dissolved organic matter—a review. *Chemosphere* **2004,** *55* (3), 319-331.

152. Skyllberg, U., Competition among thiols and inorganic sulfides and polysulfides for Hg and MeHg in wetland soils and sediments under suboxic conditions: Illumination of controversies and implications for MeHg net production. *Journal of Geophysical Research: Biogeosciences (2005–2012)* **2008,** *113* (G2).

153. Skyllberg, U.; Xia, K.; Bloom, P. R.; Nater, E. A.; Bleam, W. F., Binding of mercury (II) to reduced sulfur in soil organic matter along upland-peat soil transects. *Journal of environmental quality* **2000,** *29* (3), 855-865.

154. Haitzer, M.; Aiken, G. R.; Ryan, J. N., Binding of mercury (II) to dissolved organic matter: the role of the mercury-to-DOM concentration ratio. *Environmental science & technology* **2002,** *36* (16), 3564-3570.

155. Drexel, R. T.; Haitzer, M.; Ryan, J. N.; Aiken, G. R.; Nagy, K. L., Mercury(II) Sorption to Two Florida Everglades Peats: Evidence for Strong and Weak Binding and Competition by Dissolved Organic Matter Released from the Peat. *Environmental Science & Technology* **2002,** *36* (19), 4058-4064.

156. Duan, Y.; Han, D. S.; Batchelor, B.; Abdel-Wahab, A., Application of a reactive adsorbent-coated support system for removal of mercury(II). *Colloids and Surfaces A: Physicochemical and Engineering Aspects* **2016,** *509*, 623-630.

157. Al-Degs, Y. S.; El-Barghouthi, M. I.; El-Sheikh, A. H.; Walker, G. M., Effect of solution pH, ionic strength, and temperature on adsorption behavior of reactive dyes on activated carbon. *Dyes and Pigments* **2008,** *77* (1), 16-23.

158. Park, C. M.; Han, J.; Chu, K. H.; Al-Hamadani, Y. A. J.; Her, N.; Heo, J.; Yoon, Y., Influence of solution pH, ionic strength, and humic acid on cadmium adsorption onto activated

biochar: Experiment and modeling. *Journal of Industrial and Engineering Chemistry* **2017,** *48*, 186-193.

159. Peeva, P. D.; Palupi, A. E.; Ulbricht, M., Ultrafiltration of humic acid solutions through unmodified and surface functionalized low-fouling polyethersulfone membranes – Effects of feed properties, molecular weight cut-off and membrane chemistry on fouling behavior and cleanability. *Separation and Purification Technology* **2011,** *81* (2), 124-133.

160. Qu, F.; Liang, H.; Zhou, J.; Nan, J.; Shao, S.; Zhang, J.; Li, G., Ultrafiltration membrane fouling caused by extracellular organic matter (EOM) from Microcystis aeruginosa: Effects of membrane pore size and surface hydrophobicity. *Journal of Membrane Science* **2014,** *449*, 58-66.

161. Ramirez, J., Effect of anions on removal of Mercury(II) using FeS-Supported Crossflow Ultrafiltration. In *Ultrafiltration: Methods, applications and insights*, 2017; pp 129-151.

162. Bone, S. E.; Bargar, J. R.; Sposito, G., Mackinawite (FeS) Reduces Mercury(II) under Sulfidic Conditions. *Environmental Science & Technology* **2014,** *48* (18), 10681-10689.

163. Garcia, C.; Rogel-Hernandez, E.; Flores-Lopez, L. Z.; Espinoza-Gomez, H., Effect of the Membrane Characteristics and Operation Modes in the Fouling of Ultrafiltration Membranes by Natural Organic Matter (NOM). *Journal of the Chilean Chemical Society* **2012,** *57* (2), 1083-1086.

164. Maurer-Jones, M. A.; Gunsolus, I. L.; Murphy, C. J.; Haynes, C. L., Toxicity of Engineered Nanoparticles in the Environment. *Analytical Chemistry* **2013,** *85* (6), 3036-3049.

165. Deonarine, A.; Hsu-Kim, H., Precipitation of Mercuric Sulfide Nanoparticles in NOM-Containing Water: Implications for the Natural Environment. *Environmental Science & Technology* **2009,** *43* (7), 2368-2373.